2019

The Manufacture and Testing of Self-Sensing CNTs Nanocomposites for Damage Detecting Applications

Al-Bahrani, Mohammed

UNIVERSITY OF PLYMOUTH

The Manufacture and Testing of Self-Sensing CNTs Nanocomposites for Damage Detecting Applications

by

Mohammed Naeem Al-Bahrani

A thesis submitted to the University of Plymouth in partial fulfilment for the degree of

DOCTOR OF PHILOSOPHY

School of Engineering

University of Plymouth

October 2019

‘My success can only come from God.
In Him I trust, and unto Him I look’

[Hud 88]

Abstract

Composite materials are widely used in various important applications due to their good engineering properties. However, these properties can be reduced when subjected to different type of loads. This thesis experimentally, theoretically and statistically investigates the possibility of using multi-walled carbon nanotubes (MWCNTs) as a filler to fabricate self-sensing nanocomposites for fracture and damage sensing applications. Self-sensing composite based MWCNTs can be used to diagnose early stage damage in order to prevent a fatal fracture that could occur in the structure during its working life. Here, different concentrations of MWCNTs were evenly distributed either in an epoxy resin using high frequency sonication or by depositing them onto the glass fibre surface to make it electrically conductive. Scanning electron microscopy (SEM) and Raman spectroscopy were used to investigate the presence of the MWCNTs and their interaction with the matrix. These self-sensing nanocomposites were subjected to different types of failure such as low velocity impact, static and cyclic compression test under varied temperature, anticlastic deformations including flexural and bending tests. During such testing the mechanical, electrical, impact damage, damage sensitivity, flexural, and piezoresistive properties were examined experimentally and statistically. The results of SEM microscopy showed that the MWCNTs were well distributed inside the matrix, although some agglomeration occurred at high MWCNTs concentrations. Moreover, electrical conductivity measurements indicated a steadily increasing directly proportional relationship with increasing the MWCNTs concentration. In addition, the observed changes in the electrical resistance of specimens increased with increasing impact energy, and temperature. Conversely, the resistance decreased with increasing compression loads, and during flexural and anticlastic testing up to a certain level and then increased due to specimen distortion. In terms of the strain sensitivity, there are two strain sensitivities, in opposite directions obtained, during anticlastic testing and only one obtained under flexural and compression testing conditions.

This study has confirmed that the properties of a self-sensing composite are strongly dependent on the method used to deposit the MWCNTs onto the surface of glass fibres layers, the types of test, deformation after testing and the operative test conditions (i.e. temperature). Given these results, it is possible to correlate the degree of damage incurred due to the external loads with the changes in electrical resistance of the

MWCNTs-GE nanocomposites both during, and after, loading. Therefore, this type of self-seing nanocomposites shows excellent potential for use in many strain and fracture sensing applications.

Acknowledgments

Firstly, I would like to express my sincere gratitude to my advisor Dr. Alistair Cree for the continuous support of my PhD study and related research, for his patience, motivation, and immense knowledge. His guidance helped me throughout my research and during the writing of this thesis. I could not have imagined having a better advisor and mentor for my PhD study.

Besides my advisor, I would like to thank the rest of my thesis committee: Dr. Jasper Graham-Jones and Dr. Zoltan Gombos, for their insightful comments and encouragement, but also for the hard question which gave me the incentive to widen my research from various perspectives.

The author would like to express gratitude to staff at University of Plymouth, for their guidance and advice, especially the technician's team, Terry Richards, Mike Sloman, Dr. Richard Cullen. They provided and helped me with anything I needed during my study.

Special thanks to my friend Mohammed Ridh Al-hakeem for his assistance to support me during my PhD studying. Without his help, I cannot complete my study easily.

Last but not least, I would like to thank my family including my parents, brothers, my wife and my sons Hussein and Ahmed for supporting me spiritually throughout my PhD study and the writing of this thesis.

Author's declaration

At no time during the registration for the degree of Doctor of Philosophy has the author been registered for any other University award without prior agreement of the Doctoral College Quality Sub-Committee.

Work submitted for this research degree at the University of Plymouth has not formed part of any other degree either at the University of Plymouth or any other establishment.

Several papers, posters and seminars were presented and published at relevant conferences, and in scientific journals.

Word count of the thesis: **44552** words

Figure count of the thesis: **71** figures

Table count of the thesis: **8** tables

External Contacts:

Emails: mwcnt5@yahoo.com and mohammed.naeem@plymouth.ac.uk

Research gate: https://www.researchgate.net/profile/Mohammed_Al-Bahrani

ORCID: https://orcid.org/0000-0003-0680-0116

Signed……

Date……..

External and internal training attending

- Academic English for research student, March-September, 2015, Plymouth University, UK
- Managing Working Relationships: Students and supervisors – 14 March 2016 Plymouth University, UK
- Introduction to EndNote, 2 December 2016, Plymouth University, UK
- Application forms and writing tailored CV's, 2017, Plymouth University, UK
- Careers session for Science and Engineering researchers 24th February, 2017 Plymouth University, UK
- Ph.D. course: "Fracture Mechanics for Laminated Composite Structures", 13-17 Nov. 2017, Aalborg University, Denmark

Publications

A) Journal publications

- Mohammed Al-Bahrani and Alistair Cree, *A simple criterion to evaluate the degree of damage in composite materials after sudden impact loads by exploiting the MWCNTs piezoresistive property*. Carbon 150 (2019) p.505-517.
- Mohammed Al-Bahrani, Zoltan J Gombos and Alistair Cree, *Investigation of the constancy of the MWCNTs on the fibres surface for manufactured self-sensing composites*. Composites Part B: Engineering, 173 (2019), 106998.
- Mohammed Al-Bahrani, Muhsin Aljuboury and Alistair Cree, *Damage sensing and mechanical properties of laminate composite based MWCNTs under anticlastic test*. Materials Research Express, 2018. 6(3) 035704.

- Mohammed Al-Bahrani, Zoltan J Gombos and Alistair Cree, *The Mechanical Properties of Functionalised MWCNT Infused Epoxy Resin: A Theoretical and Experimental Study*. International Journal of Mechanical & Mechatronics Engineering IJMME-IJENS, 2018. 18(1): p.76-86.
- Mohammed Al-Bahrani; Alistair Cree and Sung-Hwan Jang, *On the electromechanical and temperature dependent behaviour of an epoxy resin-based nanocomposite incorporating multi-walled carbon nanotubes*. Submitted to the construction and building materials journal and currently it is under review.

B) Conference publications

- Mohammed Al-Bahrani, Zoltan J Gombos, Alistair Cree., *"Studying the Effect of Carbon Nanotubes on the Mechanical Properties of Epoxy-Nanocomposite for the Oil Field Applications"*, 19th International Conference on nanostructure Materials and Nano-synthesis/ICNMN/25-25 Sep.2017, UAE.
- Mohammed Al-Bahrani, Zoltan J Gombos, Alistair Cree, *"Theoretical and experimental studying the adding of Ni-MWCNTs on the mechanical properties of epoxy-nanocomposite for the oil field applications"*, Postgraduate Society Research Showcase, Plymouth University, 4th Dec. 2017. UK
- Mohammed Al-Bahrani, Alistair Cree, Sung-Hwan Jang., *"Integrated strain and fracture sensing in carbon nanotubes reinforced composites for energy infrastructures"*, 5th PRIMaRE Conference, Bristol University 5-6 July 2018, UK
- Sung-Hwan Jang, Mohammed Al-Bahrani., *"Carbon Nanotube Coated Fiber Reinforced Epoxy Composites for Oil and Gas Pipeline"*, Engineering Mechanics Institute Conference (EMI), Massachusetts Institute of Technology, Boston, NY, USA, 2018.

- Mohammed Al-Bahrani, Alistair Cree, Sung-Hwan Jang., *"Carbon nanotubes reinforced nanocomposites for strain and fracture sensing in engineering structures"*, 13th International Conference on Surfaces, Coatings and Nanostructured Materials, 11-14 September 2018, Gdansk, POLAND.

Note: All published papers were written by the first author, based on the experimental work conducted by him. The contributions from the other authors were only minor editorial changes. Their names were added to acknowledge these contributions. Supervisory team: Dr. A. M. Cree and Dr. Zoltan Gombos.

List of contents

List of Figures

List of Tables

Nomenclature

CNT	Carbon nanotube
MWCNT	Multi-walled carbon nanotube
SWCNT	Single-walled carbon nanotube
COOH-CNT	Carboxylic functionalised carbon nanotube
GFRP	Glass fibre reinforced polymers
C_h	Chiral axis
nm	Nano-metre
μm	Micro-metre
AFM	Atomic force microscopy
E	Modulus of elasticity
σ_{ts}	Tensile strength
RTM	Resin transfer moulding
wt.%	Weight fraction
vol.%	Volume fraction
SEM	Scanning electron microscopy
SENB	Single edge notch bending
K1C	Plain strain fracture toughness
CVD	Chemical vapour deposition
ILSS	Inter-laminar shear strength
PU	Polyurethane
PI	Polyimide

PS	Polystyrene
PF	Polypropylene
σ_C	Electrical conductivity of CNTs
GF	Glass fibre
GE	Glass-epoxy
SHM	Structural Health Monitoring
v_i	Initial impact velocities
v_r	Rebound velocity
FAI	Flexural After Impact
σ_f	Flexural stress
P_f	Flexural force
t	Thickness of the sample
ε_f	Flexural strain
l	Span length
h	Sample high
w	Sample width
σ	Electrical conductivity
R	Resistance in Ohm
ε	Strain
L	Sample length
A	Cross-section area
ANOVA	The Analysis of Variance
S	Siemens

ψ	Damage Factor
E_{ab}	Absorbed energy
E_i	Initial kinetic energy
E_r	Final kinetic energy
m	Mass of the impactor
J	Joule
ΔR	Change in resistance
R_0	Initial resistance in Ohm
λ	Electric damage parameter
R_{tunnel}	Tunneling resistance
e	Charge of an electron
h	Planck's constant
m	Mass of an electron
β	Energy barrier
d	Space between Carbon Nanotubes
D	Diameter of a Carbon Nanotube
L	Length of CNT
w_c	Carbon nanotube critical concentration
σ_0	Scaling factor
Tg	Glass transition temperature
σ_b	Flexural bend
F	Force
DC	Direct Current
GRP	Glass reinforced polymer

E_x	Young's modulus in x-direction
E_y	Young's modulus in y-direction
ε_x	Strain along x- direction
ε_y	Strain along y- direction
M_x	Moments in x-direction
M_y	Moments in y-direction
EPD	Electrophoretic deposition
g	Gram
χ	CNTs non-straightness
ρ_m	Density of matrix
f	Volume fraction of the CNT
H	Depolarisation factor
σ_e	Electrical conductivity of the CNTs nanocomposite
σ_m	Electrical conductivity polymer matrix
α	CNT aspect ratio
t	Time
EPT	Electrical percolation threshold

Chapter 1
Introduction and Background to Research

1.1 Overview

As modern engineering materials, composites are widely used in many important industries such as oil and gas, aerospace, and the marine sector. This is due to their superior properties such as being lightweight, having high specific strength, and thermal stability as well as low creep and good corrosive resistance [1]. Moreover, as part of the design process composite materials can provide good flexibility to control, and tailor, multiple physical and mechanical properties through the selective choice of reinforcement and matrix materials. With a laminated composite the structural materials consists of two main phases mixed at the macro-scale. The first phase is a fibre discontinuous reinforcement phase, which provides strength and stiffness while the second phase is called the matrix, which is a weaker but tougher phase and is usually a polymeric material, either thermosetting or thermoplastic. The matrix encapsulates the fibre and therefore is considered to be the main load transfer carrier for loading through the laminate composite materials [2].

However, there are disadvantages and problems associated with composites which can arise both during manufacturing / processing or when the composite is in service. For example, cracks can initiate in the matrix material and cause delamination between the laminate layers, i.e. debonding or separation between the matrix and the fibres. This type of failure is the major drawback when using laminate composite materials. The propagation of cracks inside the composite components can lead to the sudden catastrophic failure and degradation of the structure.

Furthermore, a composite can usually be characterised as an anisotropic material when compared with metals and alloys. This is because composite materials are manufactured using a variety of processing techniques, which have to account for a numbers of different fabrication variables. These variables lead to increased opportunities to create many failure-promoting defects. Therefore, damage detection, prevention or delay is a major challenge to address, because damage usually occurs inside the composite structure [3]. Due to the demanding requirements for safety in the energy and aerospace sectors, it is very important to develop real-time structure health monitoring which can be used in service. Such a system could be used to indicate the physical conditions of the structure so reducing the maintenance time. This could also help to prevent sudden catastrophic failure. Current structural health monitoring (SHM) techniques include optical fibres, strain gauges and piezoelectric sensors, which detect any changes in the condition of a structure during operation. Using these sensors to provide data at a restricted position is often difficult and therefore it might be necessary to place them in adjacent less sensitive location near to where failure is likely [4]. One of the most effective ways to monitor the structure health is by creating a large network area of strain sensors on the surface of the structure which can give an effective response.

However, this type of technique suffers from serious shortcomings and is therefore not perfect, can be costly and requires a very complex network system to function well. In addition, it is very difficult to embed sensors inside the composite structure because they might be chemically incompatible with the composite components. For example, embedded optical fibres inside composite laminates may cause early cracking in the matrix, since another potentially debonding interface is created. These embedded

sensors may make the composite weak in use, so minimising their potential applications [5].

To overcome these issues, it is necessary to manufacture a multi-functional composite, often called a smart composite, which has the ability to sense in itself any change in its structural state during operation. The 'self-sensing' concept is achieved by employing the electrical methods to sense the internal health condition of the structure. The advantage of the self-sensing technique is to secure the composite from sudden damage by preserving all of the original mechanical properties, whilst potential internal defects can be monitored and sensed [6]. Carbon fibre reinforced polymer (CFRPs) are electrically conductive and can be used as a smart composite material. However, the failure mode in the CFRPs depends on fibre breakage and this damage most often occurs near the end of the structures life. Hence, early detection of damage, such as delamination or matrix cracking, is essential as part of a self-sensing technique which seeks to monitor the structural integrity of the structure.

Moreover, glass fibre reinforced polymers (GFRPs) are not considered within this concept since they are not electrically conductive. In order to make GFRP composites sensitive they must be conducting, and so have ability to detect the damage at an early stage. This can be achieved by two methods: either by embedding nano-scale fillers within the matrix polymer, or by modifying or coating the fibre surfaces using conductive nano-scale fillers.

Amongst the types of conductive fillers available, carbon nanotubes (CNTs) are considered to be a suitable candidate to make a GFRP composite conductive due to their very good electrical conductivity, effective mechanical properties, low density and high aspect ratio [7, 8]. They can be employed inside the non-conductive matrix

or on the surface of the fibre, so making them conductive materials due to the formation of a conductive CNTs network structure. Using CNTs as fillers in GFRPs could also provide a possible method of monitoring the structural health without the need for sophisticated electronic equipment, so improving the monitoring efficiency whilst reducing the cost.

CNTs are not only used as conductive materials but also to improve mechanical properties such as the interlaminar shear strength or toughness of the composite [9]. They do this by enhancing the interfacial connection between the matrix and surface of the reinforcing fibres. In this context, most researchers [10, 11] have tried to improve the smart composite by using an optimised method using CNTs. However, these always tend to agglomerate at high levels of concentration. In addition, they also suffer from a lack of homogenous and even distribution on the fibre surface.

Therefore, the main aims and objectives of this research study are as follows;

1. To manufacture a self-sensing nanocomposite for crack damage detection under harsh operating conditions. Therefore, in this part, self-sensing MWCNT/epoxy nanocomposites containing different concentrations of MWCNTs will fabricated. Following this an investigatigation of their electromechanical properties will be conducted during static and cyclic compression tests at different temperatures.
2. To fabricate a smart composite using glass fibres containing MWCNTs for damage sensing under different loading conditions, such as might occur during anticlastic bending. Therefore, it would appear that previous researchers have concentrated only on the standard tests such as tensile or bending. However, the anticlastic-bending test is also very important to investigate the static

failure behaviour of composites when they are used in plate or sheet form. The main aim of this test is to study the effect of the MWCNTs, when mixed with the polymer resin at different concentrations, on the mechanical and electro-mechanical behaviour of the composites during two different types of bend tests. These tests were (i) the anticlastic bend test, (ii) a pure flexural bend test for comparison. The purpose of these tests was to investigate the effects of the distributed MWCNTs in the matrix of the composite on the reversibility of the mechanical properties of a laminate composite during anticlastic loading. These tests also aimed to investigate the damage accumulation in the composites as determined by the piezo-resistivity and the strain sensitivity of the composite during a specific strain deformation.

3. To carry out a full examination of the effectiveness of applying CNTs directly onto the fabric surface during epoxy infusion. The main aims here were to firstly; investigate the use of a fixing adhesive on the glass fibre surface which held the MWCNTs in their desired location during the resin infusion process. Secondly; to investigate any variations in the mechanical, electrical and strain sensitivity properties (viz. any property gradient) along the composite panel length. In particular, a numerical study was also carried out to investigate the changes in the tunnelling distance between individual MWCNTs in relation to their volume fraction along the composite panel length.

4. From the previous studies it is clear that after the addition of CNTs to the glass fibre composite, the damage after impact load can be sensed and detected. However, these studies, and others, have concentrated only on the change in

electric resistances before and after impact without making any evaluation of the changing relationship between the electrical resistance of the structure, and other properties such as degradation in mechanical properties or the absorbed energy, during the impact. Therefore, a simple method was developed to evaluate the correlation between the energy absorbed by the target after low-velocity impact and the change in the electrical resistances under the same impact test conditions. Here, the epoxy resin had different MWCNTs concentrations added (i.e. 0.5, 1.0, 1.5, 2.0 wt.%) to fabricate a nanocomposite matrix material for the glass fibre composite. The results achieved give a clear path towards developing a self-sensing composite which can sense any damage occurring due to impact as a real-time event.

For clarity, the thesis structure, and the project development, is outlined in the flow diagram Figure 1.1.

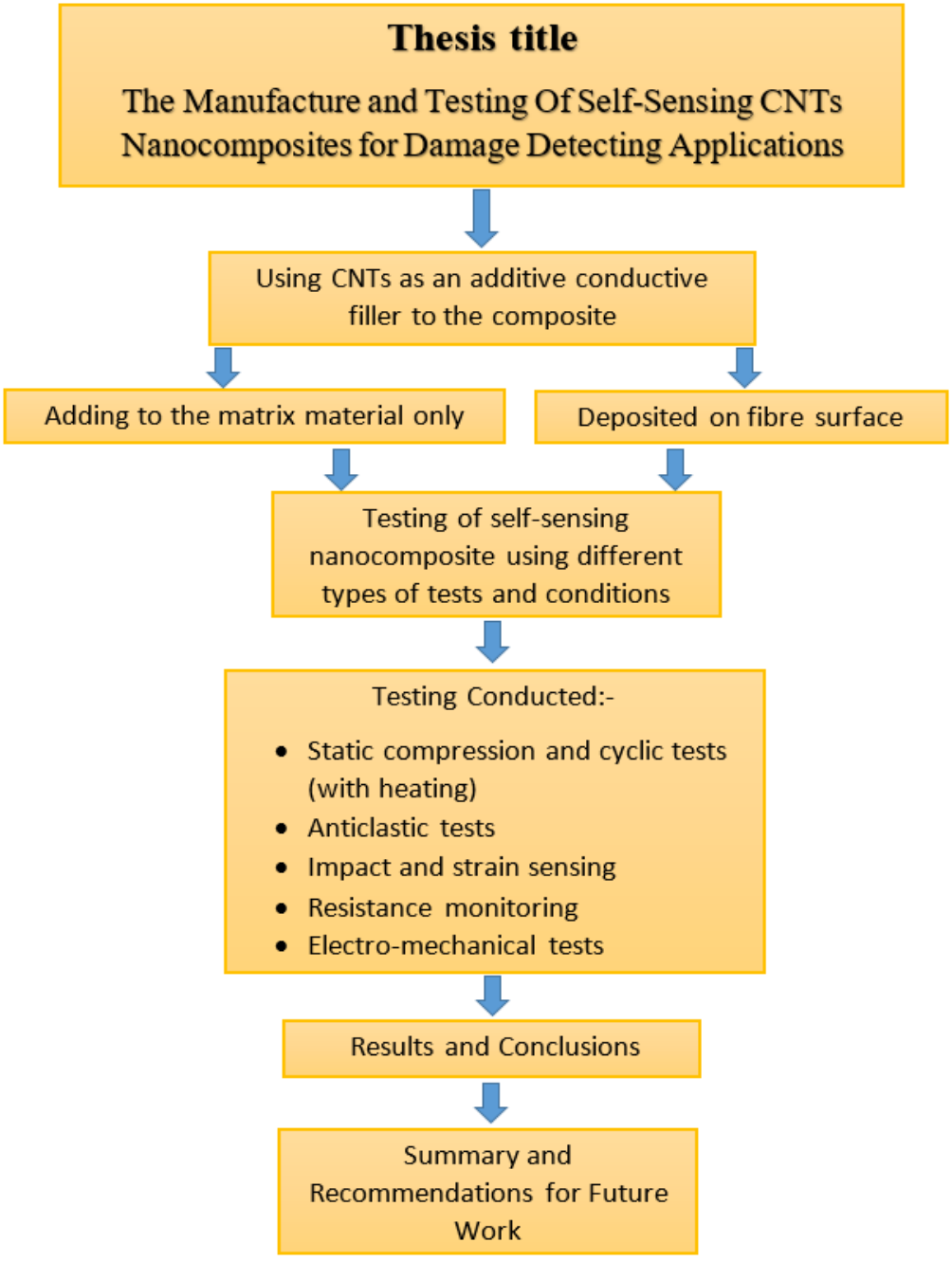

Figure 1.1: Outline of thesis

The outcomes of the experimental work conducted during this research study are represented as individual chapters in this thesis. Each chapter is concerned with a specific area of study (as defined above) and reports the work conducted and the relevant findings obtained. Each chapter concludes with the suitable conclusions to be drawn.

Chapter 2

Literature Review: The use of Carbon Nanotubes in Composite Materials

This chapter reviews the current state of the art in relation to the incorporation of carbon nanotubes in composite materials.

2.1 Nanotechnology

The term 'Nanotechnology' deals with the design, fabrication and applications of materials at nanoscale levels typically 1-100 nm. It is applied in physics, material science, chemistry, interface science, medical, robotics, chemical, mechanical, biological and electrical engineering. At the nanoscale, it has been observed that the materials possess very different properties when compared with the same material at the macroscale. This opens up exciting new opportunities in science and technology which might lead to the manufacture of mini components that have more efficient, lighter, stronger, and more effective properties than those currently available [12].

There are two main approaches to the synthesise of nanomaterials, the bottom-up approach and the top-down approach [13]. In the bottom-up approach, the materials are built and prepare from atomic levels by using self-assembly techniques. In a top-down approach, milling or grinding are used to making nanoparticles.

As discussed above, there are many excellent potential applications for nanotechnology in materials science and engineering. These are represented in:

1. Obtaining on lightweight, high strength materials.
2. Nanocomposite materials, with novel properties.
3. Thin coatings to protect structural and components from corrosion.
4. Making the composite ``self-sensing`` to changes in externally applied conditions such as temperature, gas leakages, pressure and strain.

2.2 Historical Development of Carbon Nanotubes

In 1991, Iijima discovered the 'seamless' single wall carbon nanotube [14]. A seamless (SWCNT), shown in Figure 2.1 can be prepared by rolling up a sheet of graphene. Similarly where multiple concentric tubes are produced then a 'multi-walled' carbon nanotube (MWCNT) results [15].

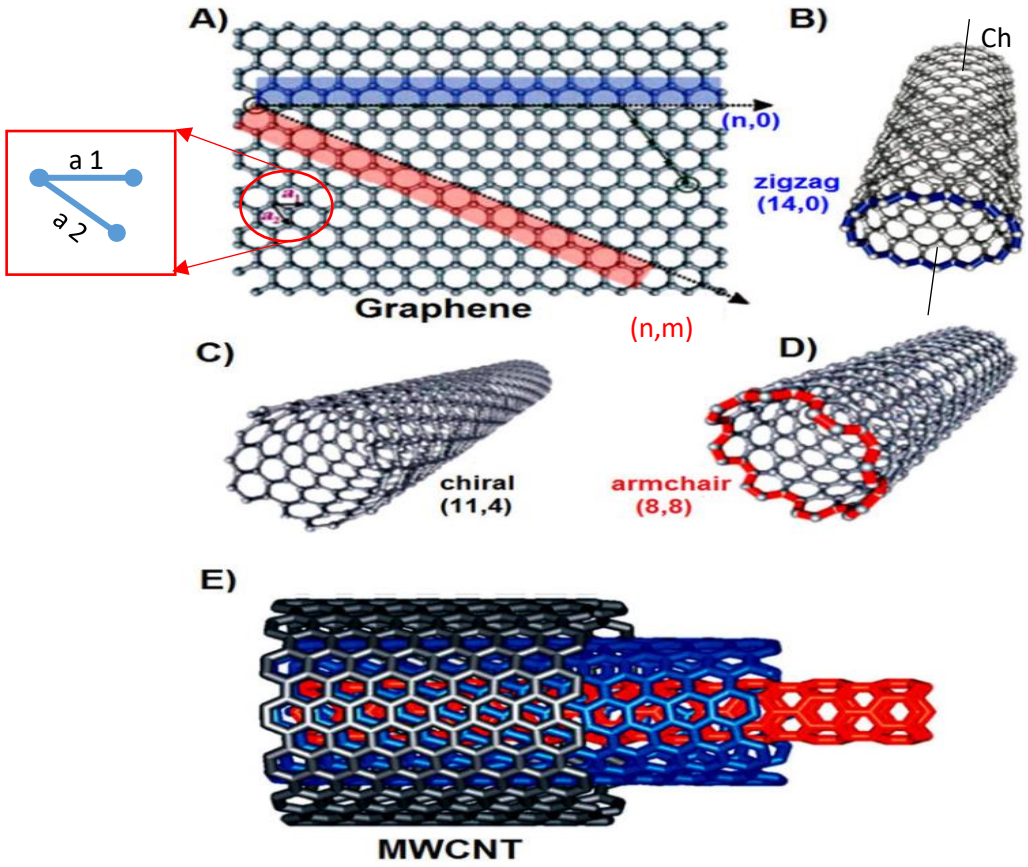

Figure 2.1: (a) Schematic showing the formation of sheet of graphene, by rolling it along different directions and the resulting gives SWNTs as in (a), (b), (c), (d) and MWCNTs as in (e) [15]

When the sheet of graphene is rolled into a cylindarical shape along the length of its chiral axis Ch, then a nanotube of circumference equal to the length of the chiral axis is created. The integer parameters of n and m are indicated in the chiral axis, are expressed in equation (2.1):

$$C_h = na_1 + ma_2 \tag{2.1}$$

In the above equation, a_1 and a_2 are vectors of lattice translation as shown in Figure 2.1. The diameter of the final nanotube would depend on these (n, m) parameters. The diameter of a single wall carbon nanotube is therefore given by equation (2.2) [16]:

$$diameter = a \times \sqrt{n^2 + m^2 + n\,m}\,/\pi \tag{2.2}$$

Where; a = 0.264 nm indicating the size of the lattice vector. If (n) is equal to (m), then the 'armchair' nanotubes are formed. If (n) or (m) equal to 0, then 'zigzag' nanotubes are formed. When the hexagonal atomic arrangement is around the circumference, these lead to both 'armchair' and 'zig-zag' configuration [16]. Along the hexagon axis then 'Armchair' nanotubes are formed, while along a diagonal axis then 'zig-zag' nanotubes shape are formed. For 2 - 50 concentric tubes then (MWCNTs) are formed. In summary, the performance of SWCNTs is very sensitive to purity and chirality, which are very hard properties to control. MWCNTs are more economical and can be grown cheaply to a high degree of purity [17].

2.3 Mechanical Properties of Carbon Nanotubes (CNTs)

Carbon nanotubes (CNTs) have excellent mechanical properties because their atomic structure is isotropic in 3D space as shown in Figure 2.1. These properties were obtained from the results of stress-strain testing [18-20]. CNTs have excellent strength and stiffness characteristics, which are equal in all their directions. The comparative mechanical properties of CNTs are shown Table 2.1.

Table 2.1 The properties of SWCNT, MWCNT and traditional steel [18-20] in the longitudinal direction at room temperature.

Physical property	SWCNT	MWCNT	Steel
Density ($g \cdot cm^{-3}$)	~1	1.4-2.1	7.8
Melting point (°C)	3550	3550	1538
Thermal conductivity ($W.\ m.\ K^{-1}$)	~3500	~3000	80
Electrical resistivity ($n\Omega \cdot m$)	10	10	100
Tensile strength (GPa)	13-53	11-150	0.4-1.5
Elongation to break (%)	16	~10	15-50
Young's modulus (GPa)	1000	1000	200

These properties can depend on the shape, the diameter of CNTs and the measurement method [7]. The Young's modulus of the CNTs can be up to 1.4 TPa and with tensile strengths of up to 63 GPa [18]. It is also known that the mechanical properites of multi-wall carbon nanotubes can be slightly less than those for single-wall carbon nanotubes due to the presence of defects within their structure. These defects form during the synthesis process when some layers are easily broken [19]. In addition, atomic force microscopy (AFM) has been used to measure, by a way of a measured deflection, the

modulus of elasticity of individual CNTs in tension. The results indicate that tensile strength of the CNTs is over 150 GPa. That means that, they are ≈ ×100 stronger than steel [20].

2.4 Using CNTs as a Reinforcement Filler in Smart Composite Materials

Composites, which are made from the fibre with epoxy, are suitable for many important applications due to their good specific stiffness ($\frac{E}{\rho}$) and specific strength ($\frac{E}{\sigma_{ts}}$). However, there are some problems which still need to be considered. These include their in-plane (fibre) and out of plane (matrix) mechanical properties. The out-of plane properties (matrix) are relatively weak and still represent a major obstacle [21]. These aspects will be considered further in section 2.5. It has been noted that the brittle nature of the epoxy and its poor bonding characteristics with the fibre surface are the main factors responsible for the weakness of the (out-of-plane) properties.

As discussed in chapter one, it was revealed that the addition of even a small amount of CNTs in the matrix can help to enhance the interface properties between CNT-matrix resulting in improving the overall toughness of the composites. Therefore, the weak properties of the traditional composite can be enhanced by the introduction of a nanoscale reinforcement material to the composite components. In particular, the weak properties of the composite can be improved by adding a nanoscale filler. This could be carried out by introducing a uniform dispersion of CNT within the matrix or by impregnating the fibre by deposition of the CNTs directly on the surface or by combining both approaches as shown in Figure 2.2.

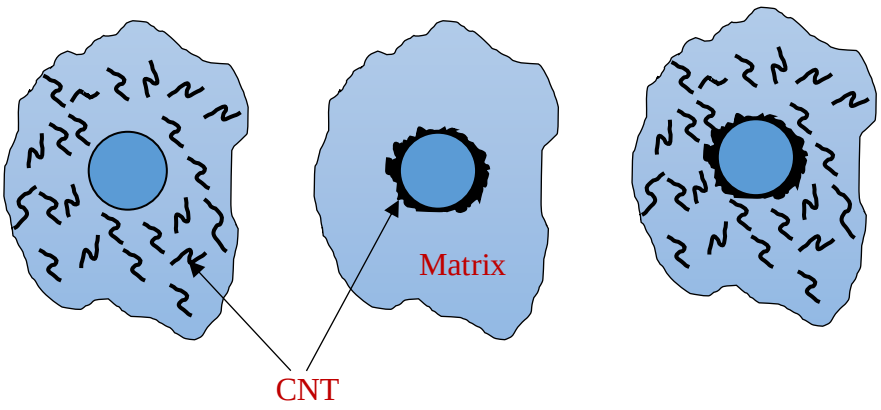

Figure 2.2: Schematics of the different material structures based CNTs

Due to the nanoscale size of CNTs, they can penetrate and distribute deeply in the narrow zone between the tows of fibre and the matrix. Thus, CNTs hold the potential to be able to tailor the structural properties and change the micro-scale damage mechanisms of the composite. The challenges related to embedding CNTs within the composite structure to create a multifunctional composite still need to be fully understood. Section 2.5 will explore these issues.

In this section, some of the results and critical issues associated with the development of smart composite and utilising CNTs to *in situ* damage detecting in composite materials.

2.5 Dispersion of CNTs and Consequent Matrix Properties

2.5.1 Incorporation of CNTs in the Matrix

The embedding of CNTs into the matrix, to produce a smart composite, can be achieved using the common of manufacturing processes for composites, such as resin transfer moulding (RTM), prepreging and pultrusion. Adding CNTs into an epoxy matrix, with homogeneous distribution, can improve the structural performance due to both an increase in strength and modulus. For example, Bal [22] prepared (MWCNTs) with epoxy resin composites by using ethanol as the dispersing agent for

low content (0.2% wt.) of multi-wall carbon nanotubes in the epoxy resin. Optical microscopy was used to analyse the MWCNTs dispersion epoxy matrix. By varying the amount of MWCNTs, the nanocomposite can have variable electrical and mechanical properties, when compared to using epoxy resin only. This is likely to be due to the excellent electrical conductivity of MWCNTs. However, there are some challenges associated with dispersing the CNTs in the polymer resin. For example, potential agglomeration; CNTs have a tendency to remain as entangled agglomerates when dispersed in the matrix. This makes its difficult to untangle and disperse them effectively. Agglomeration is due to very strong attractive Van der Waals forces which exist between the individual CNTs. This issue leads to the non-uniform dispersion of them within the polymer. Kim *et al.*[23] used the ultrasonic technique to disperse carbon nanotubes in epoxy resin. In their experimental work, 0.1, 0.5 and 2 vol. % of the MWCNTs were the first dispersed in a methanol-based epoxy solution for 2 hours using sonication. The sonication processing was then continued for a further six hours at 35°C in order to fully remove the methanol. All the samples were dried at 50°C for 7 days using a vacuum oven. The SEM images obtained clearly showed the increased CNTs entanglement in the matrix, with this significantly increasing with an increase in the CNTs content.

In addition, a high concentration of CNTs also leads to an increase in the viscosity of the polymer so creating difficulty in wetting out the fibre during infusion processing. Therefore, the adding CNTs to the polymer directly is limited to low concentration addition of CNTs. Despite these dispersion issues, some promising increases in the mechanical properties of the matrix have been observed. Gkikas *et al*. [24] showed the effect of the dispersion state of MWCNTs on the mechanical properties of the epoxy resin. A 3-point bending with single edge notch (SENB) was used to estimate the

toughness magnitude of the nanocomposite. The results show that after adding 0.5wt. % MWCNTs reinforcement, and then using ultrasonic technique with maximum amplitude (100%) for 60 minutes, the toughness was increased by 95% when compared with pure epoxy. Besides the mechanical properties, if the CNTs are uniformly dispersed in the matrix, with good penetration between the fibre bundles, then the electrical properties of the nanocomposite also improves due to a well-defined network of CNTs formed inside the nanocomposite structure. This observation is important to making the nanocomposite electrically conductive so enabling the ability to sense changes to the extremal applied conditions such as pressure, temperature and strain using an electrical technique [25].

Previous work and also [26, 27] have indicated that the addition of CNTs to the matrix materials (resins) can improve their mechanical properties. However, the results obtained were not fully explored regarding the difference between my mixing methods and CNTs type on the mechanical properties of the resin. Therefore, in the context of the present study some preliminary experimental work was conducted to evaluate these aspects. The results of this preliminary work are presented here in order to support the experimental methods which are detailed in later sections of this thesis. During this preliminary work, an investigation was conducted to determine the influence of mixing method and CNTs type on the mechanical properties. Particularly modulus, tensile strength and fracture toughness. The result obtained are shown in Figure 2.3. All of the specimens used for this were manufactured an tested by the author of this thesis.

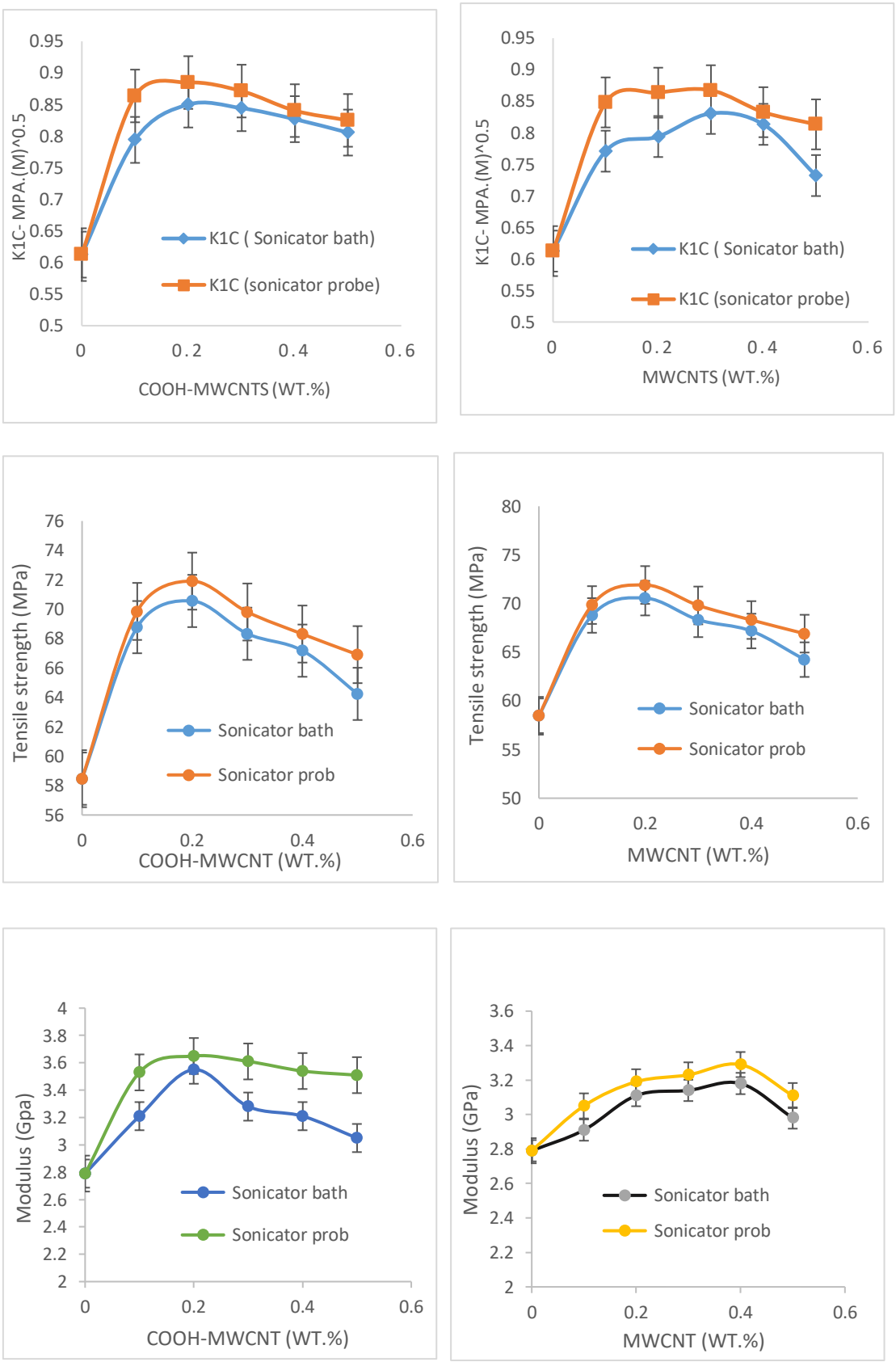

Figure 2.3: Mechanical properties of nanocomposites prepared from two types of MWCNTs and by two sonicate method.

From Figure 2.3 it can be concluded that there is a difference between the bath and probe sonication methods. The probe sonicate showed high mechanical properties compared to the bath sonicate method and this could be due to the probe sonicate provide a high-energy wave which helps to improve the mixing than those in the bath sonicate. It should also be noted that in every case the inclusion of MWCNTs can also result in slightly enhanced properties at all concentrations.

2.5.2 Deposition of CNTs on Fibre Surface

As mentioned in the previous section, using a limited concentration of CNTs in the matrix can be beneficial. Another method of introducing CNTs as reinforcement into the composite exists, this is deposition. Depositing CNTs on the fibre surface, as shown in Figure 2.4 can help to increase the possibility of using high CNTs concentration but this needs a new technique to achieve it [28]. Such techniques include; grafting CNTs, impregnating CNTs into fibre sizing and electrophoretic deposition and chemical vapour deposition (CVD). As discussed previously, these techniques have their own drawbacks and potential benefits. Gao *et al*. [29] developed a fibre sizing method for depositing CNTs uniformly onto glass fibre surfaces and then studied the composites electrical properties and compared them to composites with CNTs dispersed within the polymer. They revealed that the depositing of CNTs on the fibre surface can be easily controlled. The measured results for the composite, such as electrical conductivity, were shown to have improved in the 3D transverse, axial, and through-thickness directions.

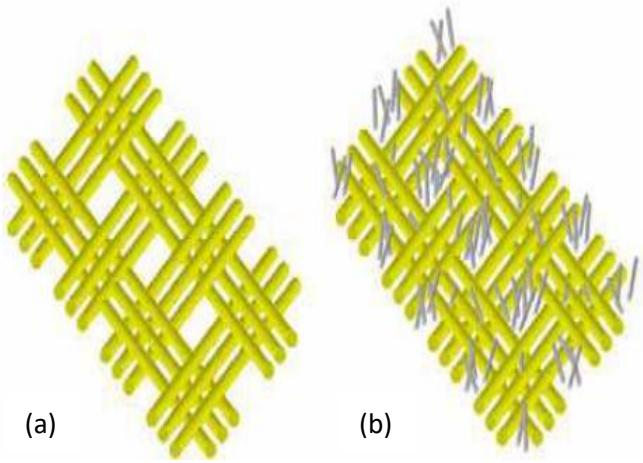

Figure 2.4: Illustration the reinforcement of CNTs through-thickness: (a) fabric with resin only (b) fabric impregnated by MWCNT-resin [28].

An *et al.*[30] used the CVD method to prepare vertically aligned CNT arrays onto a carbon fibre fabric. Their results show that the tensile strength for single fibre was slightly degraded (≈10%) for all different lengths of fibres, whilst the modulus of the fibre was not been significantly decreased. However, the interlaminar shear strength (ILSS) for single fibre pull-out tests increased from 65 MPa to 135 MPa (≈110%) when compared to the as-received carbon fibres. Bekyarova *et al.* [31] used an electrophoresis method, as shown in Figure 2.5, in which a negatively charged carboxyl functionalised CNTs was attracted to a positively charged carbon fibre. The processing was carried out for 2 hours. SEM images revealed that CNTs were uniformly deposited on the fabric surface as shown in Figure 2.6. The results obtained following testing of the composite showed a ≈ 30% improvement in the interlaminar shear strength as compared to the unmodified condition and the out of plane electrical conductivity was also significantly enhanced.

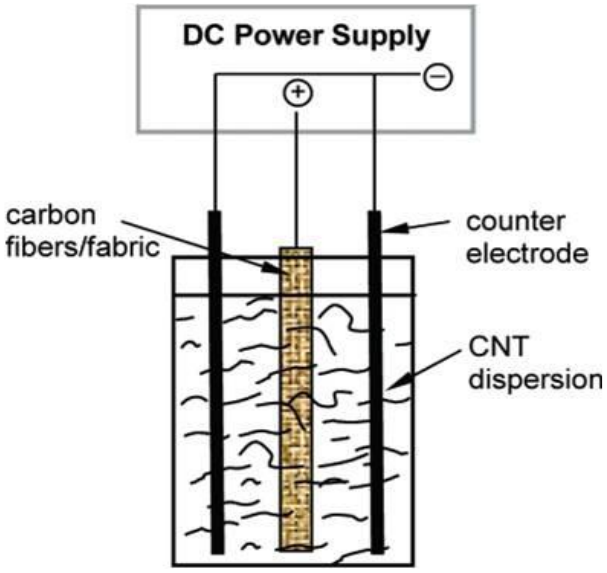

Figure 2.5: Deposited CNTs on to carbon fibre surface by electrophoresis deposition method [31].

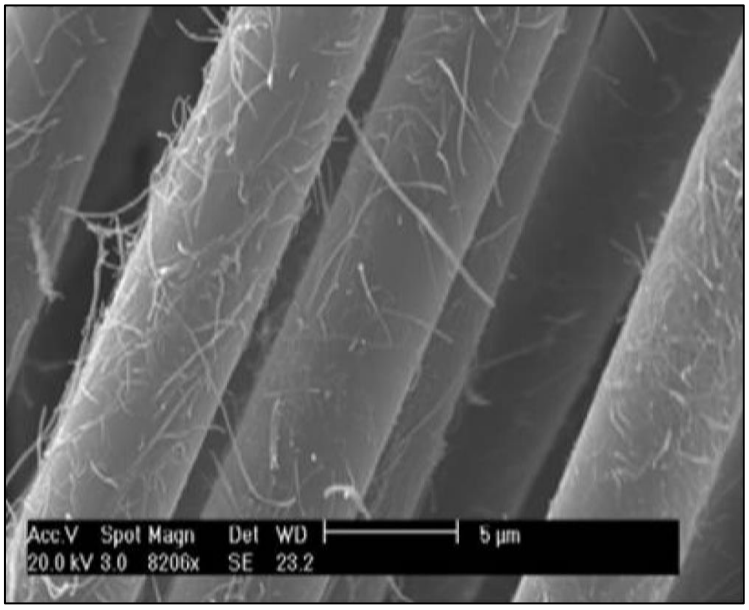

Figure 2.6: MWNTs deposited electrophoretically on the composite fibre [31].

However, the above methods are time consuming and costly, therefore they are not effective for mass production processing. A spraying method is considered a simple

approach for depositing CNTs on the fibre surface. Zhang *et al.*[32] utilised a spray coating method as an effective way to deposit CNTs onto fabric as shown in Figure 2.7. This approach is considered a simple, as well as useful technique, for industrial scale-up compared to more traditional methods for depositing CNTs within or on the composite. Using this technique Zhang *et al* showed, the carbon fibre laminates fracture toughness (K1c) to be increased by ≈ 50% at low CNT concentrations (0.047 wt. %). This modified composite showed good potential for *in-situ* damage sensing during structural health monitoring activities.

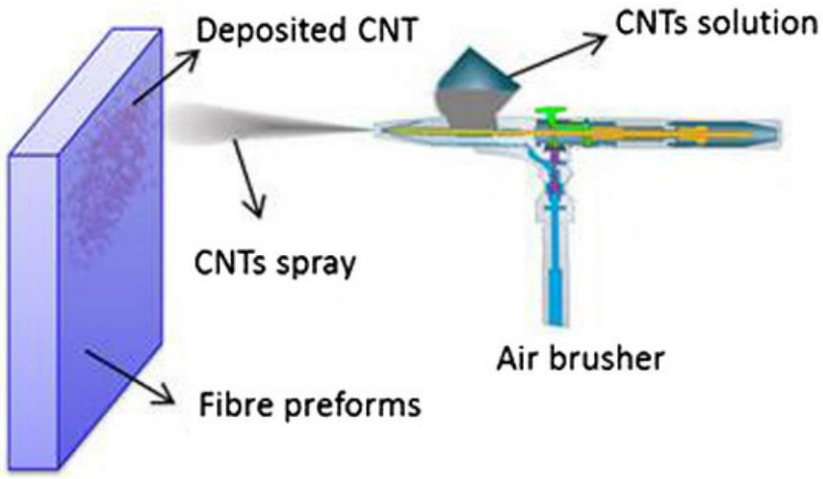

Figure 2.7: MWNTs deposited on the composite fibre spray method [32].

In summary, the impregnation of CNTs onto the fibre surface to make a multiscale fibre composite still faces some significant issues. In spite of these problems, good results have been reported. However, some researchers have concluded that the interfacial adhesion between the CNTs and the fibre surface remains as the most important issue still to be addressed [33].

2.6 Some Challenges when Incorporating CNTs in Smart Composites

As previous described, the excellent mechanical, thermal and electrical properties of carbon nanotubes make them a good candidate material for the fabrication of smart composites, so providing a variety of scientific and industrial opportunities. To date, in terms of industrial application, these efforts have mainly concentrated on incorporating them within the polymer resins, e.g. epoxy, polyurethane (PU) and polyimide (PI) and other type of the thermoplastic polymers including polystyrene (PS), polypropylene (PF) and nylon in order to enhanced the composite properties. The mechanical, thermal and electrical conductivity and other properties have been studied for a wide range of applications. However, improving the performance of the composite remains an important goal. Consequently, there remains some issues and challenges to be met with using suitable CNTs in the composite. These include controlling CNTs alignment, effective dispersion, creating path network for electrical conductivity and the morphological structure of the CNTs within the matrix. In the next section, some of the critical problems closely associated to the nanocomposite properties will be considered.

2.6.1 CNT Aspect Ratio

Despite being able to mass produce, and synthesise, CNTs using CVD, arc discharge and laser ablation techniques, the prepared CNTs do not possess reproducible intrinsic characteristics [34]. For example, the aspect ratio of CNTs which is considered one of the most defining properties, is strongly dependent on the preparation method. Aspect ratio is the important factor that can directly influence the nanocomposite properties [35]. For example, the load transfer characteristic between the CNTs and matrix can be maximised by using a suitable aspect ratio of CNTs. In this way, the mechanical

properties can be improved. Moreover, nanocomposites containing high aspect ratio CNTs possess a higher tensile strength and modulus when compared to those with a short aspect ratio and similar filler content [36]. Li *et al.*[37] also concluded that it was easier to form electrical networks along the tangled carbon nanotubes in the matrix with a high aspect ratio of CNTs.

2.6.2 CNT Dispersion

The potential for good dispersion of CNTs within the matrix, as a reinforcement to fabricate smart composite, is limited since the CNTs always tend to tangle during the mixing process. Therefore, CNTs dispersion within the polymer is an important issue when creating an effective nanocomposite. Good dispersion not only improves the interfacial bonding zone between the CNTs and the polymer, it also prevents stress concentration around the CNTs agglomerate points [38]. However, the issues which need to be overcome include CNTs length, the viscosity of polymer and the potential entanglement of CNTs. These need to be addressed in order to obtain a nanocomposite with uniform CNTs dispersion. However, it should also be noted that above a certain concentration of CNTs, the mechanical properties of the nanocomposite are degraded. This problem is due to the inhomogeneous nature of the CNTs dispersion at high concentrations and the possible bad chemical reaction between the CNTs and the polymer at these high CNTs concentrations [39]. Functionalising the CNT surfaces can help to solve the bad reaction issue.

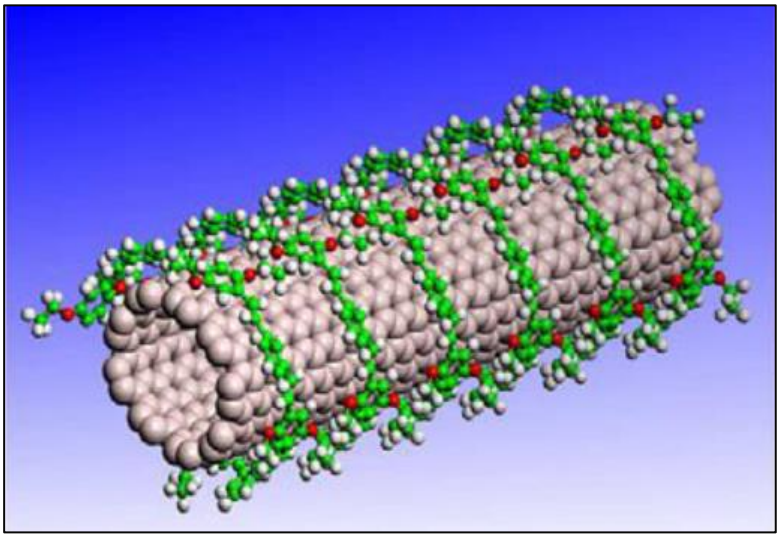

Figure 2.8: Schematics of CNT functionalisation [41].

In order to obtain a better and homogenous dispersion of CNTs inside the polymer, a number of different methods have been employed [40]. These methods include, using ultrasonic waves, ball milling, high shear mixing, etc. In addition, there are two additional modification approaches that can be used to achieve better CNTs dispersion. The first method is to modify the CNTs surface i.e. functionalisation as shown in Figure 2.8 [41]; The functional groups that can be used include hydroxyl, amino and carbonyl molecules. These methods can improve the chemical interface reaction between the CNTs and the matrix by generating strong cross-links between them [42]. However, the functionalising properties can be affected when using some surfactant chemicals [40]. These surfactants destroy the surface bonds on the CNTs such that the nanocomposite properties are reduced. The second method is to coat the CNTs with some non-covalent material such as nickel. This method could increase the chemical activity, and cross-links, between the CNTs surface and the polymer. Despite the functionalisation method being able to enhance the mechanical properties it can, at the same time, reduce the electrical conductivity due to the functionalisation layer acting to isolate and prevent the ease of electron transfer between the individual CNTs

[43]. Table 2.2 summarises using different dispersion techniques and their influence on the mechanical properties of the resulting nanocomposite [40].

Table 2.2 Effect of using different methods to dispersion of CNTs on the flexural properties of nanocomposites [40].

CNT dispersion technique	Flexural modulus (GPa)	Flexural strength (MPa)
Neat epoxy	3.43 ± 0.01 (+0.00%)	140.0 ± 2.3 (+0.00%)
Probe sonication	3.47 ± 0.06 (+1.17%)	142.7 ± 1.7 (+1.93%)
Sonication in water bath	3.41 ± 0.04 (-0.58%)	144.1 ± 1.8 (+2.93%)
Calendaring	3.65 ± 0.02 (+6.41%)	145.2 ± 0.82 (+3.71%)
Shear mixing	3.36 ± 0.09 (-2.08%)	140.4 ± 2.4 (+0.29%)

2.6.3 CNT Orientation

In addition to the CNTs within the matrix dispersion issue, the orientation of the CNTs in the matrix is another key problem to be considered when developing an effective nanocomposite. Such a geometric consideration, i.e. the difference between the random and aligned orientated of CNTs, can significantly affect the various properties of the nanocomposite [44]. Sulong *et al.*[45] investigated the effect of CNTs orientation on the mechanical properties of the nanocomposite. They reported that the mechanical properties such as tensile strength increases with an increase in the degree of CNTs alignment with the loading direction. In an electrical context, strain sensitivity is very dependent on the CNTs orientation and alignment. Previous results revealed that with high CNTs alignment, higher strain sensitivity was obtained [46]. However, it is very difficult to obtain fully aligned CNTs inside the matrix of the nanocomposite. There are some techniques available to achieving this, such as using a magnetic field [47], electrospinning [48], shear flow [49], injection or extrusion [50] etc. All of these are used to align CNTs within the matrix with the loading direction.

The degree of orientation of CNTs in the nanocomposite can also be controlled by additional factors such as CNT content and CNT diameter. At higher concentrations of CNTs, this leads to decreases in their alignment due to agglomeration. In summary, Figure 2.9 and Figure 2.10 show the effect of CNTs orientation on the properties of the nanocomposite such as Young`s and storage modulu`s. The storage modulus is an indication of the ability of nanocomposite to store deformation energy in an elastic manner. This is directly related to the extent of cross-linking. The higher the degree of cross-linking, then the greater the storage modulus [44].

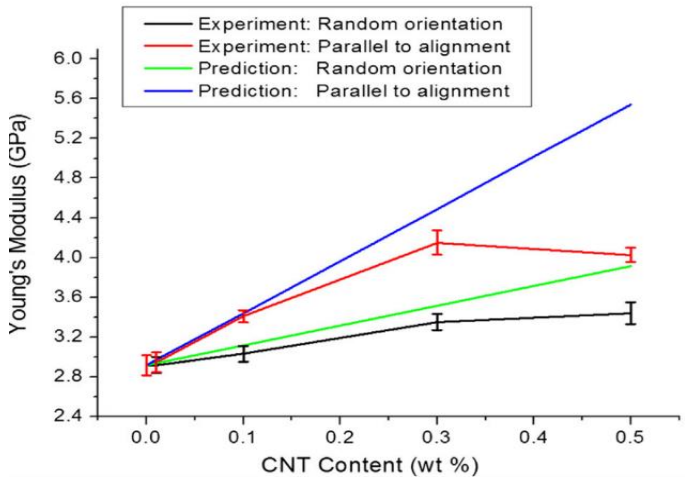

Figure 2.9: Young's Modulus of nanocomposite as a function of CNTs content and orientation [44].

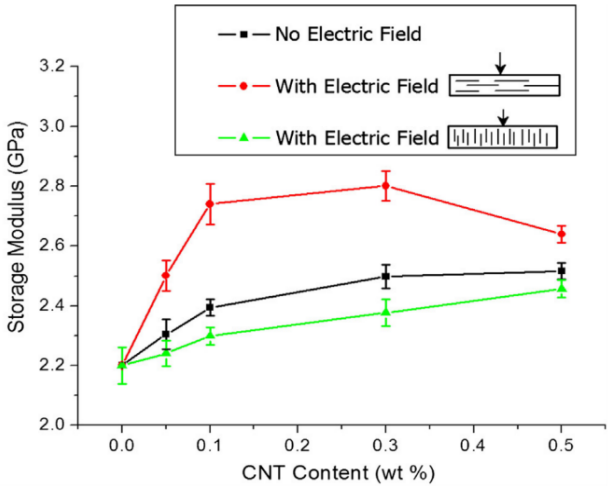

Figure 2.10: Storage modulus of nanocomposites as a function of CNTs content and orientation [44].

2.6.4 Interfacial Zone Issues between CNTs and Matrix

Achieving a strong interfacial bond between CNTs and matrix due to an enhanced effective load transfer mechanism is another challenge to be considered. The load transfer from the CNTs to the matrix depends on three mechanisms. The first is the bond strength of the weak van der Waals force between the carbon nanotubes and the polymer .The second is the chemical bond strength between CNTs and polymer. The third is the micromechanical interference between the CNTs and the matrix as shown in Figure 2.11 [51]. This interference may be insignificant in the CNT/polymer nanocomposites when the nanotubes have a smooth surface. For each of these three mechanisms, it is possible to improve the load transfer between CNT and matrix by using different conditioning solutions [9]. For example, using small CNT, it is possible to put their surfaces into very close contact at the interface. This will improve the van der Waals bonding. In addition, treating the CNTs surface chemically and physically i.e. functionalisation significantly enhance the interfacial contact region between CNTs and the matrix [52]. In terms of interference between the CNTs and the polymers, the presence of CNTs can be enough to block, and prevent, the movement of polymer chains as well as helping to propagate micro–cracks [53].

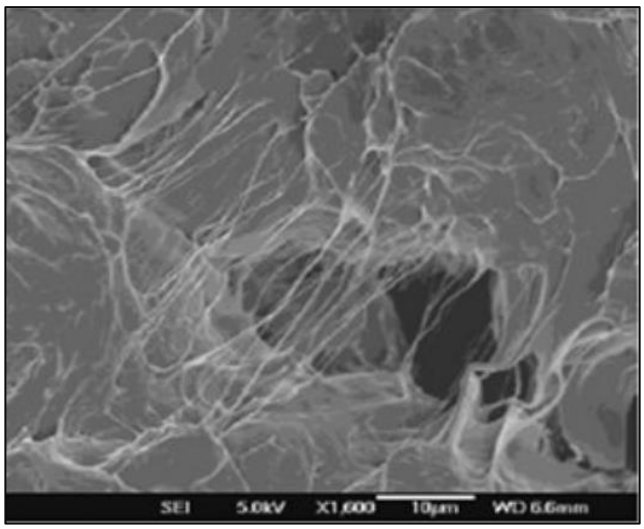

Figure 2.11: SEM of micro-cracks linked between CNTs and matrix [51].

2.6.5 Electrical Properties of CNTs

CNTs have another important property, that is their good electrical conductivity, which allows easy electron transfer between individual CNTs without dragging from impurities and other energy dissipating features [7]. The electrical conductivities of most nanocomposites based on CNTs are in the range 5–10 Sm^{-1} [54]. For epoxy resin containing CNTs, electrical conductivity is possible even at very low CNTs content [55]. This is due to the development and appearance of suitable conductive pathways at specific CNTs concentration threshold levels [56]. Below this threshold, a network of conductive pathways does not exist. While above it, effective conductive pathways are formed which facilitate the easy electron transfer through them. However, there are some factors which can affect the electrical conductivity of a smart composite. For example, modification of CNTs usually reduces the electrical conductivity of the nanocomposite, even if there is a good dispersion within the matrix. In general, the electrical conductivity of a smart composite is considered to be the key factor for sensing any damage (fracture events) occurring in the composite. Therefore, in the following section a brief description of the type of damage, which can occur in a smart composite, is considered.

2.6.6 Crack Types in Polymers and Composites

Most types of composites are subjected to environmental and mechanical loading during their manufacture, when in storage or during their service life. This can create and form micro-cracks or other forms of damage in the composite. Moreover, environmental conditions such as changes in temperature, pressure and chemistry can also help to cause and form cracks. This type of damage in the composite can cause serious issues such as delamination and debonding and as a consequence, catastrophic failure can occur. Figure 2.12 [57] shows the different types of cracks, which are

predicted to occur in a composite. Cracks in the composite are considered more complicated than those are in the traditional materials. This is due to failure mechanisms in the composite such as of matrix fracture, debonding at the fibre matrix interfaces and fracture of the fibres themselves.

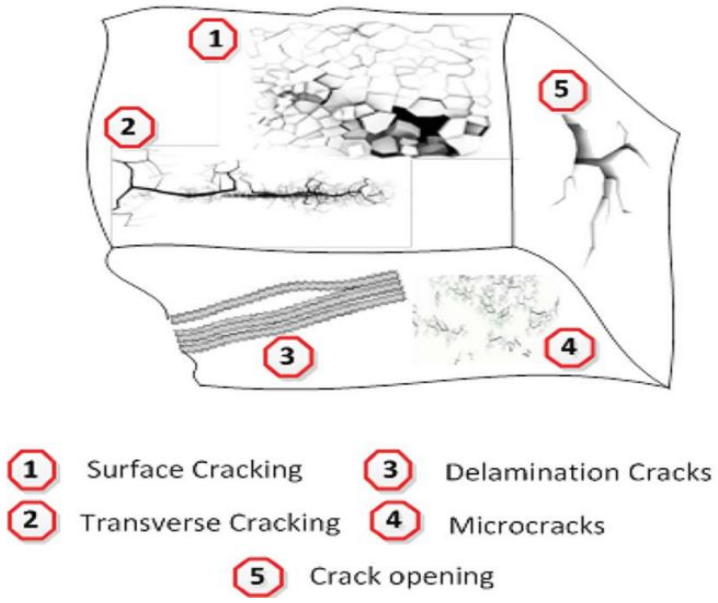

Figure 2.12: Types of cracks in the composite [57].

Some studies [57] have suggested failure models for a nanocomposite system in which an indicated micro-crack can penetrate the polymer matrix and reach the reinforcing fibres. If the fibre in the composite adheres well to the polymer matrix, the matrix micro-cracks are stopped by the adjacent fibre. However, if the load is increased, then the micro-cracks can pass around the fibre and continue to grow. The availability of CNTs helps to maintain a good interfacial bond. However, possible fibre interfacial shearing forces can cause debonding so facilitating further micro-crack growth. As a consequence, fibre fracture and breakage will occur at the weakest point inside the nanocomposite material. The total failure of the nanocomposite takes places when all the fibres are broken. The formation of internal micro-cracks in a normal composite is

often difficult to detect. Therefore, expensive non-destructive methods are usually necessary to detect the cracks in the composite.

2.7 Current Damage Detection Systems for Composite Materials

Recently, a number of non-destructive methods have been developed and are now widely used to detect micro-cracks in composites [58]. More detail of these will be considered in the following sections.

2.7.1 Visual Inspection

This technique is considered to be simple and practical since it only uses the naked eye for inspecting. This method has been used widely in many fields such as energy, aircraft and so on to detect obvious structural damage. In this method, the surface should be illuminated and clean enough to get better results. However, the method is limited to the inspection of the surface only [3]. Relying on human judgment can also be prone to error, when damage is missed during inspection.

2.7.2 Strain Gauge Method

A strain gauge can be defined as a piezoresistive metallic gauge. A strain gauge can only be fixed on the structure surface, otherwise, it will form a defect if embedded inside the composite. The gauge measures the change in the resistance across the gauge length when the surface displacement, which can lead to damage, occurs. This testing method is also simple and relatively inexpensive with easy data acquisition. This is the main benefit of using the strain monitoring method. However, because of size limitations, this technique required many strain gauges since each gage can only cover a small area of the composite structure. In addition, the maximum gauge factor developed will not exceed 2.1 and gauges are known to have poor sensitivity to micro-cracks [59].

2.7.3 Acoustic Emission

This technique is a non-destructive method in which the sensor (piezoelectric type) is embedded or bonded in the structure. Its working principle depends on the release of energy waves when the structure is dynamically loaded. The piezoelectric sensor will pick up the surface vibrations and filter them to give an acoustic emission signal. With this technique, matrix cracks, delamination and fibre fracture, can be readily detected. However, the signal may be affected (attenuated) by the presence of electromagnetic interference signals (EMI) caused by neighboring devices. Consequently, a degradation in the performance results. As a consequence the result will be not very accurate [3].

2.7.4 Optical Fibre Technique

This type of sensor can also be embedded in structure or attached to its surface. Fibre optic sensor are able to provide strain measurement data along the structure, including micro-crack formation. Therefore, this type of sensor is very useful for structural health monitoring. Figure 2.13 below shows the results obtained when optical fibre sensors are embedded in a 200×200 mm composite laminate plate. The sensors covered all the composite area in order to predict the strain changes occurring across the plate when it was subjected to a load. The visual results obtained show that the optical fibre technique is a very effective method for measuring the strain, since the optical fibre inside the composite laminate can detect, and show, barely visible impact damage. The strain map produced in this way is representative of the state of the structure. This is clearly seen by the red peaks in Figure 2.13 [60].

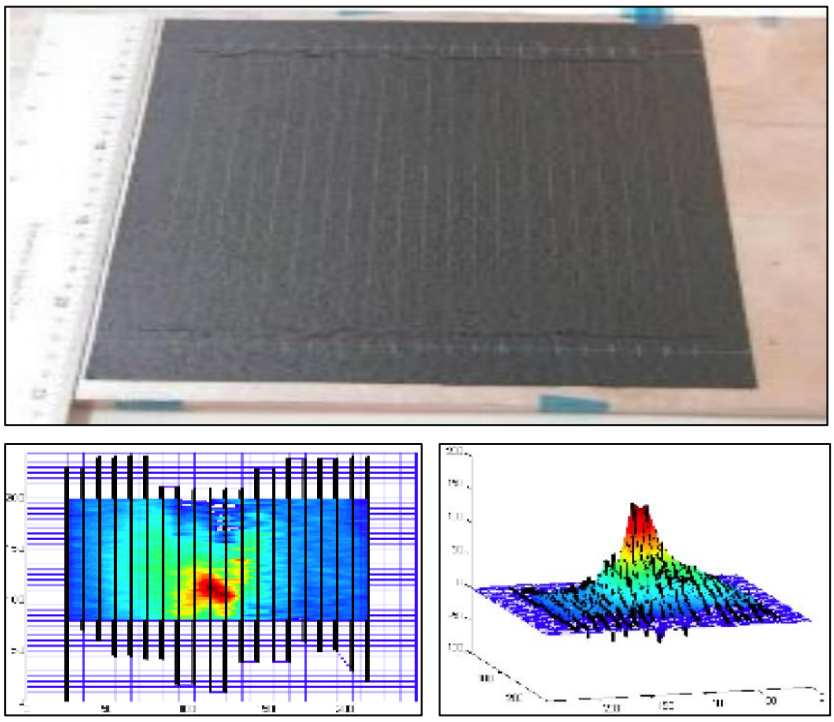

Figure 2.13: Strain data due to cracks initiation in composite plate [60].

Although it is a useful sensor, still some limitations exist when using an optional fibre sensor to observe strain changes in structure. These are due to the brittle nature of fibres. In addition, a large number of optical fibres would be needed to detect the damage in a large structure. Consequently, this make the technique quite costly. The next section outlines a new technique which has the potential to overcome the aforementioned concerns and issues.

2.8 Impact Damage Assessment in Composites containing MWCNTs

Polymer matrix composite materials have been widely used in various important industrial sectors such as aerospace, oil and gas energy and military applications due to their lightweight, high strength to weight ratio and anticorrosion properties [61]. However, their behaviour under sudden loading, such as experienced during impact, is considered one of the major issues to be overcome [62]. Since the point of impact

failure could be previously initiated during the composite manufacture, during maintenance or during assembly operations or during its service life, then it is important that such damage can be identified. If this is not done then catastrophic failure is possible. Previous studies [63-65] have reported that the main consequence of impact is usually matrix cracking, fibre fracture or delamination. These failure mechanisms will reduce the structural integrity and strength, so putting the structure at risk. Therefore, one of the critical challenges to keeping structurally important components functioning correctly is their ability to sense damage whilst in-service. This issue is important for predicting the remaining service life of composite components as well as to avoid a sudden catastrophic failure.

Currently, there are many techniques for damage evaluation which can be employed to assess the degree of damage in a composite. For example, X-ray [66], eddy current [67], thermography [68] and ultrasonic [69] techniques. These methods are not in-service inspection techniques and are often slow to evaluate the damage and to target when the component should be taken out of the surface for inspection as well as replacement. The practical real-time detection, damage location and its quantification in a large composite structure before a sudden failure event is very time consuming. Therefore, other techniques and sensors have been developed to sense the damage in a composite structure during loading. For this, fibre optic [70] sensors and piezoelectric sensors have been used [5]. However, these methods and others [71] affect the performance of the structure and need a large number of attached sensors to the surface of the structure, as well as having them embedded them within the composite itself. These attachments can create additional pre-cracks, or other defects, which initiate failure.

Therefore, there is an urgent requirement to develop a new method (non-destructive) to detect and sense the damage in composite materials at the moment of impact or failure. The use nanotechnology could provide a possible solution for sensing issues in current non-destructive methods through manufacturing smart composites or so called ''self-sensing'' composites [72]. To achieve this, carbon nanotubes (CNTs) could be used as a multifunctional additive to the glass fibre composite in order to make it a self-sensing composite. Since CNTs have superior mechanical, electrical and thermal properties [73, 74], then incorporating them as a nano-filler conducting material, even at low content into a resin matrix, will help to form electrically conductive networks around the fibres within the composite structure. When the glass fibre nanocomposite is subjected to an external load, the CNTs conductive networks will deform and if the load is further increased, cracks in the matrix will initiate. These cracks will destroy the CNT conductive networks configuration and as a result, the electrical resistance of the nanocomposite will change as a piezoresistive effect.

Recently, the piezoresistive properties of glass fibre nanocomposite were utilised to assess both microstructural and deformation damage using changes in the electrical resistance concept [75]. Many studies can be found about the self-sensing composite behaviour after impact loading. For example, Naghashpour *et al.* [76] added Multi-Walled Carbon Nanotubes (MWCNTs) to the matrix a glass fibre laminate composite. They demonstrated that electrical resistance measurements through the glass fibre/epoxy/ MWCNTs composite thickness are affected when the composite is subjected to load. Gao *et al.* [75] dispersed CNTs in epoxy resin to make them a nanocomposite matrix in a glass fibre laminate composite. The samples were subjected to impact loads and they reported that the electrical resistance of the composite increased with increases in the impact energy. Monti M *et al.* [77] employed

MWCNTs as a filler in the epoxy matrix of a composite containing glass fibre in order to make the matrix electrically conductive. A low-velocity impact was then applied to the surface of the composite samples. The results showed that the nanocomposite is able to provide an electric signal when subjected to impact due to changes in the CNTs networks sustained during damage impact. Arronche *et al.* [78] used 0.5 wt.% of CNTs to make the epoxy resin electrically conductive. The modified resin was added to the woven glass fibre fabric to obtain a self-sensing composite. The electric resistance was measured before and after an impact test. The results showed that at very low impact energies, the electric measurement device is not able to detect the damage caused by the impact.

2.9 The Electro-mechanical and Temperature Dependent Behaviour of Composites contaning MWCNTs

CNTs possess excellent mechanical, electrical, electronic, optical, chemical and thermal properties which, when combined with their very high aspect ratio and large surface area, have made them an excellent candidate for smart composite materials [79-82]. In this context CNT reinforced composite materials have been investigated for smart composite applications such as for gas detection [83], structural integrity self–sensing [6] and actuators [84]. Unlike conventional materials, CNT reinforced composites have many advantages such as being relatively light in weight, having good corrosion and water resistance, and with the potential for self-sensing applications. For example, Ku-Herrera *et al.* [11] studied the strain sensitivity of nanocomposites containing a small concentration of CNTs. They found that the mechanical properties of the nanocomposite were improved during compression testing reaching a maximum value, in terms of gauge factor, at 0.3 wt.% MWCNTs

content. Ayatollahi *et al.* [35] investigated the effect of adding MWCNTs on the mechanical and electrical properties of a MWCNTs/epoxy nanocomposite. They found that both of the mechanical and electrical properties were improved, especially for a 1.0 wt.% addition of MWCNTs. The strain sensing capability of CNT nanocomposites is considered to be a key requirement for future structural health monitoring techniques and applications. Thus, these nanocomposite materials, being lightweight and having good strength, stiffness and anti-corrosion properties, show a lot of potential for this type of application, *viz*. structural health monitoring, in the oil and gas industries. Here safety is paramount and potential failure must be monitored continuously. Consequently, this incurs high installation, calibration and maintenance costs. To overcome these problems and requirements, some studies have tried to develop novel self-sensing nanocomposites for these types of applications [11, 85-88]. Bouhamed *et al.* [81] fabricated a MWCNT/epoxy nanocomposite and focused on the behaviour of the nanocomposite under strain applications. The results showed that a higher change in resistance occurred at low CNTs concentrations. In addition, Dinh *et al.* [89] investigated the behaviour of adding MWCNTs to epoxy when fabricating a self-sensing nanocomposite structure. They found that for an applied and changing cyclic pressure, the electrical resistance of the structure increased with increasing the pressure and decreased with decreasing pressure. At room temperature, the nanocomposite structure remained stable and showed excellent reproducible results.

Shen *et al.* [82] studied changes in electrical resistance of self-sensing CNTs in an epoxy nanocomposite during compression testing. They observed that when the compression load increased the electrical resistance of the nanocomposite decreased, so indicating that it exhibited a measurable piezoresistive effect. However, these researches did not consider the possible temperature dependent behaviour of the

nanocomposite during the cyclic compression testing. This omission leaves a gap in our understanding of the phenomena since we know that when the temperature increases, so the stiffness of the combined matrix and CNTs is likely to decrease. Under these conditions the electrical resistance of the CNTs themselves will also decrease [90]. The extent of these changes remain largely unknown.

2.10 Damage Sensing in Composites containing MWCNTs during Anticlastic Bending

Due to their laminate geometry, the mechanical properties of fibre reinforced composites are relatively low in the out of plane direction, particularly their interlaminar shear strength. In addition, due to the use of discrete layers of unidirectional or woven fibres that are impregnated with epoxy, micro-scale cracks can form during loading and this can facilitate delamination, interfacial debonding, fibre breakage and matrix fracture [91]. Therefore, the mechanical properties in the interfacial zone are crucial to the transfer of the load easily from the matrix to the reinforcing fibres. Recently, it has become important to be able to fabricate new strong multifunctional composite, such as smart composites or self-sensing composites, which can form part of a structural health monitoring (SHM) system. Strain gauges and optical fibre have been previously used for this purpose to detect damage when the composite is loaded or stressed. However, embedding these types of sensors into composite laminates could can themselves lead to the creation of a pre-crack or region of stress concentration, inside the matrix so creating an additional interface will make the composite weak in use [92]. Many researchers [3, 93-96] have tried to fabricate these multifunctional composites by embedding nanofillers within the matrix. Carbon

nanotubes (CNTs), which were discovered by Iijima [97], are the one of these fillers. They have good mechanical, electrical, thermal and flame-retardant properties [21, 52, 81, 98]. The use of CNTs even at low concentrations have been seen to improve the mechanical properties and strain sensitivity of a composite material [11]. Kathi *et al.* [99] studied the addition of 0.2% CNT to epoxy resin and the results showed that there is an approximate 18% improvement in flexural strength over the untreated epoxy. Kim *et al.* [100] reported that the addition of 2.0 wt.% of CNT to a CF/epoxy composite resulted in 42% and 6% increments in flexural strength and flexural modulus, respectively. Additionally, Fan *et al.* [101] also investigated adding 2.0 wt.% of MWCNTs to reinforce a glass fibre/epoxy composite and found a 33% increases in the interlaminar shear strength of the resulting composite. Moreover, CNTs not only improve the structure properties but can also be considered as a nano sensor which can be used to detect damage initiation. The main advantage of such a self-sensing technique is that all the original mechanical properties of the structure are protected *viz.* there are no stress concentration effects, whilst micro internal damage can quickly be sensed and monitored before full development into failure [102, 103]. Other studies have also embedded CNTs into the matrix to fabricate self-sensing composites, which were tested these under different loading conditions, such as tensile [104], bending [105], fatigue [106] and impact [78]. It is well established that carbon fibre/epoxy composite laminates can be damaged easily during normal use due to stress and other environmental factors. The generation of damage and its accumulation, in composite materials will also lead to an acceleration of the ageing process in the material [107]. Consequently, a serious reduction in the lifetime, and the resistance to harsh environmental conditions, could lead to catastrophic failure.

2.11 The Drift Properties of MWCNTs in Composites during Manufacture

Uniform filler dispersion in a self-sensing composite is very important to improve the mechanical properties when the composite structure as well as to get reliable electrical resistance values when the structure is being exposed to external loads [108]. Therefore, such improved mechanical and electrical properties are essential to keep the smart composite functioning even after being subjected to changes in operating conditions where high static and cyclic loading and temperature variations may be encountered. To overcome these potential problems, it may be necessary to improve the strength and toughness of the composite by incorporating additional strengthening materials, but without affecting the weight of the composite. Carbon nanotubes have been widely used in this role as a nanoscale filler to reinforce a number of different composites in order to create a self-sensing, and strong, composite. Such a response can be achieved since CNTs possess excellent mechanical, electrical, optical and thermal properties [86, 109-113]. This unique combination of electrical and mechanical properties, in addition to their morphological features (high aspect ratio and nanoscale), have made them an excellent candidate material for this purpose. To use CNTs in this way, they must somehow be incorporated into the fibre composite. This can be achieved in two ways; (i) by adding the CNTs directly into the resin matrix material and (ii) by impregnating the surface of fibre with the CNTs in order to improve the mechanical properties in that region as well as to make it electrically conductive.

With regards to the matrix modification technique, Chang [114] studied the mechanical properties of GFRP/epoxy composite laminates with embedded Multi-Walled Carbon Nanotubes (MWCNTs) and compared the results obtained with the

unmodified composite. His results showed that a significant improvement of the mechanical properties of the composite was achieved, especially with regards to the flexural and impact strengths, which increased by 22.1 % and 44.3 % respectively, when compared with the unmodified GFRP laminate condition. Liu *et al.* [115] added CNTs to epoxy resin in order to develop a smart nanocomposite material. The results they obtained showed a good improvement in the Young's moduli (E) which increased by 62.6% (from 2.5 GPa to 6.69 GPa). The material also displayed a good response to strain, generating a gauge factor of about 2.68. However, significant agglomeration issues were observed, caused by adding a high concentration CNTs, so increasing the viscosity of the matrix resin and this issue is also observed by other study as well [116].

This processing problem remains the major challenge that has yet to be fully addressed. In addition, using a large quantity of CNTs during the fabrication of a large component or structure will markedly increase the manufacturing cost. Coating the fibre surface with CNTs, as suggested here, could significantly reduce this cost penalty. Several approaches have been employed to directly coat the composite fibre surfaces instead of adding them to the resin matrix. These methods include direct growth [117], electrophoretic deposition (EPD) [118], dip coating [119] and spray gun lay-up [94]. All such methods have successfully deposited the CNTs onto the fibre surface and have improved composite properties. For example, De Greef *et al.* [117] deposited the CNTs directly on the fabric surface using a chemical vapour deposition (CVD) technique in order to strengthen the weak interface region between the fibre and matrix. The obtained results showed improvement of the composite properties. Deng *et al.* [118] used electrophoretic deposition (EPD) to embed the CNTs on the fibre surface. Their study, using scanning electron microscopy (SEM), showed surface

roughening of the reinforcing fibres so leading to a change in the fibres, natural surface morphology. This method enhanced the interlaminar shear strength (ILSS) of the resulting composite by 60.2%, when compared to normal processing. In general, the main purpose of these fibre surface treatments is to eliminate the outer surface layer of the fibre, which is often seen as a weak region, so increasing the reactivity of the reactive groups at the interfacial surface region [55, 120].

However, the mechanical stability of MWCNTs on the surface of fibre has yet to be fully understood. Most researchers have concentrated only on the nature of the deposition of MWCNTs onto the fibre surface without fully exploring the changes to both the mechanical and electrical sensing properties of the resulting glass fibre/MWCNT/epoxy composite.

2.12 Using CNT as a Sensor for Damage Detection in a Smart Composite

As discussed previously in the introduction, composite materials are now used in various important industrial sectors due to their good mechanical properties. However, a composite can be very sensitive to various types of damage such as matrix cracks, fibre fracture, debonding, delamination and so on. Therefore, during a structure`s service life, many of its parts need evaluation, and regular inspection, in order to monitor their health and to prevent sudden failure. To meet these concerns there is a need to develop a new method to detect the damage in the early stages of failure. The damage in the composite materials usually starts as a matrix micro-scale crack or by delamination. Matrix damage can happen even at very low strain levels, and this can lead to catastrophic fracture. As a result, the durability of the structure will reduce. Although, non-destructive methods are available to predict the damage in the initiation

stage, these still need further improvement. This requirement is essential for service life prediction. Employing the electric resistance principle for composites containing fibres has been shown to be one of the most promising ways to detect damage when a structure is subjected to dynamic or static loading [121]. In this method, as applied to carbon fibre composites, the inherent electrical conductivity of the fibre can be affected by the applied load on the structure. Therefore, the influence of fibre is more dominant, in terms of damage, when compared to the matrix. However, this purpose is considered to be insufficient where the damage initiated in the matrix rather than the fibre as shown in Figure 2.14. This gap between fibre and damage site promotes a sensitivity issue.

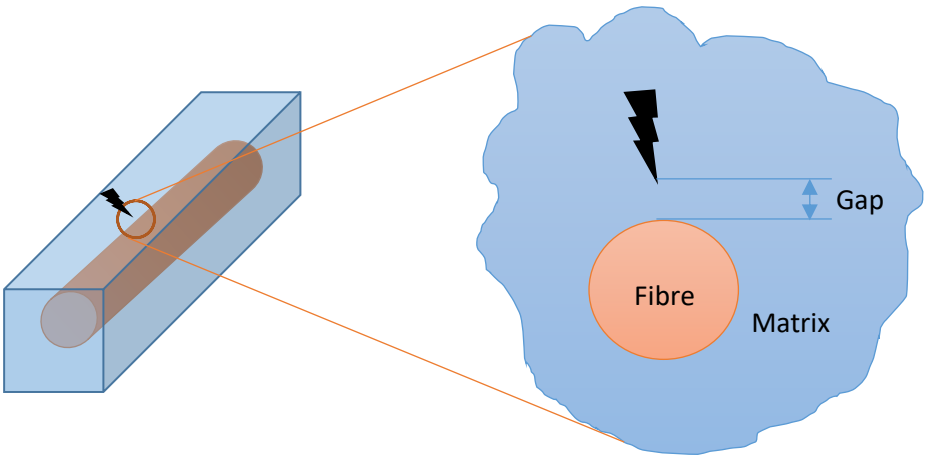

Figure 2.14: Sketch showing a matrix crack in composite.

In this case, since the fibre will not break, there will be no change in the electric resistance of the fibre. The possible solution to this problem is to make the matrix conductive by embedding high electrical conductivity fillers such as CNTs.

Some researchers have studied using CNTs as an embedded sensor material within the composite. For example, Thostenson *et al.*[105] embedded CNTs in epoxy resin as distributed sensors in order to evaluate the damage in the glass fibre/epoxy composite

laminate. Their results showed that when the load increased the resistance also increased. It then increased further when cracks began to initiate inside the matrix. This is shown very clearly in Figure 2.15.

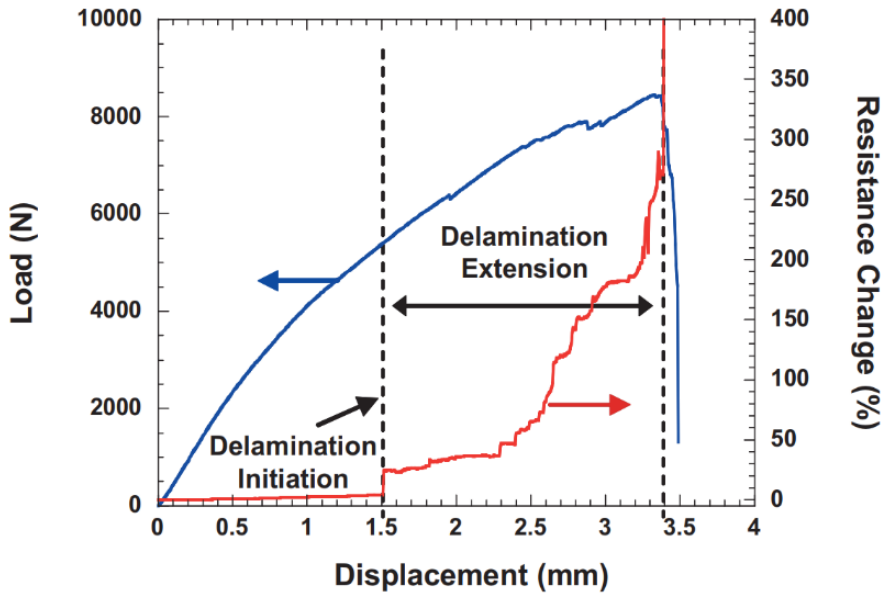

Figure 2.15: Load-displacement vs resistance curves for composite [105].

Nofar *et al.*[122] employed MWCNTs in the matrix as sensors to predict the damage and to monitor the degradation of the composite`s mechanical properties. They subjected glass fibre/epoxy composites to cyclic fatigue and tensile loadings. They reported that when the cyclic and tensile load increase, the observed changes in resistance would increase in size when failure in the composite occured. Moreover, during cyclic loading, the normalised change in resistance showed a high degree of sensitivity to the location of the crack. Kim *et al.*[58] dispersed a low concentration of CNTs in the matrix of a 3D braided composite to study the mechanism of the damage during applied loading. They reported that, during the tensile testing, piezoresistive behaviour was observed. In addition, when the CNTs` conductive networks were disrupted, the change in the electrical resistance altered in a non-linear manner, due to the developing strain increasing the inter-particle spacing.

Figure 2.16 shows the crack propagation in the matrix and leading to the break up of the CNTs network. This distortion in the CNTs network formation causes an increase in the electrical resistance [123].

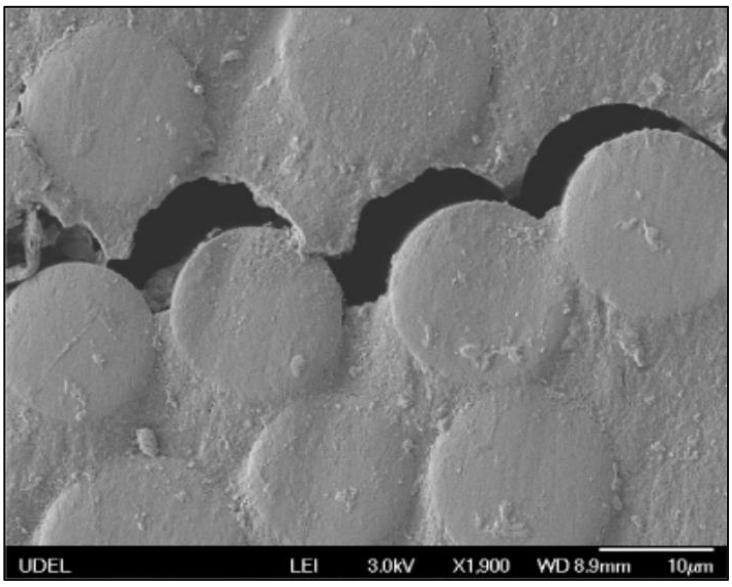

Figure 2.16: SEM image showing the microscale crack in matrix contains CNTs [123].

As mentioned above, especially as seen in Figure 2.14, the cracking can occur in the matrix but it does not reach, and so break, the fibres. In additional, with the exception of carbon fibres, the other types of fibres, such as glass fibres, do not electrically conduct and are therefore unable to sense the damage when the composite is subjected to an external load. Therefore, some studies solved this issue by coating the fibre with the CNTs instead of adding them to the matrix. Gao *et al.*[124] applied MWCNTs to composite containing glass fibres as the reinforcement material. The MWCNTs were deposited onto the surface of the glass fibre by dipping the glass fibre into MWNTs dispersion for 15 mins. They reported that, the glass fibres composites containing MWCNTs exhibited better electrical properties. They also had a lower electrical percolation threshold. Here, the interfaces between the glass fibre and the matrix were considerd to act as an in-situ multifunctional sensor. Alexopoulos *et al.* [25] embeded

CNTs fibres on the surface of the glass fibres and between the composite layers of a fabricated structural composite. The CNTs were firstly stabilised with sodium dodecyl sulfate surfactant (SDS) and then the solution was deposited on the surface of fibres. When the structure was subjected to different types of loading such as tensile and compression, the results showed that after the stress was applied, changes in the electric resistance were observed. They also calculated the accumulated damage in the modified composite and were able to correlate this with the change in the electrical resistance.

2.13 Summary and Concluding Comments

In summary, most studies have concentrated on how to use CNTs within the composite to tailor the electrical and mechanical properties. The introduction of a small amount CNTs in the composites can form an electrically conductive network, which could render the composite capable of sensing damage for structure monitoring purposes. Different types of manufacturing methods were used to prepare the nanocomposites. Table 2.3 summarises, with references the type of damage and detection possibilities for a smart composite which has been fabricated via typical manufacturing methods.

Table 2.3: Summarises studies to explain the effect of using different types of CNTs under different manufacturing methods on the damage sensing results.

Composite type	CNTs type and location	Processing type	Damage type (detection aim)	Typical results
GF/epoxy [106]	0.3wt.% MWCNTs in epoxy	Calendering	Crack propagation during tensile testing	CNTs have successfully identified damage propagation
GF/epoxy [125]	SWCNT coated surface of GF	Spray	Micro-crack initiation under tensile testing	SWCNT-coated glass fibre have provided *in-situ* sensing of the deformation under testing

GF/epoxy [126]	MWCNTs coated GF surface	Electrophoretic deposition	Cracking	Coated GF worked well as an in-situ sensor for propagation the cracks
GF/epoxy [127]	0.5wt.% MWCNTs in epoxy	Sizing agent and three-roll milling	Crack sensing under tensile testing	localisation and dispersion of CNT affected sensing results
GF/epoxy [75]	MWCNTs in epoxy resin	Using sizing agent for dispersion	Impact damage	Showed potential of electrical sensing during impact
GF/epoxy [128]	0.5 wt.% MWCNTs in epoxy	Ultrasonic	Sensing under tensile testing	strain sensitivity was improved compared to neat GFRPs
GF/epoxy [77]	0.1–0.5 wt.% of CNTs in epoxy	Ultrasonic and mechanical stirring	Impact damage	Resistances were increased after impact
GF/epoxy [78]	0.5 wt.% of MWCNTs in epoxy	Direct adding to the resin	Impact damage	Two probe method provided lower measurement sensing data compared to Four probes
GF/epoxy [129]	0.1–1.0 wt.% of CNTs in epoxy	Three-roll mill	Impact damage	Resistances were affected by impact testing
GF/epoxy [130]	MWCNTs in epoxy	Solution method	Damage sensing under cyclic, tensile, Impact and fatigue	sensing signals completely depended on the sizing, dispersion and treatment of CNTs
GF/epoxy [91]	MWCNTs coated GF surface	Spray	Interlaminar shear stress and delamination	Percolating and networks of CNTs are achieved at low CNTs content
GF/epoxy [131]	0.5 wt.% of CNT coated GF	Spray	Fatigue test	Good correlation between AE signals and electrical sensing results under fatigue testing

GF/epoxy [132]	CNT growth on the surface of GF	Embedded fibre	Damage sensing under tensile testing	A potential using coated glass fibre as a strain sensor

With regards to the matrix resin properties, it can be concluded that;

i) The addition of MWCNTs to the matrix resin has a small but measurable affect on modulus, tensile strength and fracture toughness (K1c).

ii) Probe sonication is the most effect method for dispersing the CNTs in the resin matrix and shows better works than bath sonication. This experimental method will be used in the later section.

However, the uniform distribution of CNTs and the processing to embed them in the matrix and on the fibre surface still the main issues to be overcome, especially for industry scale mass productions.

Chapter 3

Materials and Experimental Techniques

This chapter discusses the experimental work conducted to fabricate and characterise of the self-sensing nanocomposites material under different preparation conditions. However, to achive this, this study required an accurate calculation of the various parameters necessary for specimen preparation in addition to the actual testing. The challenging issues to be overcome during sample preparation were as follows:

1. Selection of an appropriate matrix material
2. Selection of suitable type of carbon nano tubes for conductivity and reinforcement
3. Selection of an effective type of solvent for dispersion of the CNTs
4. Selection of the wt.% of CNTs in the epoxy matrix
5. Selection of a good and effective dispersion technique
6. Selection of a suitable composite preparation method for laminate samples as well as the casting method for nanocomposite samples. This includes choosing material, size, shape and casting mould material. Morovere, selection a suitable release agent and casting conditions was also needed.
7. Finally specimen preparation prior to testing

In addition to the above isses, the testing methods also involved the selection of various test parameters such as: (i) Selection of test cross-head speeds and (ii) Number of test samples for each type of test to obtain good set of accurate results for the nanocomposite properties being measured. The sections which follow describe these aspects.

3.1 Impact Damage Assessment In Composites containing MWCNTs

3.1.1 Experimental Methods

3.1.1.1 Materials

To fabricate the MWCNTs-glass epoxy i.e. (MWCNTs-GE) nanocomposite, the MWCNTs, as shown in Figure 3.1, and as produced by chemical vapour deposition (CVD), were added to the epoxy resin. The average length and average diameter of these MWCNTs were 50 μm and 5-15 nm respectively. The purity of MWCNTs obtained from Research Nanomaterials Inc, USA was > 95% and their specific surface area was ≈ 233 (m^2/g). The glass fibres used were plain woven 290 $g.m^{-3}$ in mat form. The epoxy resin used was a slow cure time type EL2, with its hardener (AT30). Both materials were supplied from the same company, (Easycomposites, UK).

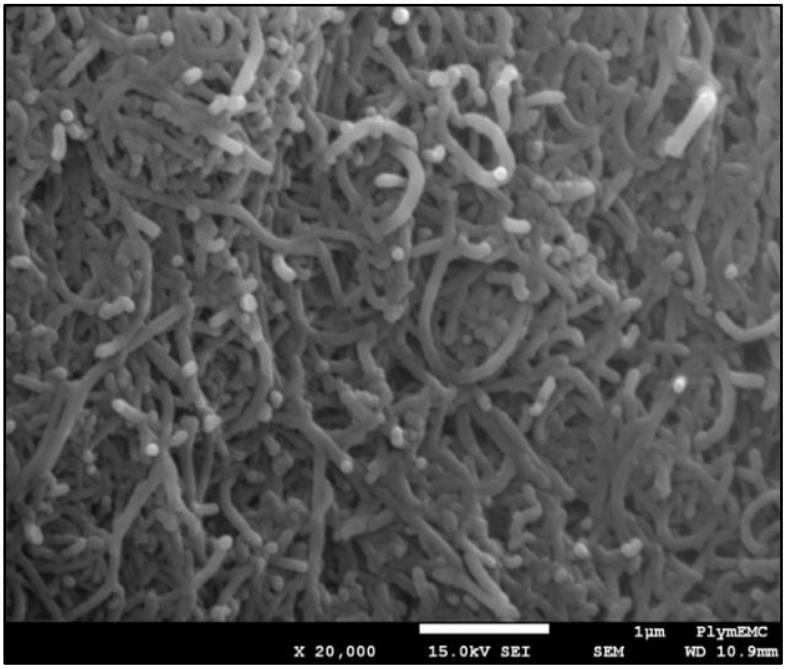

Figure 3.1: SEM image of as-received MWCNTs.

3.1.1.2 Preparation of MWCNT-GE nanocomposites

In the as received condition, MWCNTs usually exist as an agglomerated mass. Therefore, to disperse them, a pre-calculated weight of MWCNTs was added to a 50 ml of high purity organic acetone in a clear beaker. Sonication, using a high-intensity ultrasonic probe (BR-20MT-10L, 1000W), was then carried out for 10 minutes. The MWCNTs/acetone mixture was then mixed with the required amount of epoxy resin and the solution was further sonicated again for 20 minutes using a pulse mode of 40 seconds on 20 seconds off. The beaker was kept in an ice bath in order to prevent the mixture from overheating. Following this, the solution was placed in an oven for 2 hours at 60 °C to evaporate the acetone. The hardener was then added to the mixture at a ratio of 100:30 (epoxy: hardener) by weight. During these procedures, there is a probability that air can be trapped within the nanocomposite. Therefore, these bubbles must be removed to prevent voids occurring inside the composite layers which will affect the properties of the structure. Hence, the mixture was degassed for 20 minutes to remove all the air bubbles.

The mechanical properties of a MWCNTs-GE nanocomposite depends directly on the geometry of the laminates, especially the thickness. Thus, according to the British Standard BS EN ISO 14125 (1998-2011), the thickness of the samples should be 2 mm. Therefore, 10 layers of glass fibre fabric with 120 g of nanocomposite were used to obtain a 2 mm thick MWCNTs-GE nanocomposite laminate. Hand lay-up steps were used to place the nanocomposite between the laminate layers using a roller. After completing the lay-up process with different MWCNTs contents i.e. (0 %, 0.5%, 1.0%, 1.5%, 2.0%), all of the laminates were placed inside a vacuum bag for 24h at room temperature to draw out any residual trapped air and excess resin. Finally, the cured

panels were post-cured at 60°C for 15 hours. Processing in this manner resulted in fully consolidated flat rectangular test panels.

3.1.2 Characterisation

3.1.2.1 Low-Velocity Impact Testing

The aim of these tests was to cause damage in the self-sensing composite panels whilst trying to understand the behaviour of the self-sensing composite during and after impact. The impact tests on the self-sensing composite samples were performed using a drop-weight impact method as shown in Figure 3.2.

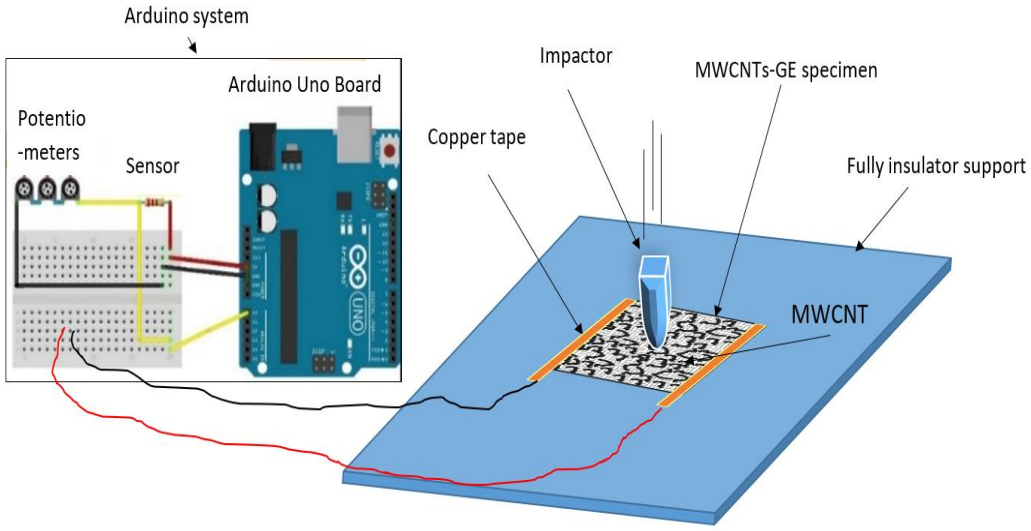

Figure 3.2: Schematic layout of the impact test of self-sensing MWCNTs-GE composites..

Flat rectangular specimens were used for this. These were cut from laminate panels with the dimensions of 100×50×2 (mm) using a diamond saw. Each sample was securely clamped to a supporting frame and then impacted exactly at the centre of the sample. The steel impactor head was hemispherical in shape with a diameter of 16 mm. A round head was used to minimise penetration of the sample. All samples were modified by additional of 0, 0.5 1.0, 1.5 and 2.0 wt.% of MWCNTs respectively. The

impact energies used were 12J, 24J and 36J. These energy levels were used to prevent the specimens fully breaking. The initial impact velocities (v_i) were calculated from the height from which the steel impactor was dropped onto the sample surface. In addition, in order to calculate the rebound (v_r) velocities, the tests were recorded using a high speed camera type (Sony RX10 II, Japan) which could capture 1000 images per second. The details of the low-velocity impact tests are shown in Table 3.1.

Table 3.1: Low-velocity impact test parameters

Drop height (m)	Drop mass (kg)	Impact energy (J)	Impact velocity (m/s)	No. of samples
0.5	2.44	12	3.13	4
1	2.44	24	4.43	4
1.5	2.44	36	5.43	4

3.1.2.2 Flexure After Impact (FAI) Testing

The post-impact strength of all impacted samples was evaluated using a three-point flexural test method, under static conditions on a universal testing machine (Instron 5582/UK195). The flexural load was applied with a constant crosshead speed of 2 mm/min with a span distance of 70 mm. The flexural stress and strain which occurred in the specimen when loaded can be calculated using the following equations:

$$\sigma_f = \frac{3P_f l}{2wt^2} \tag{3.1}$$

$$\varepsilon_f = \frac{6ht}{l^2} \tag{3.2}$$

Where, P_f is the applied flexural force. *l, w, t* and *h* are span length, width, sample thickness, and maximum deformation respectively.

3.1.2.3 The Electrical Resistance Measurement

The electrical resistance of all the self-sensing composite samples was measured without any load using a two-point probe technique at room temperature. A digital multi-meter type (Keithley 6517B, USA) was used for this purpose. In order to reduce (i.e. minimise) the contact resistance between the sample and the tip of the probes, the opposite ends of the specimens were painted with a high purity silver paint. Following this, two copper electrodes were fixed at these positions on the samples to ensure good electrical contact. The in-plane electrical conductivity of the samples was then estimated from:

$$\sigma = \frac{L}{RA} \tag{3.3}$$

Where L is the sample length and R is the electrical resistance and A is the cross-section area of the sample. Regarding the electrical resistance measurement during the impact test, due to the very short impact time period (in milliseconds), an Arduino system was used to record the obtained resistance data in milliseconds. The Arduino system is an open-source electronics platform based on easy-to-use hardware and algorithm software. The hardware features an open source hardware board designed around a 32-bit microcontroller. Current models have a USB interface, 14 digital output pins and 6 analog input pins that gives an allowance to user to attach various type of extension monitoring boards.

3.1.2.4 Scanning Electron Microscopy and Raman Spectroscopy Analysis

The distribution of MWCNTs in the matrix was examined using scanning electron microscopy (JEOL JSM-7001F, Japan) operating at 15 kV. To assist visualisation the specimens were coated with a thin film of gold by sputtering. After flexural testing, the broken specimens were also sputtered with gold using (model QUORUM-Q150TES, UK) for 12 minutes so that the MWCNTs morphology could be clearly observed. Raman spectra for the prepared MWCNTs-GE nanocomposite specimens were recorded at room temperature using a Raman Microscope. An excitation wavelength (514 nm) in the range of 1000-3000 cm^{-1} was generated from a diode laser, with power approximately 100 mW, on the sample surface. Positions, intensities and the calculation of ratios between intensities of the bands were obtained using Lorentzian routine functions fitted to the Raman raw data. Raman Microscopy is a spectroscopic technique typically used to determine the vibrational modes of molecules, although rotational and other low-frequency modes may also be observed. It is commonly used during chemical analysis to provide a structural fingerprint by which molecules can be identified. During Raman microscopy a laser light interacts with molecular vibrations, phonons or other excitations in the system. This results in the energy of the laser photons being shifted up or down. The shift in energy gives information about the vibrational modes in the system, so identifying the molecules involved.

3.1.2.5 Statistical Results Analysis

Statistical analysis of the experimental data obtained after impact testing was carried out using SPSS version 23.0 software (SPSS Inc., Chicago, USA). The one-way

ANOVA method was chosen to calculate the P-value and other statistical parameters. The P-value is statistically defined as the probability against the null hypothesis (i.e. the suggested criterion does not have a high significant effect in terms of the quantification data). The p-value is used as an alternative criterion to rejection to provide the smallest level of significance at which the null hypothesis could be rejected. A smaller p-value means that there is stronger evidence in favour of the alternative hypothesis. In this study, differences were considered to be a statistically significant only when p-values < 0.05.

3.2 The Electromechanical and Temperature Dependent Behaviour Of Composites contaning MWCNTs

3.2.1 Experimental Procedures

3.2.1.1 Materials

MWCNTs (described in section 3.1.1.1) were used as a filler to make a nanocomposite material. The matrix material used for the specimen preparation was a low viscosity epoxy resin type (IN2 Epoxy Infusion Resin) combined with a hardener (AT30 slow). Both were supplied by Easy Composite (Staffordshire, England, UK). After mixing, the viscosity of the matrix resin was 200-450 mPa s at room temperature. In its mixed state, at room temperature, the epoxy resin has a pot life of 80 – 100 minutes. The solvent used during manufacture was high purity of acetone (> 95%) supplied by Acros Organics Ltd (Loughborough, UK).

3.2.1.2 Preparation of MWCNTs/Epoxy Nanocomposite

The MWCNT/epoxy nanocomposite matrix was prepared by uniformly dispersing the MWCNTs in the epoxy resin using an ultrasonic technique. Firstly, different concentrations of the MWCNTs (0 – 2.0 weight %) were weighed out and mixed in 60 ml of acetone in a beaker. The procedure to prepare the nanocomposite samples is the same that decreased in section 3.1.1.2. The mixture produced in this way was then cast in a silicon mould to produce the desired specimen configuration needed for compression testing. Finally, the mixture was cured for 24 hours at room temperature and then for a further 24 hours post-cure at 60°C to ensure the full completion of the cure process. The cylindrical test specimens obtained in this way had a 24 mm diameter and length 25 mm. Fabrication process for the nanocomposite containing MWCNTs is shown in Figure 3.3.

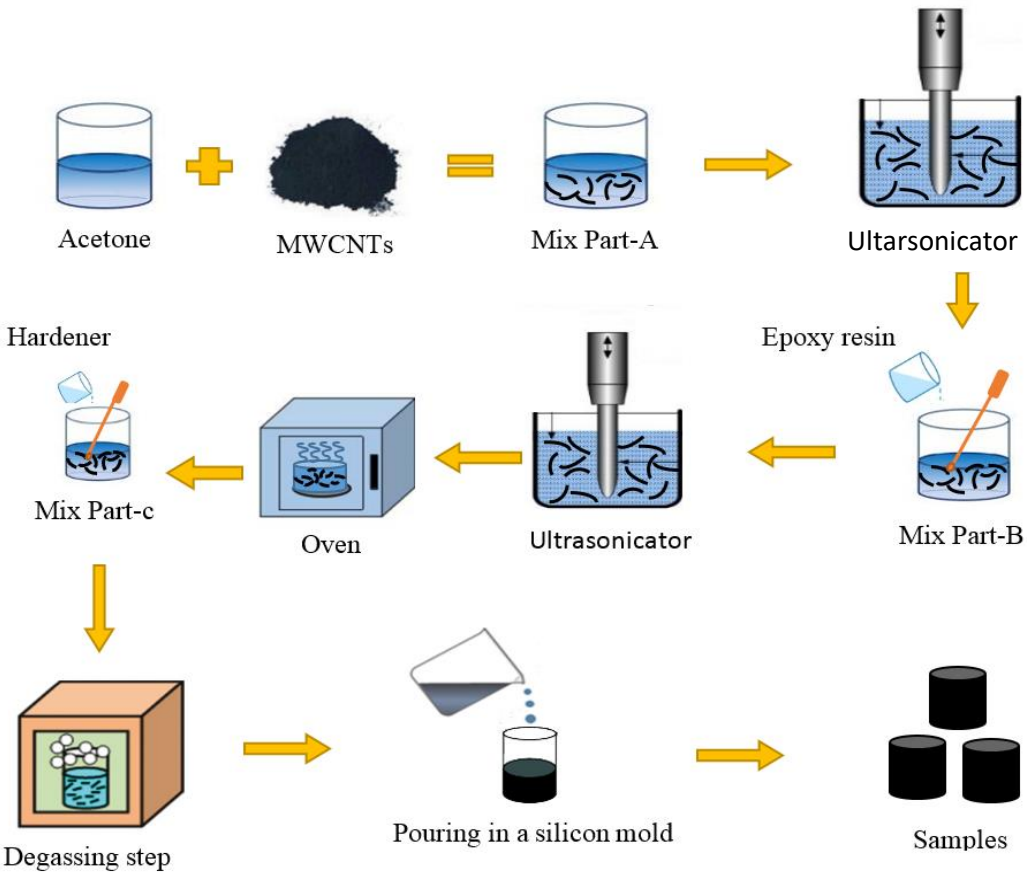

Figure 3.3: Schematic illustrating fabrication process for MWCNTs/epoxy nanocomposite

3.2.2 Characterisation and Testing

3.2.2.1 Electrical Conductivity

To assess the electrical conductivity of the prepared nanocomposite specimens a high resistance digital multi-meter (Keithley 6517B) was used. This measured the volume electrical resistance of the samples. The procedures used here were the same as those described in section 3.1.2.3.

3.2.2.2 Compression Testing

The compression testing of the samples was carried out using a universal testing machine (described in section 3.1.2.2) operating under displacement control at an appropriate crosshead speed. For accuracy, three samples (see Figure 3.4), for each MWCNT concentration studied, were tested. For the electromechanical testing of the nanocomposite, the uniaxial compressive loading was applied to the specimen at a crosshead speed of 5 mm/min. The strain sensitivity i.e. (gauge factor GF) of CNT/epoxy composites was calculated using the following equation;

$$GF = \frac{\Delta R / R_0}{\varepsilon} \tag{3.4}$$

Where ΔR represents the change in resistance of MWCNTs/epoxy samples, R_0 is the initial resistance and ε is the compressive strain. In addition, a cyclic load test was as conducted to explore the dynamic response of the MWCNT/epoxy nanocomposites and to confirm the reproducibility of this under load. An alternating displacement strain (0 - 0.4 mm/mm) was applied to the sample using a crosshead speed of 0.5 mm/min. For the temperature dependence testing, measurements were carried out, as shown in Figure 3.5, within a closed-cycle heater, with a temperature operating range of 20 to 80 °C. Prior to testing the test temperature was stabilised by holding at the

target temperature for 60 minutes. The resistance of samples was measured, and recorded, using a digital multi-meter. To assess the electromechanical response at the various temperatures, *viz*. 20°C, 50°C, 60°C, 70°C and 80°C, samples containing 0.5, 1.0, 1.5 and 2.0 weight % of MWCNT's were subjected to cyclic compression tests. During each test, the holding time at each temperature was again 60 minutes. Once the temperature was stable five compression load cycles were applied to the specimens at a crosshead speed of 0.5 mm/min.

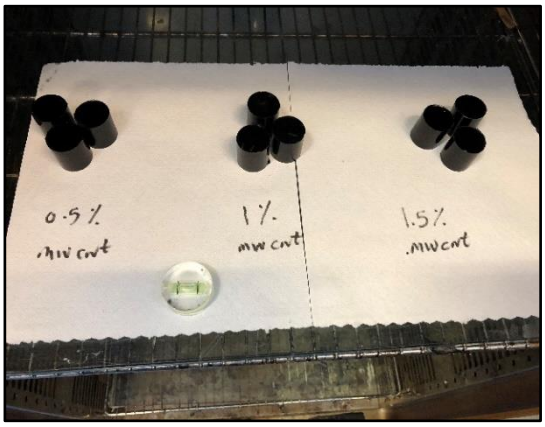

Figure 3.4: Post-curing step for samples

Figure 3.5: Electromechanical test set-up showing the test specimen inside the heating chamber.

3.2.2.3 Dispersion Assessment

Following testing the fracture surfaces of the specimens were examined using a scanning electron microscope (JEOL JSM-7001F, Japan). This was carried out to assess the extent of dispersion of MWCNTs in the epoxy. The steps to prepare the samples for SEM examination was described in section 3.1.2.4.

3.3 Damage Sensing in Composites containing MWCNTs during Anticlastic Bending

3.3.1 Experimental Procedures

3.3.1.1 Materials

The materials used to fabricate the smart composite were described previously in section 3.1.1.1. The important properties for these materials are listed in Table 3.2.

Table 3.2 Properties of the materials used during the manufacture of test panels.

Property	MWCNTs	Epoxy Resin	Glass Fibre
Density (g/cm^3)	2.1	1.15	2.54
Modulus (GPa)	1200	3	72
Strength (GPa)	63	0.07	3.4

3.3.1.2 Manufacturing of Fibre/MWCNTs/epoxy Composite Laminates

The procedure used to manufacture the matrix (nanocomposite) of the smart composite was described previously in section 3.1.1.2. Based on the British Standard BS EN ISO 14125 (1998-2011), the chosen laminate thickness was 2 mm for all samples used during flexural testing. For each test specimen, 10 layers of woven glass

fibre mat, containing MWCNT/epoxy, were used. The hand lay-up process was used to fabricate glass fibre /MWCNTs/epoxy composites. During the manufacturing process, the fabric (measuring 300 mm×300 mm) was saturated with the epoxy resin, which had been previously mixed with the MWCNTs, layer by layer to ensure that the resin was uniformly distributed on each. This was done using a roller to ensure an even distribution of the resin. After the hand layup process was completed, the composites were subjected to vacuum bagging for 24 hours. Finally, the cured laminates were placed in an oven at 60 °C for 15 hours to post cure. The glass fibre/MWCNTs/epoxy composites manufactured in this way had ≈ 50% volume fraction of glass fabric and ≈ 50 % volume fraction of epoxy resin. These were filled with 0.0, 0.5, 1.0, 1.5 and 2.0 wt.% concentrations of MWCNTs, respectively. A brief schematic description of these steps is shown in Figure 3.6.

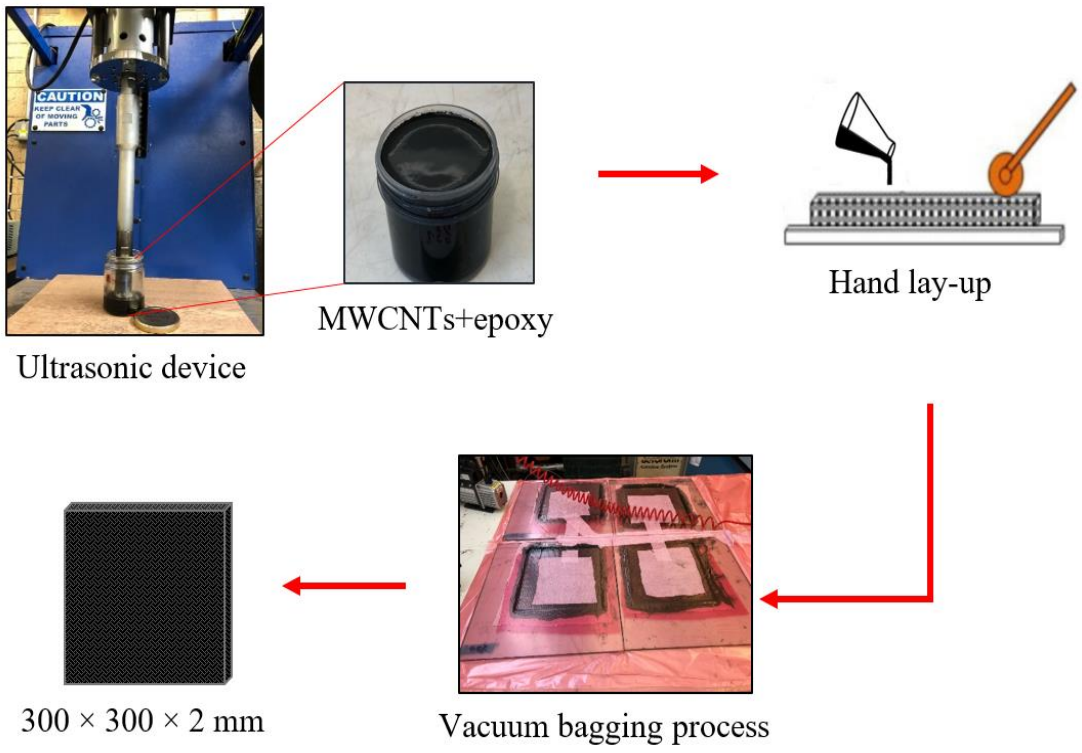

Figure 3.6: Schematic illustration of glass fibre/MWCNTs/epoxy composite fabrication steps.

3.3.2 Characterisation

3.3.2.1 Microstructural Examination

Scanning electron microscopy (SEM) was employed to investigate the MWCNTs dispersion in the matrix, and also to examine fracture surface of the composites laminate following testing.

3.3.2.2 Electrical Property Measurement

A two-point probe technique, using an advanced digital multimeter (Agilent 34401A) was used to measure the volume electrical resistance of the specimens. A silver paste was used to minimise the contact resistance between the surface of the sample and the tip of the probe. The electrical conductivity (σ) of the samples was estimated using equation;

$$\sigma = \frac{L}{RA} \tag{3.5}$$

Where L is the sample length and R is the electrical resistance and A is the cross-section area of the sample In addition, the strain sensitivity (gauge factor) of the fibre glass/MWCNTs/epoxy was also calculated using equation;

$$GF = \frac{\Delta R / R_0}{\varepsilon} \tag{3.6}$$

(Terms in Eq.(3.6) have been defined previously). To obtain these measurements, strain gauges (type L2A-XX-125LT-350) were bonded to one side of the specimen surface. The strain gauge resistance was 350 Ω and the gauge factor 2.1.

3.3.2.3 Flexural Tests

A uniaxial flexural mechanical test, as shown in Figure 3.7b, was performed using three-point bend configuration. The sample dimensions were 150×150×2 mm. The tests were carried out using a universal testing machine (Instron 5582, USA) at room temperature. The machine was operated under displacement control with a crosshead speed of 3 mm/min. For each composite laminate, at least, three specimens were tested to ensure accuracy. The flexural bend stress σ_b was calculated using equation.

$$\sigma_b = \frac{3p_f \times l}{2wt^2} \tag{3.7}$$

Where, P_f is the applied flexural force. *l, w and t* are span length, width and sample thickness, respectively.

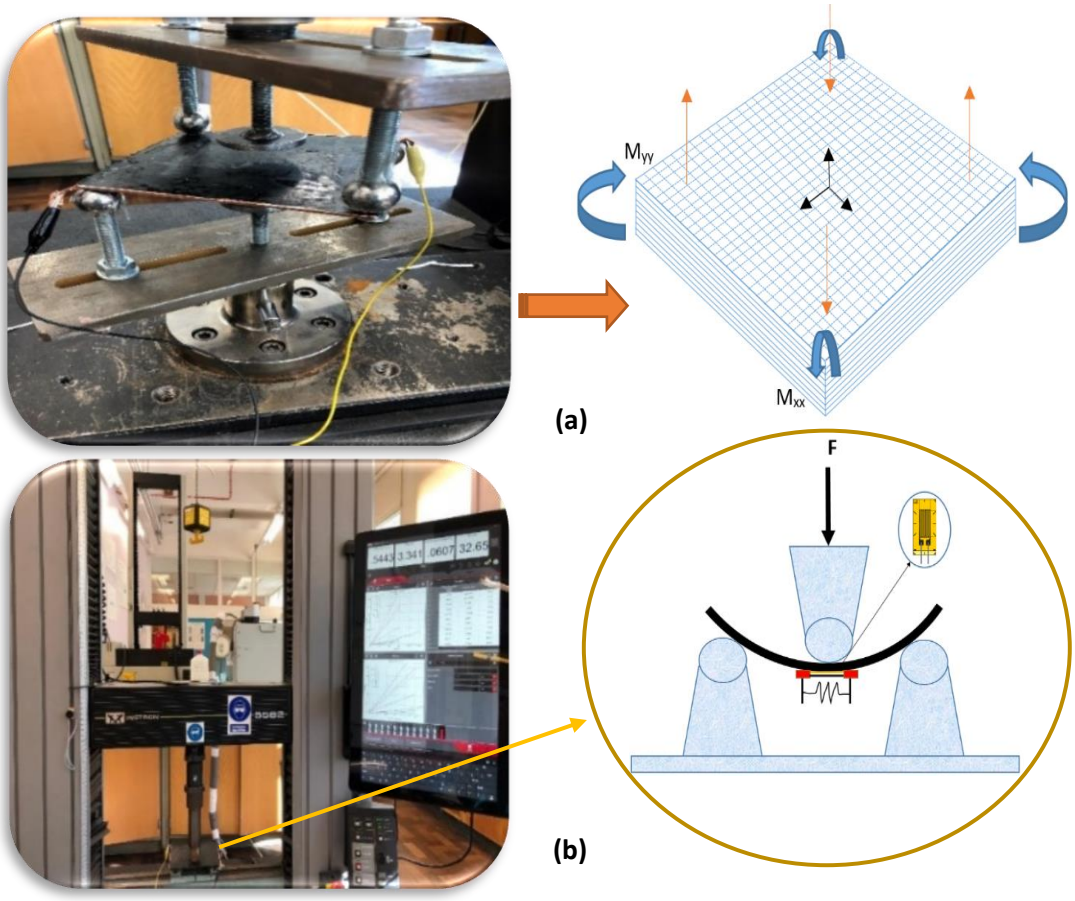

Figure 3.7: Schematic drawing of the samples on the rig (a) anticlastic test rigs (b) 3-point bending

In terms of electromechanical characterization (piezoresistive), the resistance was recorded in real-time during the static flexural testing.

3.3.2.4 Anticlastic Bend Tests

This type of test was used to study the out-of-plane failure of the composite. Testing carried out initially below the elastic limit to avoid early failure. The load was then increased until fracture in order to monitor the damage. The thickness of the test samples was also 2 mm to ensure accuracy. All of these samples were cut to the same dimensions (150×150×2 mm). The testing was carried out on the same universal machine (Instron 5582, USA) described earlier. The two part rigs used during testing (set at 90° to each other) are shown in the Figure 3.7a. The span between the loading points on the test plates (both top and bottom) was 140 mm. This span distance was chosen to ensure that no localised pure bending could occur at the centre of plate. The ball bearing placed on the top of each loading rod ensured that the load was equally distributed on each side of the composite plate. A preload of 10 N was used prior to the readings being taken to ensure the test rigs were balanced correctly. The stress obtained during an anticlastic test can be calculated from the following equation [133]:

$$\sigma_{anticlastic} = \frac{3F}{2t^2} \tag{3.8}$$

Where F indicates the load applied on the corner of the composite plate, t is the sample thickness. During testing, the plate will take on an anticlastic shape due to the applied external load on the four corner edges, as shown in Figure 3.7a.

3.4 The Drift Properties of MWCNTs in Composites During Manufacture

3.4.1 Experimental Procedures and Materials

The multi-wall carbon nanotubes (MWCNTs) used in this study were a CVD synthesised variety obtained directly from the manufacturer (US-Research Company, USA). These CNTs had a mean diameter of approximately 50 nm and an average length of 20 μm. Their purity was > 95% with a density of ≈ 2.1 $g.cm^{-3}$. The reinforcing glass fibres used in the test panels were of a commercial plain-woven E-type glass, of the density of 2.54 $g.cm^{-3}$. The epoxy matrix resin was slow curing EL2 laminate (bisphenol-A) type with a density of 1.15 $g.cm^{-3}$. In addition, a low viscosity resin and curing hardener (type AT30) were chosen since these are widely used in many industrial applications. The adhesive used to fix the MWCNTs to the fibre surface was a simple adhesive spray (Fusion Fix GP Spray Adhesive). The E-glass fibres, the epoxy resin and the adhesive were all supplied by the same company (Easy Composite Co, Ltd, UK).

3.4.1.1 Specimen Manufacture

To prepare the MWCNTs/glass/epoxy composite (i.e. MWCNTs - GE), the composite laminate layers panels were prepared individually using vacuum assisted resin infusion. Figure 3.8 below shows the preparation steps used during the procedure.

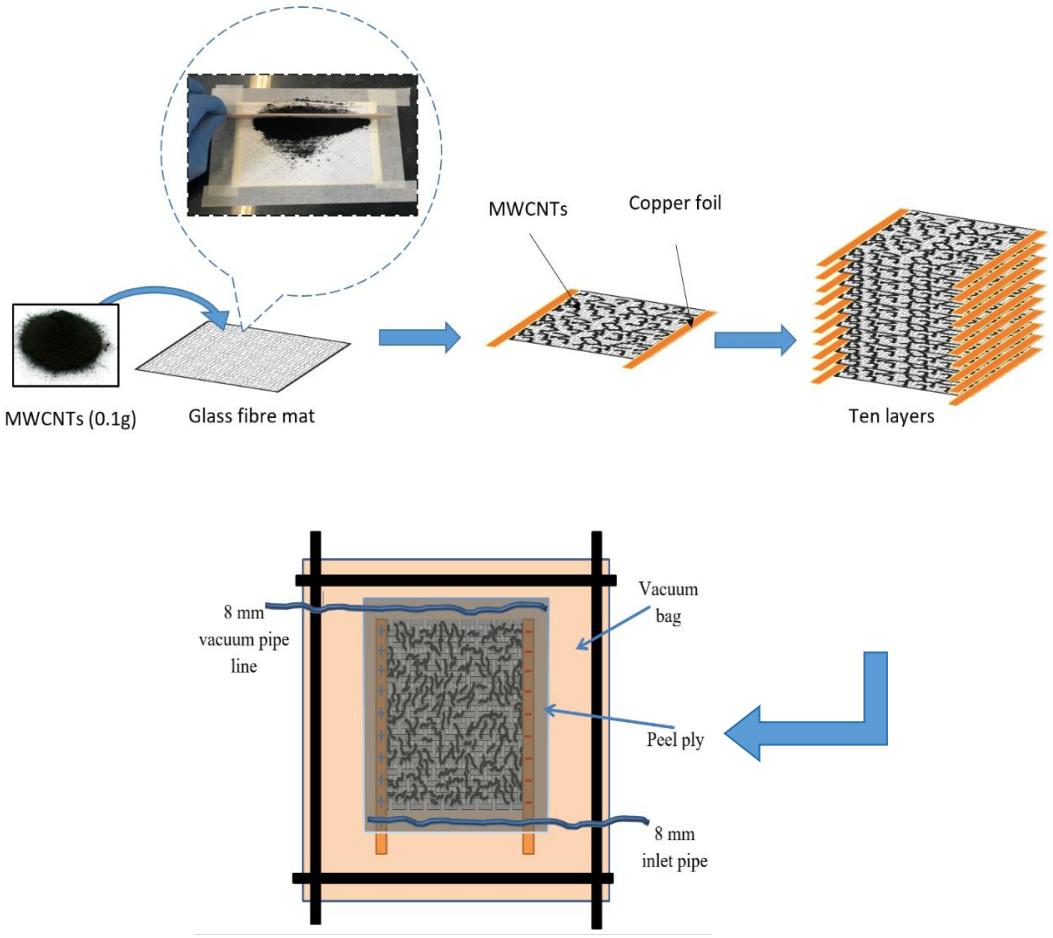

Figure 3.8: Schematic illustration of MWCNTs depositing on the top surface of composite layers (for both groups with and without adhesive) and then stacked together for vacuum assisted resin infusion.

Firstly, a pre-measured mass of MWCNTs (starting from 0.1g) was spread manually on the surface of the glass fibre mat, using a wooden spatula. This made them electrically conductive. This process was continued until the MWCNTs covered all of the surface area of the composite layer. In this way, a low electrical resistance (i.e. at 0.4 g of MWCNTs ≈ 613 Ω) was produced. Therefore, each layer consists of 0.4 g MWCNT, resulting in 4g being applied to the 10 layers. This is ≈ 10 wt.% of the total fabric weight. During this procedure, care was taken to ensure that no clumping of the MWCNTs occurred on the surface. The dimensions of each coated rectangular specimen area was 32 cm × 24 cm. For the targeting tests panels, 20 such layers were

prepared. From these, two test panels, comprising 10 layers each, were then manufactured. This ensured that each test panel had a nominal thickness of ≈ 2 mm, as required by the flexural tests which were conducted according to standard BS EN ISO 14125:2011E. These panels were then divided into two groups; one group was coated only with MWCNTs, the second group had the MWCNTs fixed into place using the adhesive. For the second group, the adhesive was applied to the fibre surface before the resin infusion took place. To ensure that a uniform distribution of the MWCNTs was obtained, the MWCNTs were sprinkled very carefully manually onto the adhesive layer. These techniques are shown in Figure 3.8. For electrical resistance monitoring, copper conductive tape was attached to the edge of each layer for both groups (with and without adhesive applied). This step was carried out in order to facilitate the monitoring of the electrical resistance changes which was took place during processing. Control samples were also fabricated from 10 layers of glass fibre and epoxy resin by resin infusion. The virgin glass fibre/epoxy (GE) composites had ≈ 50:50 % volume fraction of epoxy resin to glass fabric.

3.4.1.2 Mechanical and Electrical Characterisation

3.4.1.2.1 Mechanical Tests

Flexural tests were carried out on the prepared specimens in accordance with (BS EN ISO 14125:2011E) using a three-point bend configuration. These tests were conducted on an Instron (5582/UK195) 100 kN Universal Testing Machine operating under displacement control with a crosshead speed of 3 mm/min along a span length of 80 mm. The dimensions of the test specimens were 100 x 15 x 2 mm respectively. Three

samples, taken from three zones shown in Figure 3.9, were tested to provide a more accurate average response.

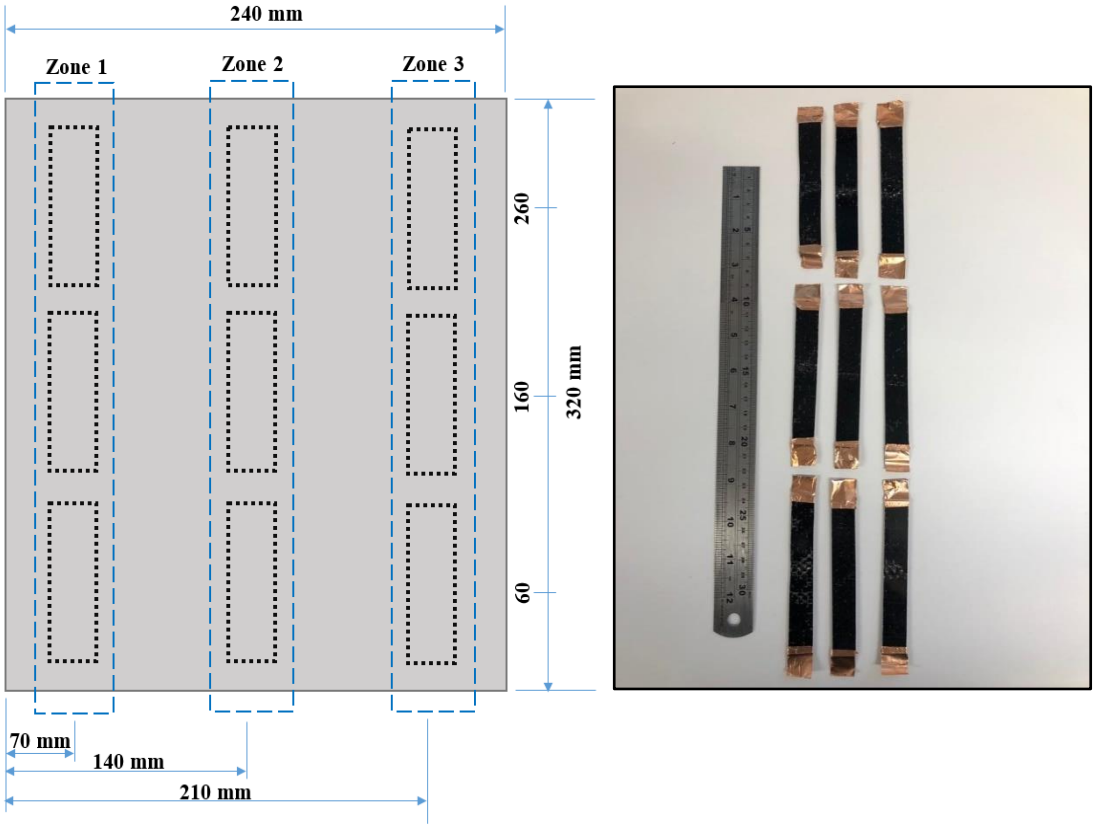

Figure 3.9: Schematic illustration of samples collected at positions along the panel (left) and the prepared flexural test specimens ready for testing (right).

3.4.1.2.2 Electrical Tests

For the electrical testing of the specimens, a DC digital multi-meter (type Agilent 34401A) was used to take the measurements. The electrical conductivity (σ) of samples was calculated using the standard equation $\sigma = L/RA$ where, L is the sample length in mm and R is the resistance in ohms (Ω) and A indicates the cross-section area of the sample in mm^2. Once again a silver conducting paste was used to coat the tip of each specimen to minimise the contact resistances encountered. The three samples tested (10×10×2) mm were taken from five different zones positioned along the sample length starting from the infusion inlet to the end of the MWCNTs-GE

composite panels. These are shown in Figure 3.10. To quantify the strain sensitivity (via the gauge factor), the piezo resistive response of MWCNTs-GE composite was calculated for composite samples subjected to flexural loading. The electrical resistance was measured at two contact points during the test, as shown in Figure 3.11b. The gauge factor was calculated from the equation $GF = (\Delta R/R_0)/\varepsilon$, where $\Delta R = (R-R_0)$ is the changes in resistance caused by the applied load. R_0 is the initial sample resistance without applied any applied strain, ε is the applied strain.

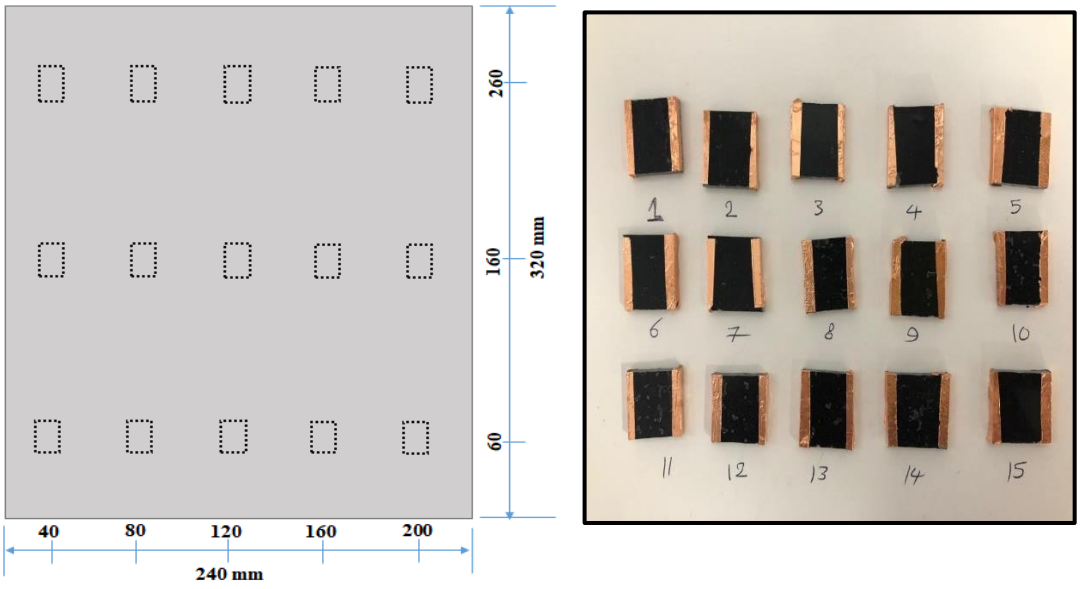

Figure 3.10: Schematic illustration of samples collected positions along the panel (left) and the prepared specimens for electrical conductivity test (right).

To monitor the real-time resistance changes taking place during infusion, both types of prepared composite test panels (as explained above) were used. To record the changes in electrical resistance, multi-meter probes were connected to the test panels using copper tape on the sides of the MWCNTs treated zone. During the infusion process, the flow rate of the epoxy resin was maintained at a constant 1 $cm.min^{-1}$ in order to allow enough time to collect the necessary multi-meter readings as shown in Figure 3.11. Scanning electron microscopy (SEM JEOL JSM-7001F, Japan) was also

used to investigate the degree of dispersion of the MWCNTs on the fibre surface. The SEM operated at an accelerating voltage of 15 kV, to ensure an appropriate magnification to clearly visualise the MWCNTs in situ. The samples were coated with gold to reduce sample charging. In addition, optical microscopy was also used to capture some images in order to show the positional state of MWCNTs along the whole length of the samples.

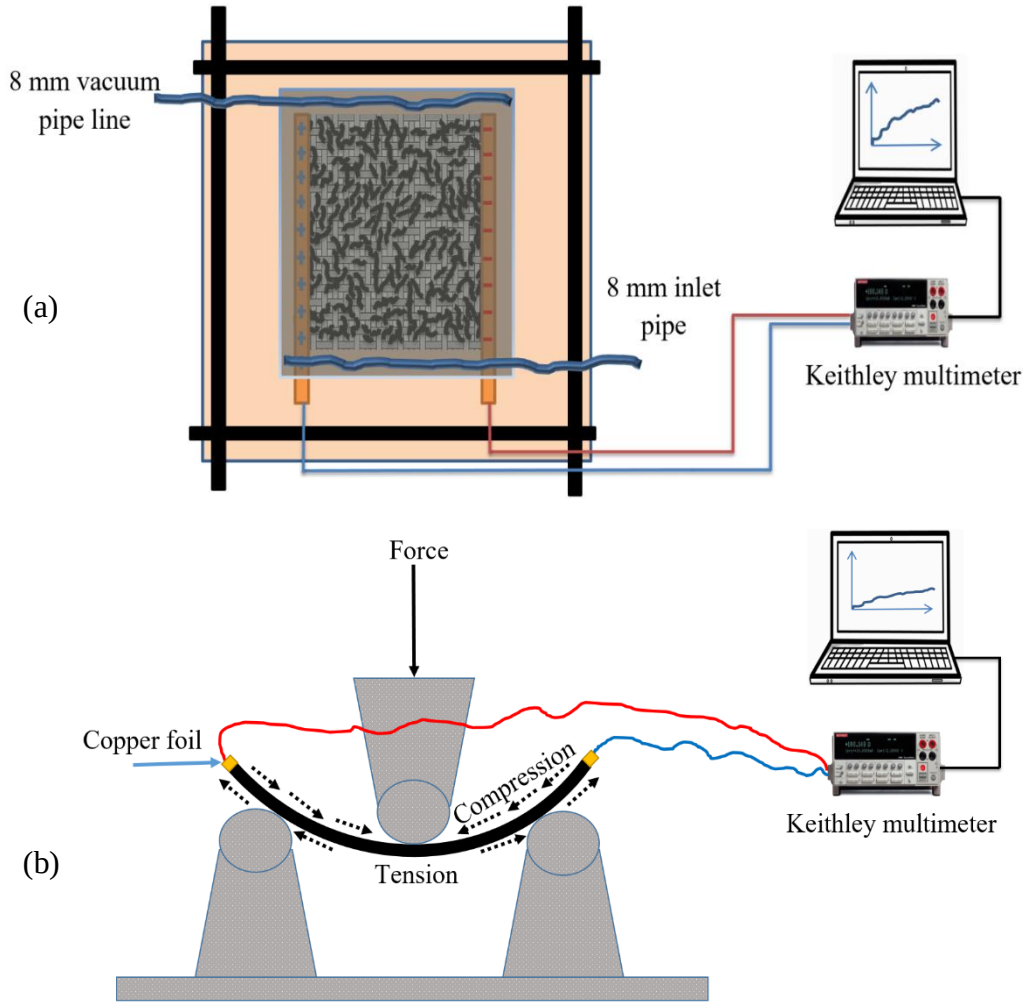

Figure 3.11: Illustration of the *in-situ* resistance monitoring of the MWCNTs deposited composite during (a) epoxy infusion and (b) flexural test.

In summary this chapter detailed the experimental work conducted in characterising the nanocomposite materials investigated.

Chapter 4

Results and Discussion

This chapter discusses the results obtained from the experimental work conducted in chapter 3.

4.1 Impact Damage Assessment in Composites containing MWCNTs

4.1.1 The Electrical Conductivity of the Self-sensing Composite

The electrical conductivity of the self-sensing specimens was measured at the zero load conditions i.e. without any strain applied. Figure 4.1 indicates the measured electrical conductivity of the self-sensing composite as a function of MWCNTs wt. % content. It is clear from the curve that the specimen shows a sharp increase in the electrical conductivity when the concentration of MWCNTs was increased from 0 to 0.5 wt.%. This occurs since above this value the MWCNTs start to form conductive networks inside the matrix.

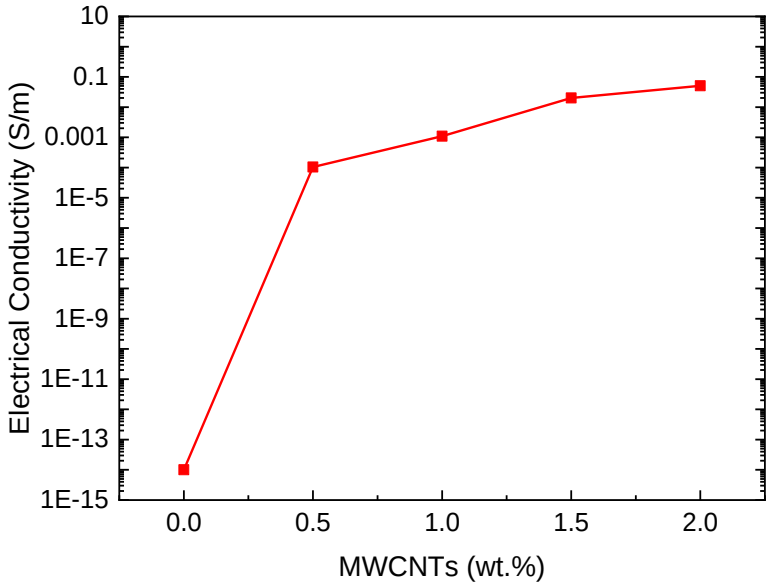

Figure 4.1: Variation of electrical conductivity of self-sensing composite with wt.% MWCNTs concentration.

The percolation threshold is defined as the turning point at which the composite changes from being an insulator to become electrically conductive due to the presence of the MWCNTs networks. This has also been observed in previous studies [134]. The electrical conductivity of the composite increased gradually after reaching the percolation threshold approaching 5.1×10^{-2} S/m at 2.0 wt.% of MWCNTs. At high MWCNTs concentration, the number of conductive networks increased inside the matrix of the self-sensing nanocomposite, and became more active, and as a result, electron transfer (conductivity) proceeded easily. The efficient electrical conductivity of self-sensing nanocomposites is a very important objective in this study in order to allow for the *in-situ* monitoring of the self-sensing nanocomposite, during, and after, impact.

The degree of dispersion (i.e. high homogeneity) of the MWCNTs into the matrix has been shown to influence the characteristics of the final nanocomposite properties (mechanically and electrically) [7]. Raman spectroscopy can be employed as a rapid, and unambiguous, technique to explore the homogeneity of the nanocomposites in terms of carbon nanotubes (CNTs) dispersion in the matrix materials. All Raman data for MWCNTs-GE nanocomposites are summarized in Figure 4.2 and Table 4.1 in terms of the changes in the Raman shift and intensities ratios. As described previously Raman spectroscopy is a sensitive tool for monitoring electronic structure in carbon nanotubes and the presence of defects. It can be speculated that there are two weak bands (D, 2D), due to their relatively small intensity peaks, to be observed when a defect occurs in the MWCNTs structure [135].

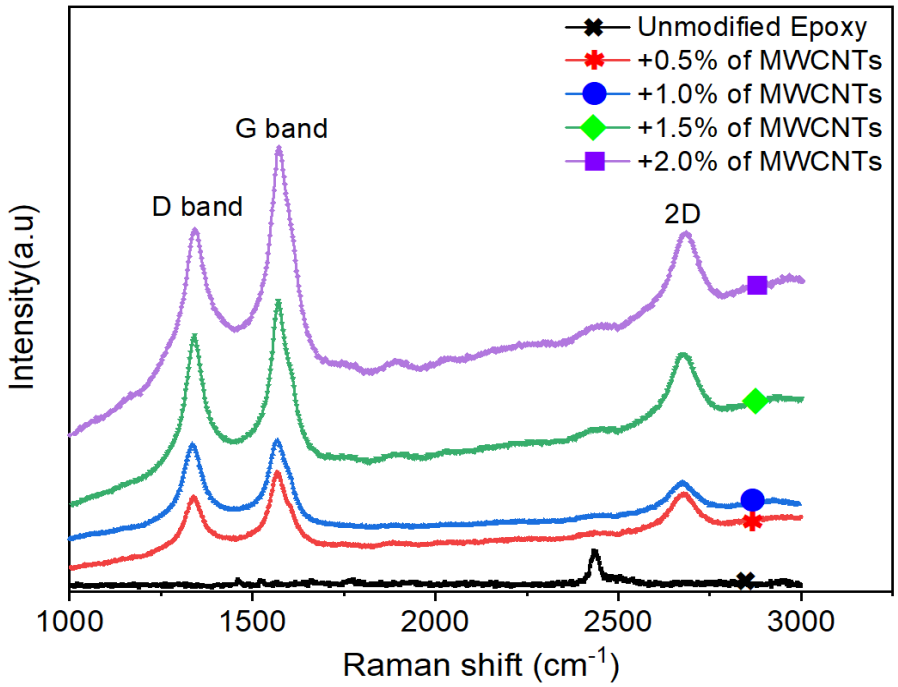

Figure 4.2: Raman spectra of unmodified epoxy and modified with different MWCNTs concentrations.

In contrast, the other Raman shifts (G-band), which was 1572.18 cm^{-1} for the 2.0 wt.% of MWCNTs) were 0.12%, 0.23% and 0.32% respectively for the 1.5, 1.0 and 0.5 wt.% MWCNTs as measured relative to the 2.0 wt.% value. The shift in the peak of G band for MWCNTs in the matrix of self-sensing nanocomposites indicates that a strong interfacial interaction between the epoxy and the MWCNTs has occurred [136].

Table 4.1: Raman intensities ratios of the self-sensing MWCNTs-GE nanocomposites

Sample	I_D/I_G	I_{2D}/I_G
0.5 wt.% MWCNTs/epoxy	0.79 ± 0.01	0.81 ± 0.009
1.0 wt.% MWCNTs/epoxy	0.98 ± 0.01	0.72 ± 0.04
1.5 wt.% MWCNTs/epoxy	0.88 ± 0.003	0.80 ± 0.01
2.0 wt.% MWCNTs/epoxy	0.81 ± 0.02	0.82 ± 0.008

Moreover, the homogeneity and lower quantity of MWCNTs defect structure inside the nanocomposite matrix could also be confirmed by the peaks ratios (see Table 4.1). The relative intensity of this mode can provide direct evidence of covalent modification, so indicating possibly defect concentration. It should be noted that the I_D/I_G and I_{2D}/I_G ratios presented have a low value (<1) for each sample which indicates a high degree of homogeneity of the MWCNTs in the nanocomposites structure.

4.1.2 Mechanical Properties of MWCNTs-GE Composite before Impact

The measured flexural strength and flexural modulus for samples with different wt.% MWCNTs concentrations are shown in Figure 4.3a, b. The ultimate flexural strength significantly increased in MWCNTs-GE composite, together with a linear increase in the stiffness (slope) relative to the virgin composite. Both flexural strength and modulus were collectively superior to the unmodified condition. When 1.5 wt.% of MWCNTs were added to the matrix of the composite (pure epoxy as Figure 4.4a), the flexural strength showed a maximum value of 577.52 MPa, with the maximum flexural modulus of 23.88 GPa occurring at 2.0wt.% of MWCNTs. This observed improvement in properties may be due to a more effective load transfer mechanism, from the matrix to the reinforcing fibres, due to the presence of the MWCNTs. Hence, it can be speculated that the maximum properties can be obtained when the nanoparticles are uniformly distributed within the nanocomposite matrix and between fibre tows, as shown Figure 4.4b, c.

(a)

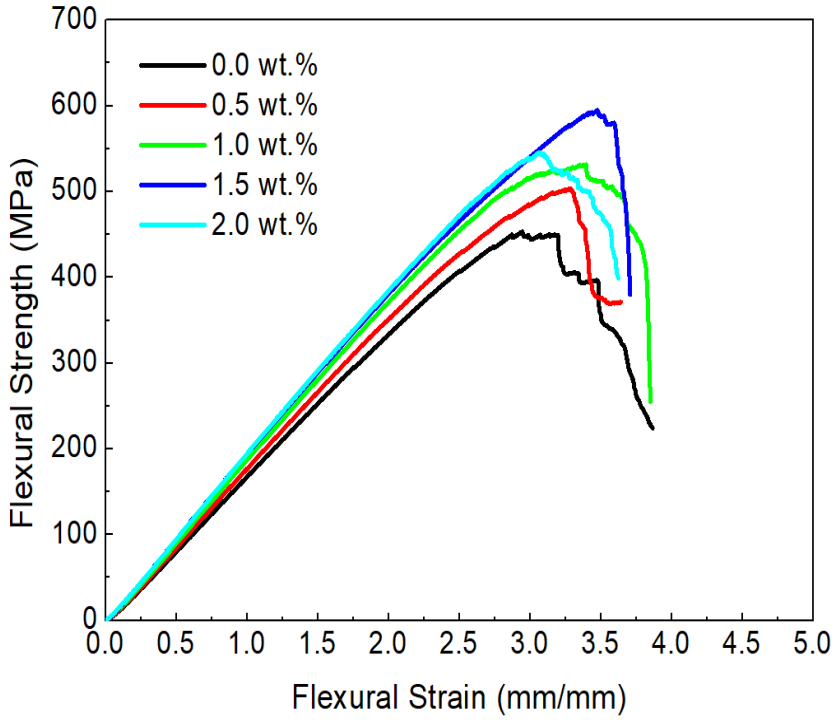

(b)

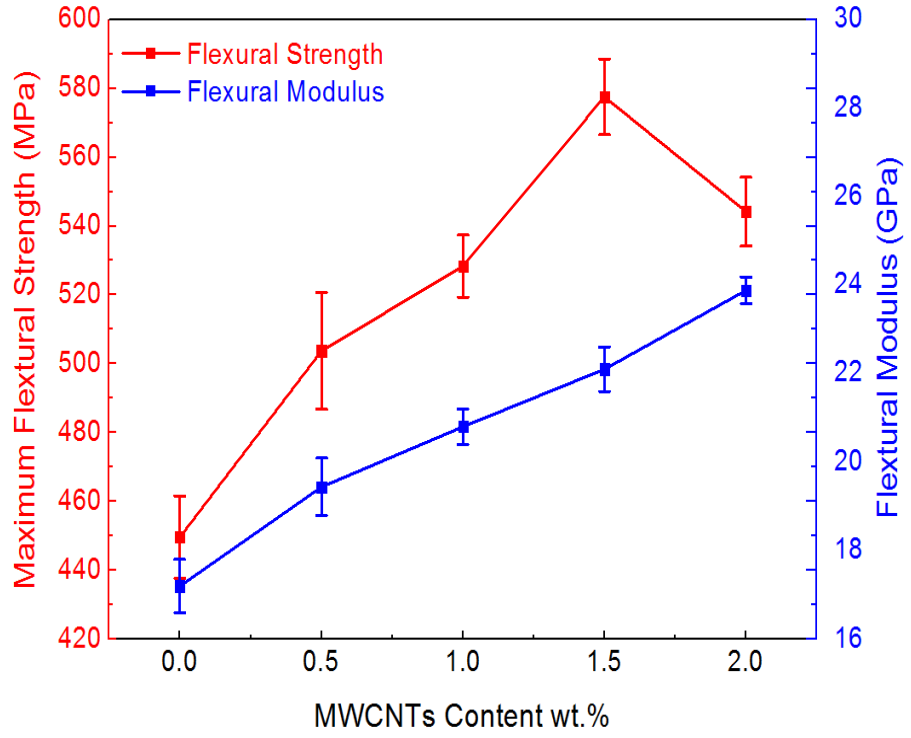

Figure 4.3: Mechanical properties of self-sensing composite as a function of MWCNTs concentration (a) Stress-strain (b) maximum flexural strength and elastic modulus.

However, the flexural strength was seen to reduce to 544.21 MPa at 2.0 wt.% of MWCNT. This was still above the virgin composite value. As is likely that this reduction can be attributed to the presence of MWCNTs agglomeration (Figure 4.4d) effects (i.e. clustering) in some places inside the matrix. This prevents the load being transferred in a straightforward manner between the nanocomposite components [137]. From the above results, it is clear that the MWCNTS are not only making the composite electrically conductive but are also improving their mechanical properties as well.

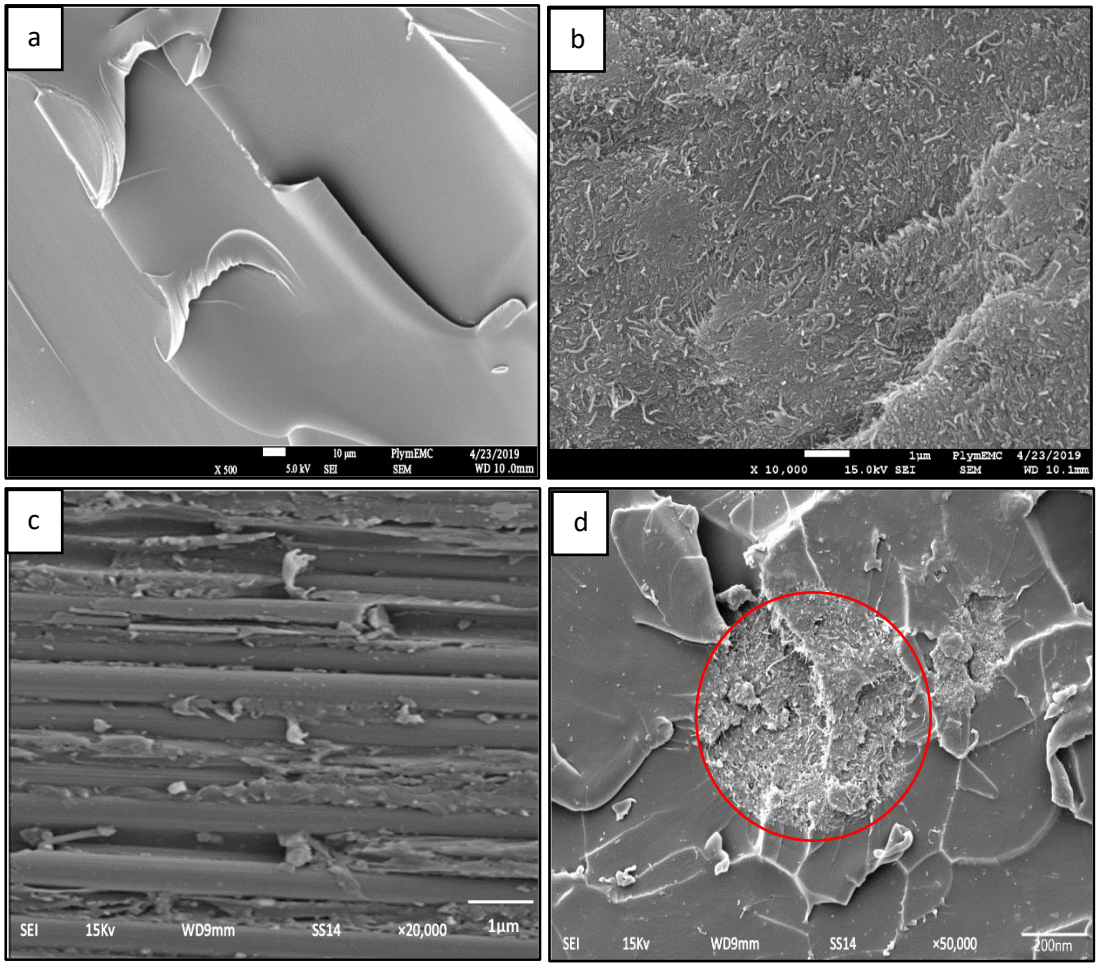

Figure 4.4: SEM images of (a) unmodified epoxy resin (b) 1.5 wt.% MWCNTs nanocomposite (c) nanocomposite between the fibre tows, (d) agglomeration of the MWCNTs inside the matrix.

4.1.3 Absorbed Energy and Damage Factor (ψ)

Analysis of absorbed energy is considered to be one of the main parameters used to evaluate the degree of damage in composite laminates following impact [138]. During impact testing, the absorbed energy can be calculated from the difference between the initial kinetic energy before impact and final kinetic energy after impact, as expressed in the following equation:

$$E_{ab} = E_i - E_r = \frac{1}{2}m(v_i^2 - v_r^2) \tag{4.1}$$

Where, m, v_i and v_r are the mass, initial impact velocity and residual velocity of the impactor, respectively. As shown in Figure 4.5, incorporating MWCNTs into the composite matrix allows for more impact energy to be absorbed by the self-sensing composite. It should be noted that, for the three impact velocities used, the absorbed energy increased significantly when the MWCNTs content was increased up to 1.5 wt. %. However, it then decreased slightly when the MWCNTs concentration further increased to 2.0 wt.%. The largest amount of energy absorbed in the samples, which occurred from the impactor at a velocity of 5.43 $m.s^{-1}$, was 22.1J at 1.5 wt. % of MWCNTs followed by 20.8J, 18.7J and 13.1J for self-sensing composites containing 2.0, 1.0 and 0.5 wt.% of MWCNTs respectively. It also interesting to observe that, under the same MWCNTs concentration, with increasing the impact velocity the absorbed energy increases as well. As shown in Figure 4.5, at 1.5 wt. % of MWCNTs, the absorbed energy increases by 142 % from 9.1J to 22.1J as the impact velocity increases from 3.13 to 5.43 $m.s^{-1}$. This trend could be due to the strong interfacial adhesion between the MWCNTs and the matrix. The same behaviour was observed with other concentrations as well. Therefore, it can be concluded that adding

MWCNTs to the composite has contributed to elevated levels of energy absorbed at different impact velocities, as indicated by the observed increase above the 0 wt.% position.

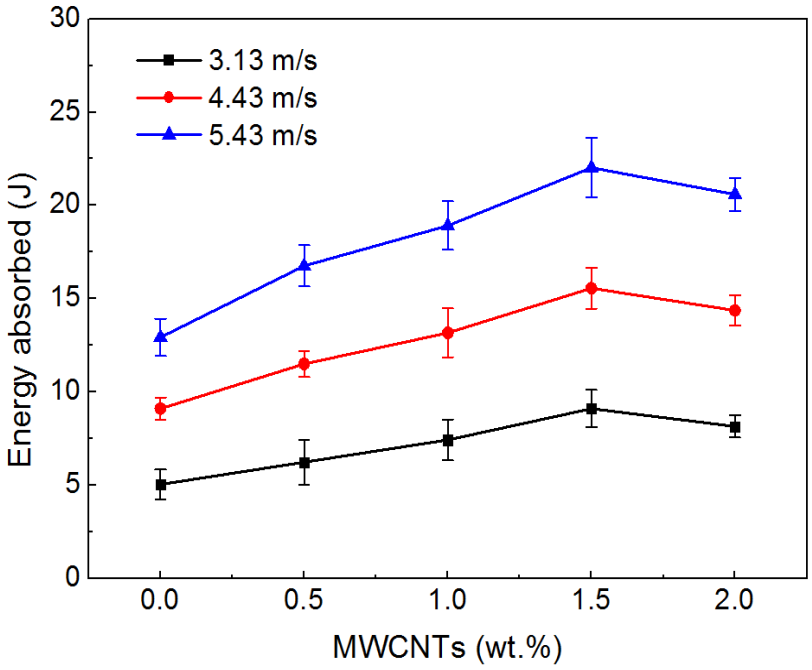

Figure 4.5: Absorbed impact energies versus wt. % of MWCNTs concentration.

To evaluate the degree of damage incurred by the specimens, the following expression for damage factor (ψ) (equation Eq.(4.2)) was used [139].

$$\Psi = \begin{cases} \frac{E_i - E_r}{E_i} = \frac{E_d}{E_i} = 1 - \frac{v_r^2}{v_i^2} & (in\ rebound\ case) \\ \\ or \\ \\ 1 & (in\ penetrate\ \text{case}) \end{cases} \qquad (4.2)$$

Here, E_d is the energy dissipated by the samples. If the damage factor ψ = 0, then $E_i = E_r$, and this indicates that no impact energy is absorbed, so of the energies are fully converted to rebound energy of the impactor. This is an ideal case which cannot actually be achieved due to friction and elastic energy. In contrast, if ψ =1, then the

sample is fully penetrated by the impactor and will show a high degree of damage. Therefore, the damage factor $0 < \psi < 1$ may indicate the degree of dissipated energy which can be used as a criterion to evaluate the ability of the composite to absorb the initial impact energy. Applying this criterion to the current self-sensing composite, then a smaller value of ψ means less damage, so is indicating a better resistance to impact.

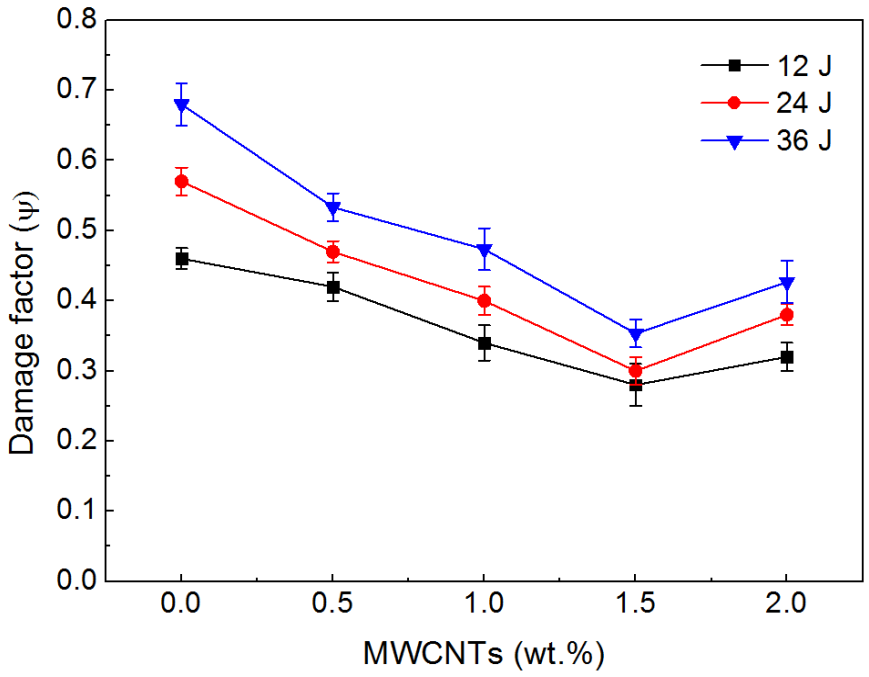

Figure 4.6: Damage factor as a function of MWCNTs concentration and under different impact energies.

As shown in Figure 4.6, the damage factor ψ at the lower impact energy decreases by 39% from 0.46 to 0.28 as the MWCNTs concentration increases from 0 to 1.5%. In addition, the damage factor for an impact energy of (24J) decreases from 0.57 to 0.3 by 47%. Moreover, at the highest level of impact energy (36J), the value of ψ progressively decreases by 48% from 0.68 to 0.35 as the MWCNTs concentration increased. From the results, it is revealed that the sample modified with 1.5 wt.% of

MWCNTs shows a minimum damage factor value which indicates the best impact resistance for all the three levels of impact energies studied. This improvement could indicate the most effective homogenous MWCNTs distribution within the matrix (Figure 4.4) as well as the strongest interfacial bonding condition between the MWCNTs and the matrix between the fibre layers as shown in Figure 4.4c. However, above this level i.e. at 2.0 wt.% MWCNTs, the damage factor increased possibly due to the agglomeration of MWCNTs within the matrix as shown in Figure 4.4b. This agglomeration prevents strain energy being released, as crack propagation occurs during impact. This type of constraint allows greater damage to occur, due to an embrittling effect.

4.1.4 Residual Flexural Strength after Impact

Good flexural strength after impact is an important characteristic for any composite since it can provide significant information regarding initiation and propagation of the damage within its structure. Therefore, a flexural test after impact for the self-sensing composite was conducted at different levels of impact energy. The maximum absorbed energy value, which was occurred at 1.5 wt.% of MWCNTs concentration as shown in Figure 4.5, was chosen for this test. Figure 4.7a, b shows the results obtained for the flexural stress-strain and the normalised residual flexural properties at different impact energy levels. As expected, the applied impact events caused a reduction in both the strength and the modulus properties of the self-sensing composite. It should also be noted that the residual flexural strength is significantly reduced as the impact energy increases, and to a greater degree when compared to the residual flexural modulus. The maximum reduction is ≈ 25% and ≈ 16% for the residual strength and

the modulus respectively. This indicated that the flexural modulus is not as sensitive to damage, when compared to the flexural residual strength.

(a)

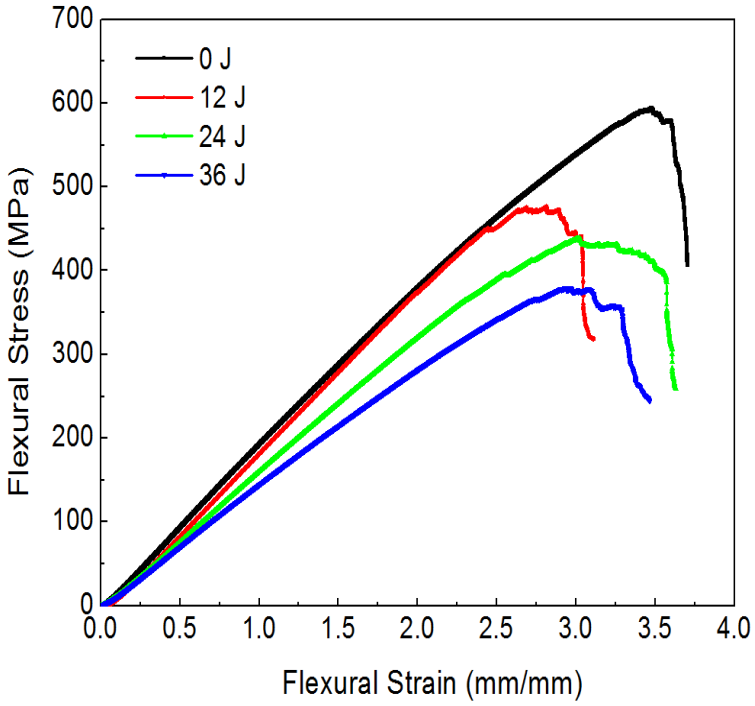

(b)

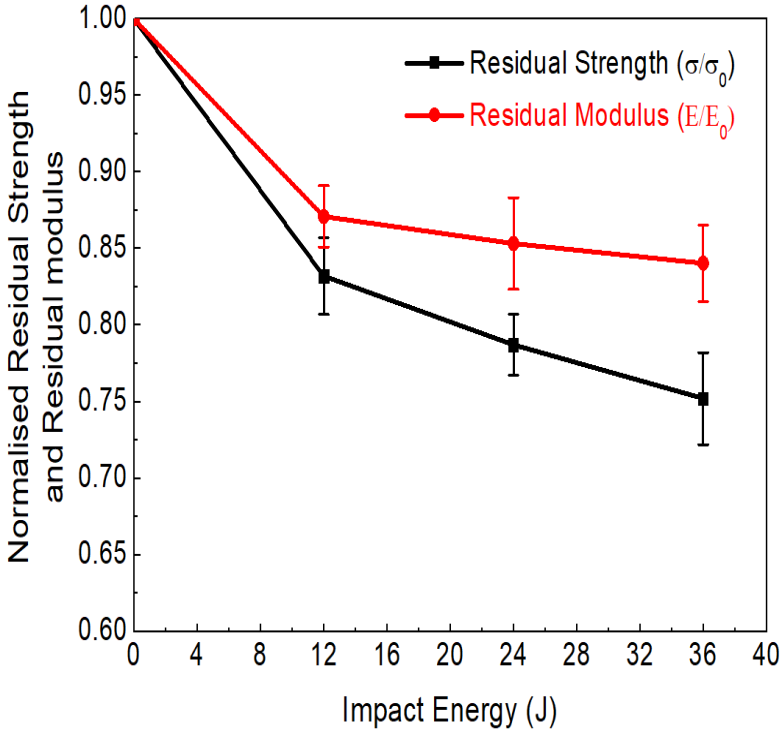

Figure 4.7: Flexural properties versus impact energy for self-sensing composite containing of 1.5 wt.% MWCNTs (a) flexural stress-strain and (b) normalised residual flexural properties.

This has also been observed in other studies [140-142]. The higher sensitivity of the flexural residual strength, to damage, can be demonstrated by the fact that the impact damage is localised to the damage site and so therefore has a minimal effect on the other macro properties such as residual modulus.

4.1.5 Self-sensing Damage Measurement using Electrical Resistance

The damage in the specimen, after impact, is generally localised. However, if the impact level increases, the damage will spread out through the thickness around the impacted area as shown in Figure 4.8. Therefore, it is important to measure the electrical resistance through the specimen volume to assess the degree of damage.

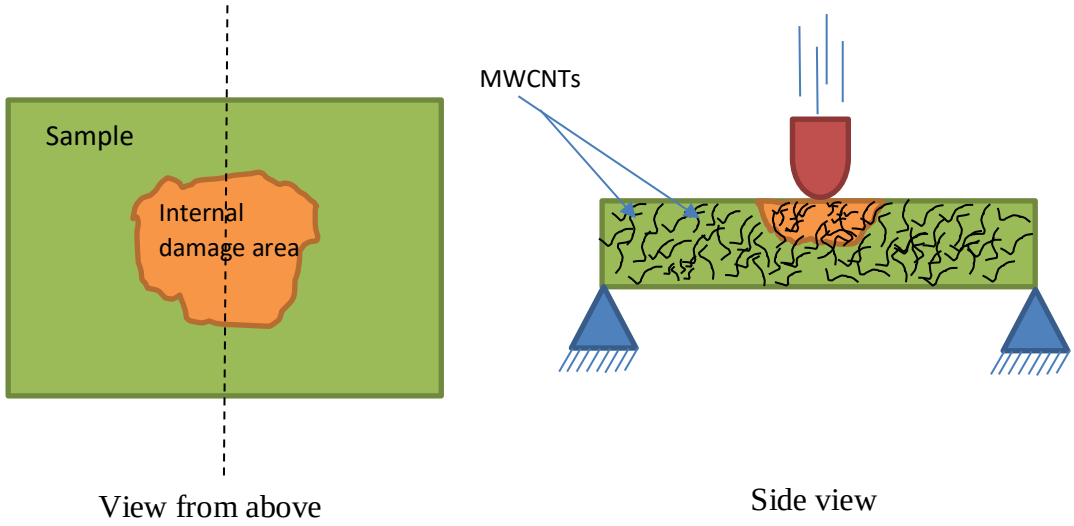

Figure 4.8: Sketch showing potential internal damage following impact.

Figure 4.9 shows the normalised change in electric resistance ($\Delta R/R_0$) as a function of the time for different levels of impact energies applied to self-sensing composites for the different concentrations of MWCNTs. $\Delta R/R_0$ is defined as the ratio of the change in resistance (ΔR) to the initial sample resistance (R_0). It is clearly observed that when the sample is subjected to an instantaneous impact load, the $\Delta R/R_0$ of all samples initially increases linearly with time, reaching a maximum value before gradually decreasing nonlinearly until a certain level (as shown in Figure 4.9a, b and

c) is reached. This change in electrical resistance is due to the MWCNTs conducting networks being disrupted during the impact event. This leads to increase in the electrical resistance. These results were also confirmed by statistical analyses and showed significant variations (P-values < 0.05).

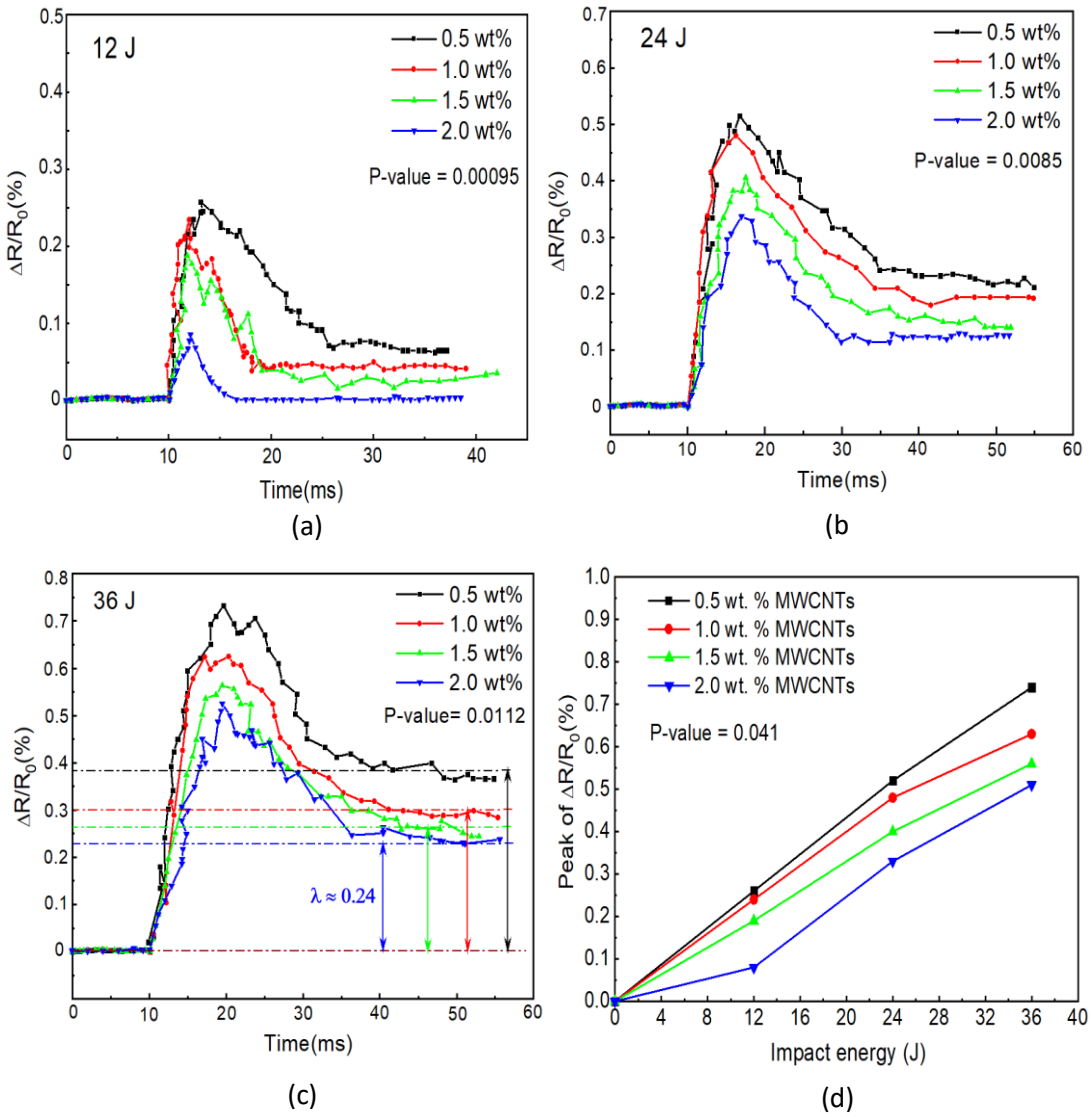

Figure 4.9: Normalised changes in electrical resistance vs time for different wt.% MWCNTs concentration at different impact energies (a) 12J, (b) 24J, (c) 36J and (d) the peak of ($\Delta R/R_0$).

When the impactor rebounds, part of the fracture area may close (elastic deformation) and so the MWCNTs contact is re-established resulting in a decrease in the electrical resistance of the sample. In addition, to demonstrate the maximum electric resistance reached, during impact, Figure 4.9 d shows the peak values of $\Delta R/R_0$ with respect to applied impact energy for different MWCNTs wt.% concentrations. It is observed that the peak value of $\Delta R/R_0$ increased with increasing impact energy level, and with a statistically significant difference (P-value < 0.05). Further, the self-sensing composites with higher MWCNTs content exhibit lower values of $\Delta R/R_0$ than those with low MWCNTs concentrations. For instance, the $\Delta R/R_0$ values at 36J impact energy are 0.51, 0.56, 0.63, and 0.74 for samples containing 2.0, 1.5, 1.0 and 0.5 wt.% of MWCNTs respectively. Similar trends, as shown in Figure 4.9d, occur for the other wt.% MWCNTs concentrations.

The smaller value of $\Delta R/R_0$ for samples with high MWCNTs content may be due to the potentially higher electrical conductivity of the sample. Using a high MWCNTs concentration leads to a reduction in the distance between the MWCNTs so improving electron transfer (conduction). As a consequence, the electrical resistance decreases [11]. Therefore, when an impact load is applied, the amount of damage to the existing conduction pathways due to the MWCNTs within the matrix will be less when compared to low MWCNTs concentration.

Interestingly, it should also be noted that the self-sensing specimen containing a high MWCNTs concentration showed a less permanent change to the electrical resistance when compared to a low MWCNTs concentration. This can be expressed by an electric damage parameter (λ) as shown in Figure 4.9c. The electric damage parameter (λ) is a measure of the damage in the composite left after impact. This is indicated by the permanent changes in the residual resistance of the structure above the initial level.

This parameter is useful to assess the degree of structural damage after impact. This will be explained in more detail in the next section.

4.1.6 An in-situ Evaluation of Changes in Electrical Resistance

The on-line structural health monitoring, *in-situ*, is still a critical issue for important applications such as energy generation, aerospace and nuclear installations. Therefore, the main objective here is to develop a simple method to detect the real-time damage of structures by monitoring changes in electric resistance during impact or other damage situations. By using this principle, the self–sensing of a MWCNTs-GE nanocomposite has been investigated to predict the internal damage, which occurs during impact loading. Figure 4.10 shows the relationship between the electric damage parameter (λ) for samples sustaining different impact energies as a function of MWCNTs concentration. The magnitude of (λ) was obtained from Figure 4.9c, and the same approach was used to achieve this for other samples in Figure 4.9a, b. It can be seen that all samples showed an almost linear reduction in the electric damage parameter (λ) as the MWCNTs concentration increased with this being dependent upon the impact energy used. For example, at the lowest impact energy (12J), the electric damage parameter (λ) decreases by about 95% as the MWCNTs concentration increases from 0.5 to 2.0 wt.%. For the highest level of impact energy (36J), the value of λ decreases by only 34% as the MWCNTs concentration increases from 0.5 to 2.0 wt.%. Thus, it can be seen that the self-sensing sample which contained 2.0 wt.% of MWCNTs showed a lower value of λ under all impact energies levels. By applying Tukey's multiple comparison test to all impact energies, the results are shown in table below Figure 4.10. The Tukey test is a statistical test used to determine if the relationship between two sets of data is statistically significant [143]. The statistical calculations show a significant difference (i.e. P-values <0.05) in terms of electrical

damage parameter (λ) for all impact energies. Therefore, in summary, those self-sensing samples, which contain high concentrations of MWCNTs, will be less sensitive to damage incurred during impact events.

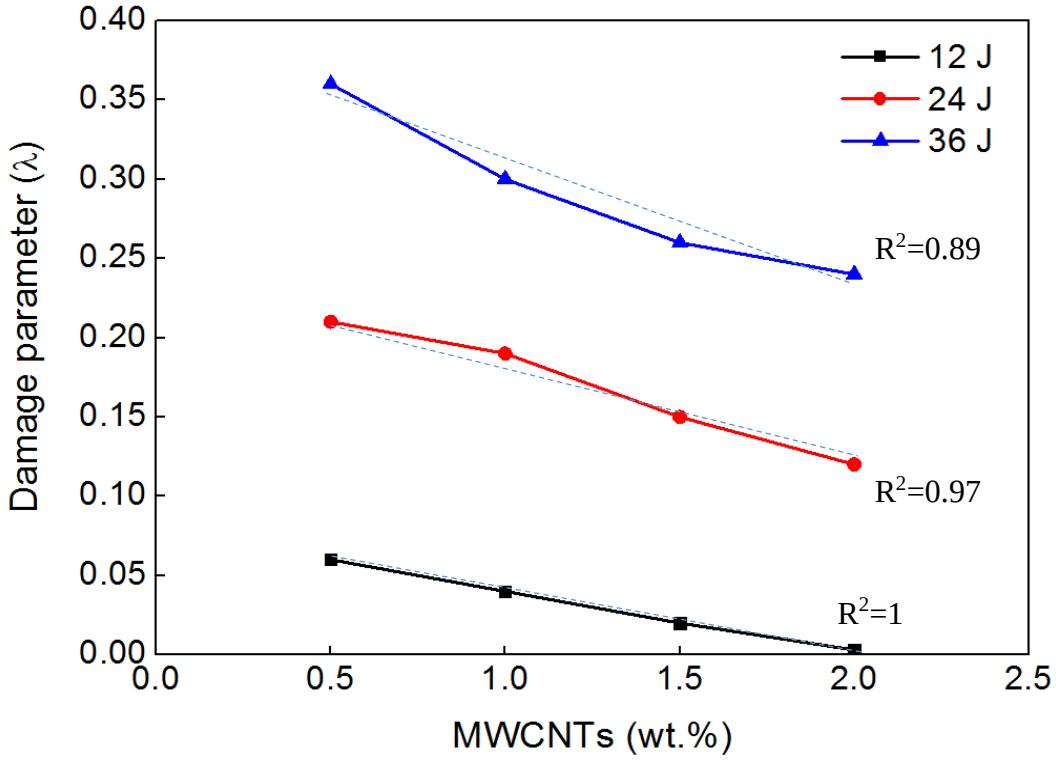

Tukey's multiple comparison tests	P- value	95% CI of difference	Summary
12 J vs. 24 J	0.008	0.092 to 0.142	<0.01
24 J vs. 36 J	0.046	0.041 to 0.048	<0.05
36 J vs. 12 J	0.002	0.180 to 0.270	<0.01

Figure 4.10: Graph to show the variation in the electrical damage parameter (λ) for self-sensing composites containing different MWCNTs concentrations for different impact energies. The table below the graph explains the statistical analysis results.

Other studies have also showed this to be the case. For example, Ku-Herrera *et al.* [11] used different concentrations of CNTs as an additive to fabricate a smart composite. They measured the sensitivity of the resulting composite under tensile loading conditions. It was found that with decreasing the CNTs content, the sensitivity of the

smart composite to damage increased linearly. Yin *et al.* [144] added different concentrations of MWCNTs to epoxy resin to fabricate a self-sensing composite. Here the testing of the samples was tensile and compressive under both static and cyclic conditions. They reported that the samples containing high concentrations of MWCNTs showed less ability to sense the damage incurred during both types of tests. However, the results obtained in the present study showed the lowest damage parameter (λ) to occur at 2.0 wt.% of MWCNTs. Therefore, samples containing 0.5, 1.0, and 1.5 wt.% of MWCNTs were only those considered for the following evaluation method.

4.1.7 Damage Factors and Damage Sensitivity

From the experimental results obtained during this study, it can be noted that there is a relative relationship between the damage parameter (λ), obtained during impact testing, and the damage factor (ψ), which was a measure of the absorbed energy during testing. This can be expressed as follows;

$$\lambda \propto damage\ factor(\psi) \tag{4.3}$$

Figure 4.11 shows the relationship between the electrical and mechanical damage following impact testing for the self-sensing samples containing different MWCNTs concentrations.

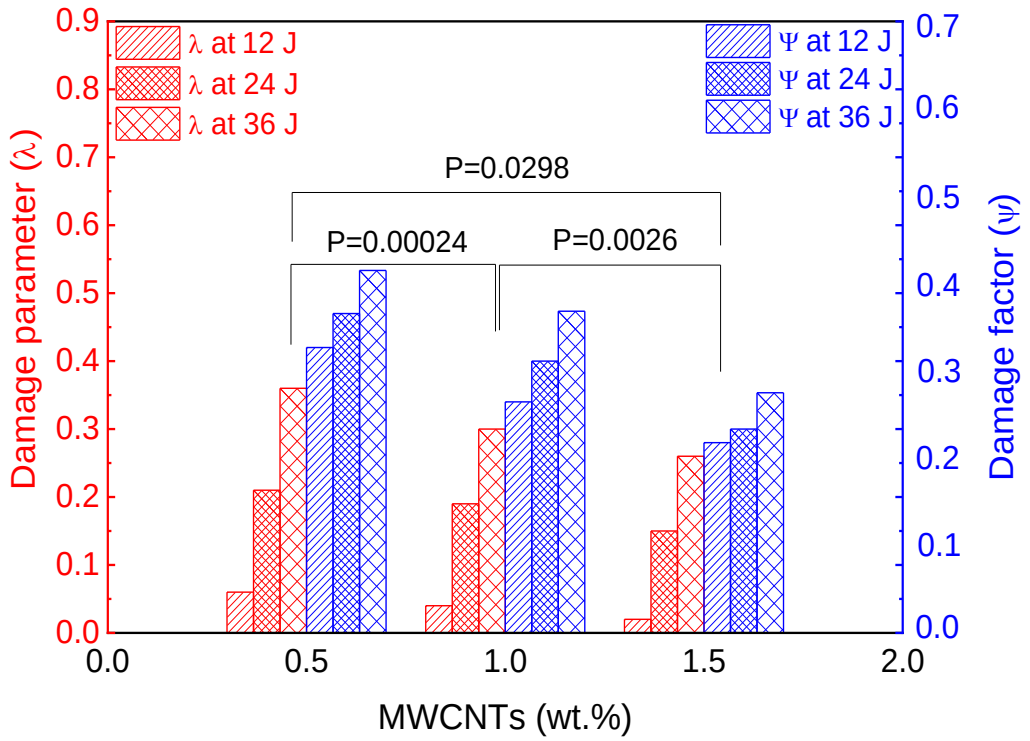

Figure 4.11: The relationship between the damage parameter (λ) and the damage factor (ψ) for self-sensing composites containing different MWCNTs concentrations for different impact energies.

It is clear that, for all impact energies, both the mechanical damage factor (ψ) and the electrical damage parameter (λ) are both significantly decreased with increasing MWCNTs concentration. For example, at 36J the damage factor (ψ) decreases from 0.53 to 0.35 (≈ 33.9%) and the electrical damage parameter (λ) by ≈ 27.7% from 0.36 to 0.26 as the MWCNTs concentration increases from 0.5 to 1.5%. Moreover, at low impact energy 12J, the mechanical damage factor ψ decreases by ≈ 33.3% from 0.42 to 0.28, and the electrical damage parameter λ decreases by ≈ 66% from 0.06 to 0.02 as the MWCNTs concentration increases. In addition, it can also be noted that there are statistically significant differences between the different concentration groups. For instance, the relation between the damage factor (ψ) and the damage electrical parameter (λ) show a significant difference (i.e. P-value <0.05 and < 0.01) when the

MWCNTs concentration increases from 0.5 to 1.0 wt.% and from 1.0 to 1.5wt% respectively. Finally, it was observed that the incorporation of higher concentration of MWCNTs, such as 1.5 wt.% within the nanocomposite's matrix, led to a significant difference (P-value < 0.001) in comparison with lower MWCNTs concentration (0.5wt.%). This improvement could indicate the most effective homogenous MWCNTs distribution within the matrix (Figure 4.4) as well as the strongest interfacial bonding condition between the MWCNTs and the matrix between the fibre layers as shown in Figure 4.4c

Based on these results, it can be observed that the damage parameter and damage factor are fully dependent on the concentration of the MWCNTs in addition to the impact energy. At lower MWCNTs concentration, the distance between CNT- CNT (i.e. tunnelling distance) [145] is high and this distance increased due to the fracture of composite matrix caused by the impact load. In this case, the conducting electrons cannot pass easily between them. As a consequence, the overall specimen resistance increases. Further, the electrical resistance of specimen after impact (R_2) can be assumed by;

$$R_2 = R_0 + \Delta R_{\text{tunneling}} \tag{4.4}$$

where R_0 is the specimen's resistance before impact and $\Delta R_{\text{tunnelling}}$ is the change in resistance (after impact) for the tunnelling distance between CNT-CNT. According to the tunnelling theory (This is defined as a quantum mechanical phenomenon where a subatomic particle passes through a potential barrier) [146], the tunnelling resistance before impact is given by;

$$R_{tunnel} = \frac{h^2[d]}{Ae^2\sqrt{2m\beta}} \exp\left(\frac{4\pi[d]}{h}\sqrt{2m\beta}\right) \quad (4.5)$$

Where e is the electron charge, m is the electron mass, h indicates the Planck's constant, β is the energy barrier (for the epoxy matrix, 0.5 eV~2.5 eV [59], and A is tunnel cross-sectional area and d is the space between neighbouring MWCNTs. Similarly, after impact, the distance between every adjacent MWCNTs will alter due to the damage in the MWCNTs network. Therefore, tunnelling resistance after impact will be assumed as;

$$\Delta R_{tunnel} = \frac{h^2[d+\Delta d]}{Ae^2\sqrt{2m\beta}} \exp\left(\frac{4\pi[d+\Delta d]}{h}\sqrt{2m\beta}\right) \quad (4.6)$$

It can be noted that the tunnelling resistance is strongly dependent on both the tunnelling distance (i.e. d) and the energy barrier of the matrix (e). Therefore, by combining Eq.(4.6) with Eq.(4.4) an equation for $\lambda = (R_2\text{-}R_0)/R_0$ can be obtained as;

$$(R_2 - R_0)/R_0 = (\lambda) = \left(1 + \frac{h^2[d+\Delta d]}{Ae^2\sqrt{2m\beta}} \exp\left(\frac{4\pi[d+\Delta d]}{h}\sqrt{2m\beta}\right)\right)/R_0 \quad (4.7)$$

Eq. (4.7) also shows that a clear relative relationship exists between the distance between CNTs and the electrical damage parameter (λ). Additionally, Figure 4.12 shows the relationship between the absorbed energy and the electrical damage parameter (λ) as a function of MWCNTs concentration.

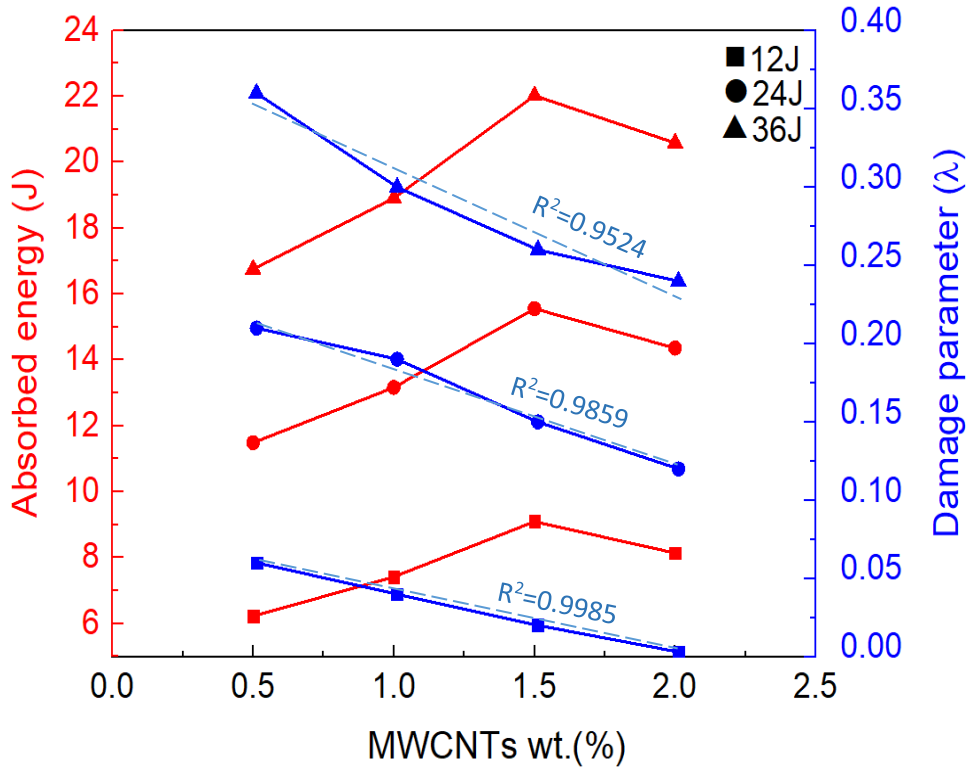

Figure 4.12: The representative relationships between the absorbed energy and the damage parameter (λ) for self-sensing composites containing different MWCNTs concentrations subjected to different impact energies.

It can be seen that the damage parameter (λ) is inversely proportional to the impact energy absorbed when the content of MWCNTs was increased up to 1.5 wt.%. Up to this concentration, the following relationship applies;

$$\lambda \propto \frac{1}{absorbed\ energy} \tag{4.8}$$

However, this relationship between the electrical damage parameter (λ) and the absorbed energy no longer applied when the MWCNTs content further increased to 2.0 wt.%. The observed reduction in the absorbed energy was due to the agglomeration as described earlier and as shown in Figure 4.4d. The agglomeration can produce stress concentration zones within the nanocomposite matrix and this issue makes the matrix

too weak to bear the impact loads [147]. Therefore, the agglomeration of the MWCNTs is considered a critical issue (limitation to detection) for this evaluation method. So, in this study, the suggested criterion is only used when the MWCNTs are well distributed within the nanocomposite matrix as shown in Figure 4.4b. Therefore, when the relation in Eq.10 and Eq.4 are placed into Eq.11, the expression will be;

$$\left(1+\Delta R_{tunnel}=\frac{h^2[d+\Delta d]}{Ae^2\sqrt{2m\beta}}\exp\left(\frac{4\pi[d+\Delta d]}{h}\sqrt{2m\beta}\right)\right)/R_0=\frac{2\times C}{m\times(v_i^2-v_r^2)} \qquad (4.9)$$

Where C is a constant which depends on the concentration of the MWCNTs within the nanocomposite and the impact velocity. This evaluation method model provides an opportunity to determine the degree of damage sustained after impact for the in-service self-sensing of the composite material without the need for inspection equipment. Therefore, aircraft pilots or technical engineers in other industries will be able to evaluate in real-time, if a structure is at risk or is safe, by monitoring the magnitude of the changes in electrical resistance.

Furthermore, the damage sensitivity of the self-sensing composite material to changes in electrical resistance after being subjected to an impact event can be identified by the following relationship;

$$\text{Damage sensitivity}=\frac{\text{damage in electrical resistance }(\lambda)}{\text{impact energy (J)}} \qquad (4.10)$$

Figure 4.13 shows the damage sensitivity of the self-sensing composite to different impact energies for different MWCNT concentrations. It can be observed that the self-sensing samples, which contained the lowest concentration of MWCNTs, showed the

highest sensitivity to damage when compared to those which contained a high MWCNTs concentration. Also, the influence of the impact energy on the damage sensitivity was investigated using three different impact energies. The samples with the highest impact energy (36J) showed the highest damage sensitivity ($0.01J^{-1}$) at 0.5% of MWCNTs, which is nearly 1.2 and 1.39 times higher than these samples at the 1.0 and 1.5 wt.% of MWCNT concentrations respectively.

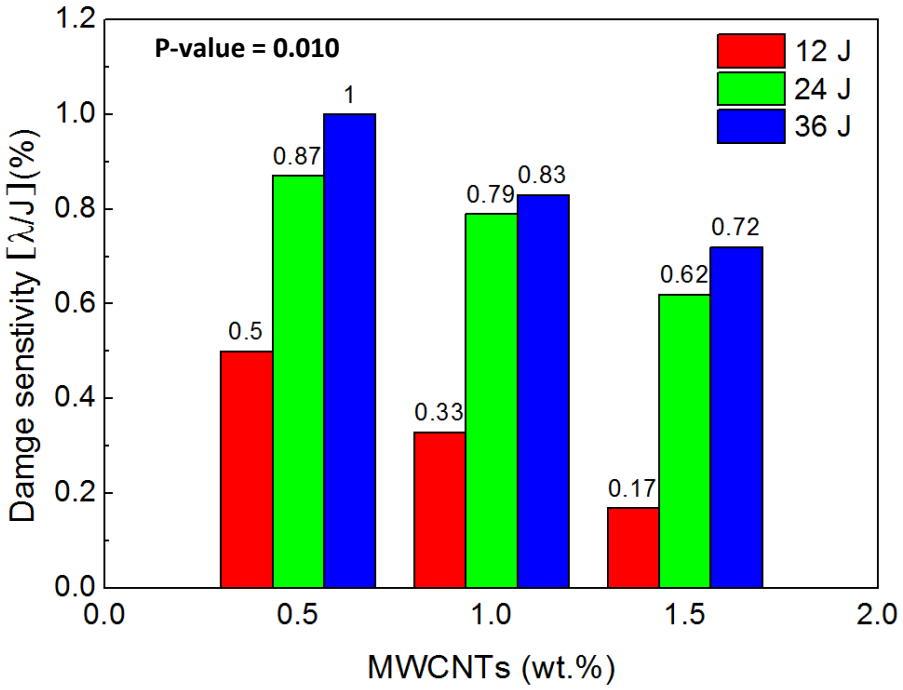

Figure 4.13: Damage sensitivity of electric resistance under impact energies vs MWCNTs concentration.

In order to study the statistical significant of the damage sensitivity results, the differences among the three concentrations of MWCNTs (0.5, 1.0 and 1.5%) undergoing the varied impact energies were calculated. A high statistical significant difference was observed in the given results (i.e. the P-value is lower than 0.05). This can be explained as follows; when impact occurs, many micro-cracks develop in the matrix materials in different locations. This causes a high level of distortion in the

MWCNTs conductive networks. This distortion in the MWCNTs conductive networks leads to an increase in the average distance between the CNT-CNT. Thus, the fewer contacts between the MWCNTs contribute to reducing the number of conductive pathways available. This may be the reason why the self-sensing composites containing low MWCNT concentrations exhibit the highest sensitivity to impact.

4.1.8 Time Response and Stability of the Method

To investigate the response time for this method, from Figure 4.9a, b and c, the experimental results are summarized in Table 4.2. By calculating the response time to peak as well as the decay time required to approach a steady state level the total response time can be considered. From the table, it can be speculated that the total response time (a period time starting from the beginning of impact, approaching the peak and then decaying down to the steady state level as shown in Table 4.2), decreases with increasing the MWCNTs concentrations. This is likely due to the high number of possible contacts between MWCNTs, which lead to a rapid decrease in specimen's resistance. However, this total time period increased as the impact energy increased due to greater damage in the self-sensing nanocomposite specimen's matrix.

The reliability (i.e. in terms of operation stability) of any developing method is necessary to its acceptance. Therefore, in this study, the stability of this method was studied as a function of time by repeating the impact energy three times on the same specimen.

Table 4.2: Response time to peak and decay time to steady state level for self-sensing nanocomposites containing different concentrations of MWCNTs subjected to varied impact energies. The diagram below the table indicates the behaviour of the impact test in term of time response.

Impact energy (J)	Response time (ms)	Wt. % of MWCNTs			
		0.5	1.0	1.5	2.0
12	R	3.0	2.6	2.5	2.4
	D	16	7.4	7.1	4.6
	Total	19	10	9.6	7.0
24	R	7.5	7.0	8.0	7.5
	D	22.5	25.6	21	14.5
	Total	30	32.6	29	22
36	R	11	10.7	10	9.0
	D	27	25	23	18
	Total	38	35.7	33	27

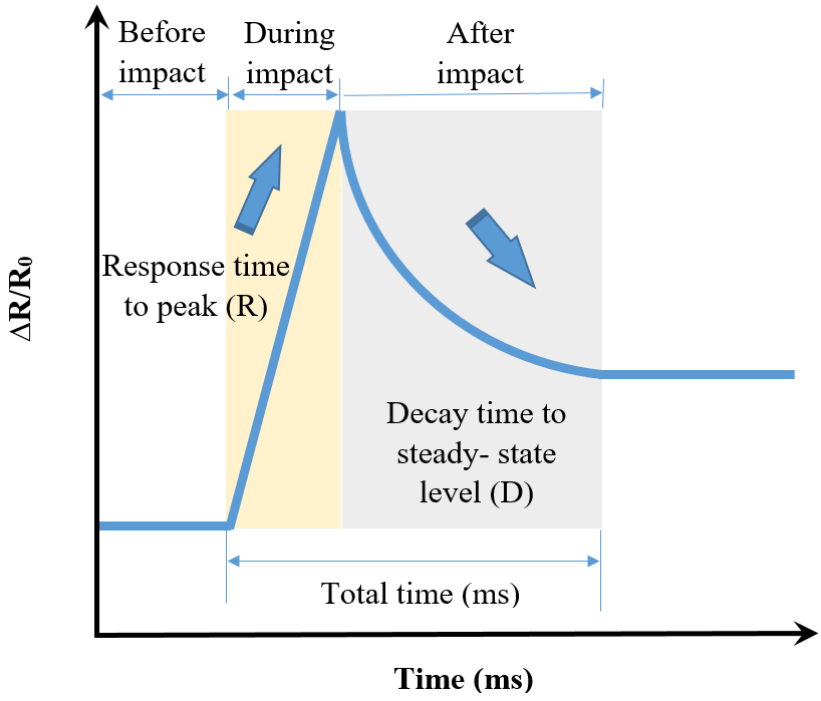

Figure 4.14 shows the effect of repeated impact test on the changing in electrical resistance of the self-sensing nanocomposite specimens containing different MWCNTs concentrations. It can be observed that both the peak of the resistance changes ($\Delta R/R_0$) and electrical damage parameter (λ) increase with the repeated impact energy. These permanent changes in resistance occurred after each impact are due to the distortion in the MWCNTs conductive pathways. Regarding the statistical

analysis, the graph in Figure 4.14 shows that there are statistically significant differences (rising peaks) between the three repeated impacts test in terms of the changes in electrical resistance $\Delta R/R_0$, (p-value < 0.01), and the electrical damage parameter λ, (p-value < 0.05). These changes in values come from the continuous distortion of the MWCNTs networks inside the nanocomposite because of the repeated impacts on the specimen.

Details of the statistic results are shown in Table 4.3. In the fourth column, the 95% confidence interval (CI) is for the mean difference values of the comparison between the each impacted pairs test is given.

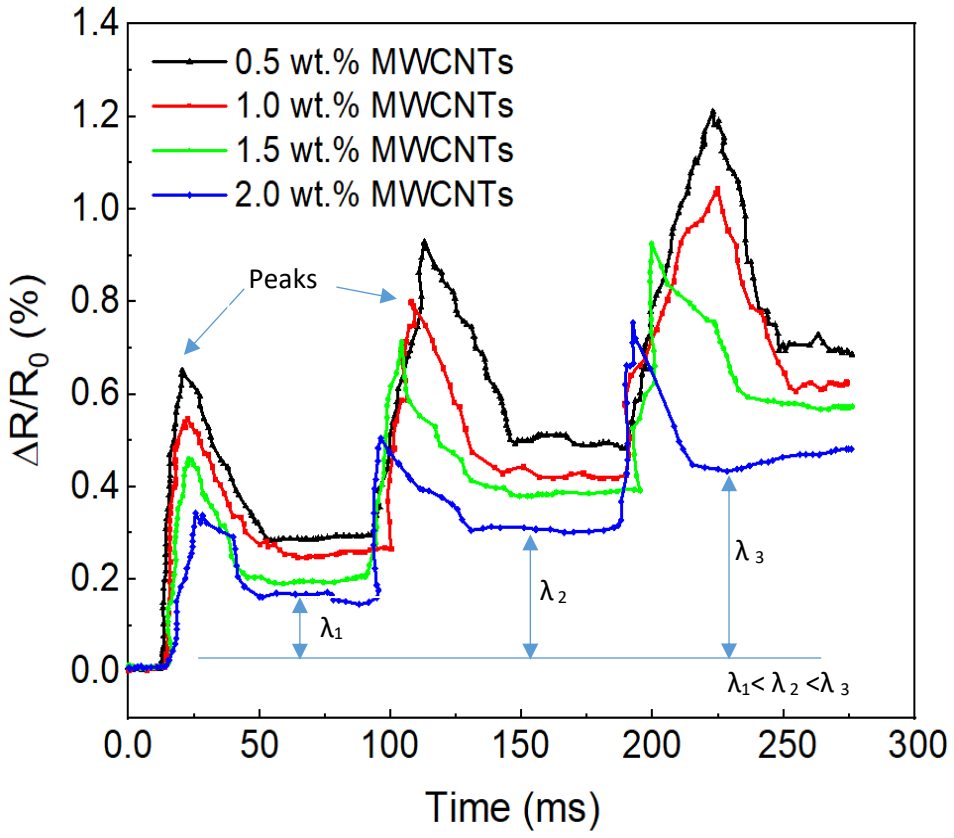

Figure 4.14: Fractional change in normalised resistance ($\Delta R/R_0$) as a function of time during three times repeated (24J) impact tests for self-sensing nanocomposites filled with different

Table 4.3: Comparison summary for all MWCNTs concentrations undergoing three repeated impact tests.

Changes	Tukey's multiple comparison tests	P- value	95% CI of difference	Summary
In Peaks	First impact VS. second impact	0.0088	-0.219 to 0.343	< 0.01
	Second impact Vs. third impact	0.0093	-0.142 to 0.533	< 0.01
	Third impact VS. first impact	0.00059	0.170 to 0.327	< 0.001
In (λ)	First impact VS. second impact	0.033	-0.193 to 0.347	< 0.05
	Second impact Vs. third impact	0.023	-0.352 to 0.405	< 0.05
	Third impact VS. first impact	0.012	-0.416 to 0.597	< 0.05

4.2 The Electromechanical and Temperature Dependent Behaviour of Composites contaning MWCNTs

4.2.1 Mechanical Properties

The excellent mechanical properties possessed by carbon nanotubes ($E \leq 1.4$ TPa, $\sigma_{TS} \approx 63$ GPa), and their very high aspect ratio ($L/D \approx 5000$), make them an ideal reinforcing material for multifunctional nanocomposite materials [148, 149]. The results obtained here, during compression testing, are shown in Figure 4.15.

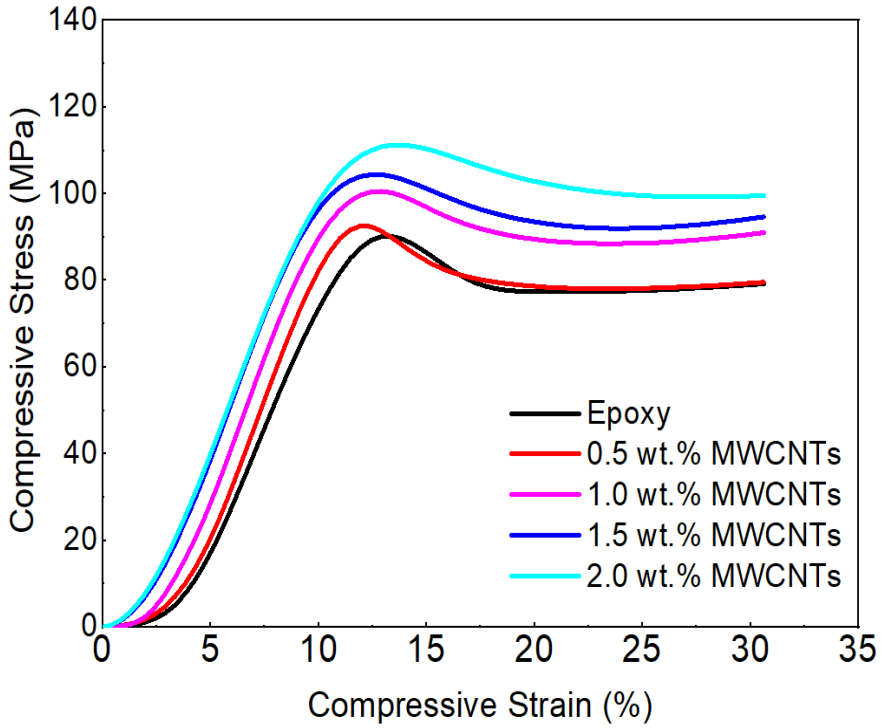

Figure 4.15: Compressive stress-strain relationship for nanocomposite.

The stress- strain curves show approximately linear behaviour between stresses in the range 20 ~ 70 MPa was reached beyond this, nonlinear behaviour can be seen. It can also be noted that both the compressive strength and modulus of elasticity are directly proportional to the weight % content of MWCNTs, each showing an increase with increasing weight %. However, at higher concentrations agglomeration can also have an influence, due to a possible saturation effect beyond 1.5 wt.%. The maximum compressive strength and the modulus of elasticity reached during testing in this study were 110 MPa and 3.85 GPa respectively as shown in Figure 4.16. It should be noted that the results of this three tests conducted (see chapter 3) were very similar. These were seen to occur at a 2.0 weight % MWCNTs concentration. These enhanced properties are most likely due to the homogenous nature of the distribution of the MWCNTs observed in the matrix material as compared with unmodified epoxy, as shown in Figure 4.17 (a,b). This even distribution provides for effective load transfer, and an entanglement effect, across the interface between matrix and the reinforcing MWCNTs during loading [150]. In effect, the presence of the carbon nanotubes can delay the onset of permanent plastic deformation until a higher stress level is reached. This increases the strength of the nanocomposite [151].

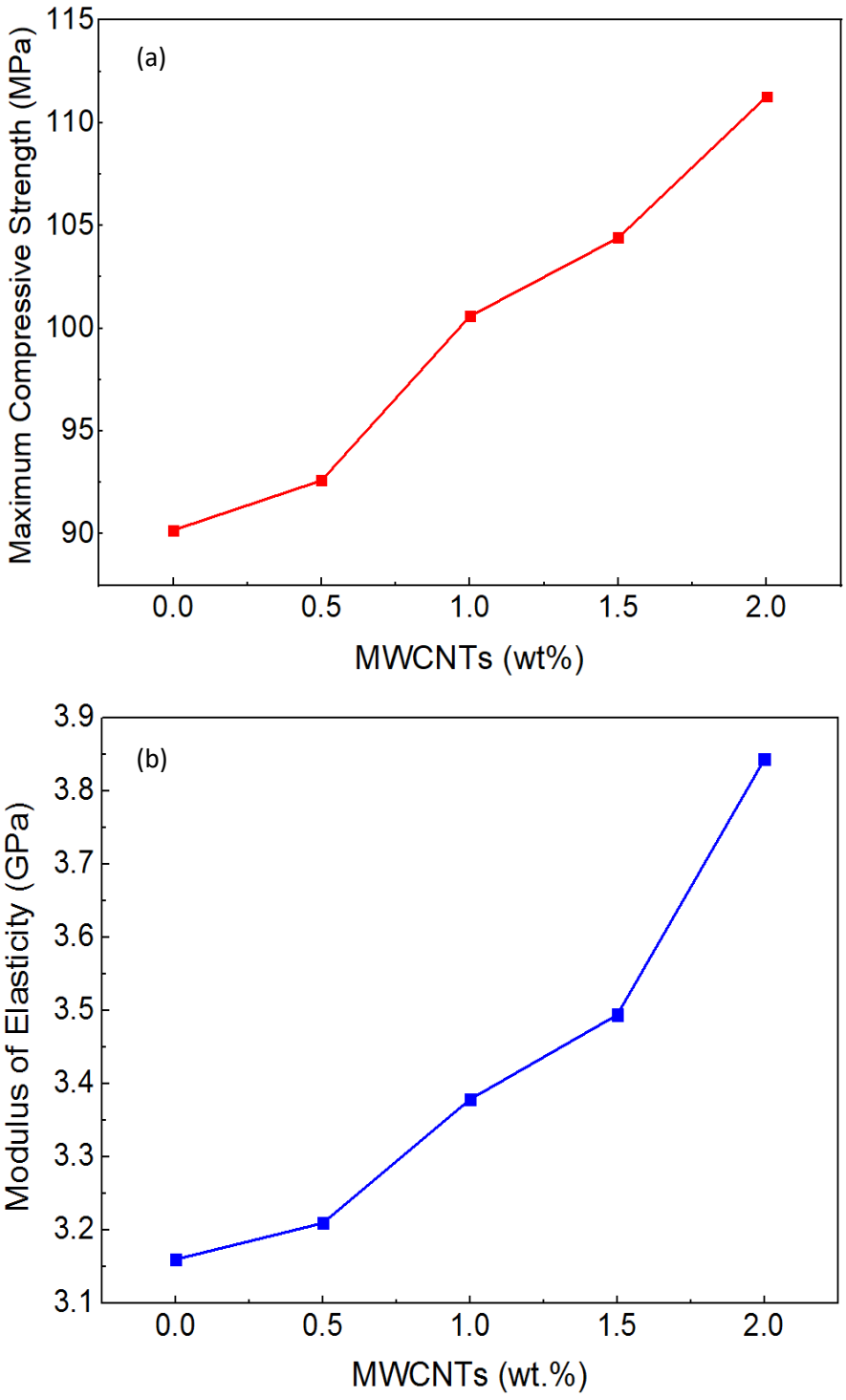

Figure 4.16: Maximum compressive properties as a function of MWCNTs content, (a) strength and (b) elastic modulus.

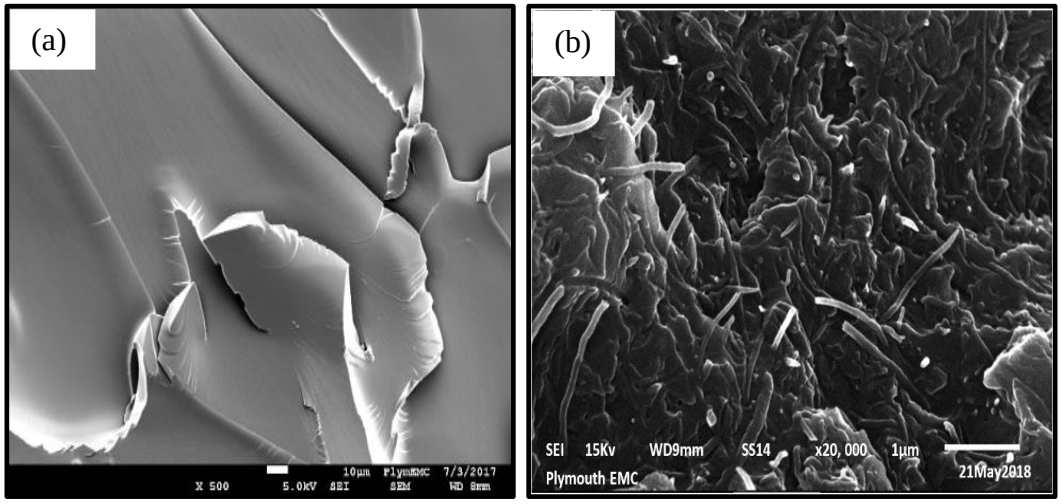

Figure 4.17: SEM images of (a) pure epoxy and (b) nanocomposite with 2.0 wt.% MWCNTs.

4.2.2 Electrical Conductivity

The electrical conductivity measurements for the MWCNTs/epoxy nanocomposites are shown as a function of weight % MWCNTs concentration in Figure 4.18. Here it is also necessary to determine the electrical percolation threshold (EPT), i.e. the minimum weight % of MWCNTs content in the matrix after which no significant change in the electrical conductivity was observed. It can be seen here that a significant increase, after the EPT has been passed, in the electrical conductivity was observed when the concentration of MWCNTs increased from 0.1 weight % to 0.5 weight %. Thereafter the observed change in conductivity, up to 2.0 weight % MWCNTs, was more gradual. To do this the statistical power law equation $\sigma = \sigma_0 (w-w_c)^t$ was used to find the critical percolation threshold of the electrical conductivity (w_c). Here, σ, σ_0, w and t are the composite`s electrical conductivity, scaling factor, filler weight fraction and critical exponent, respectively. This equation applies when $w > w_c$. The experimental data were analysed using a log-log plot of the filler concentration versus electrical conductivity as shown in (Figure 4.18 inset).

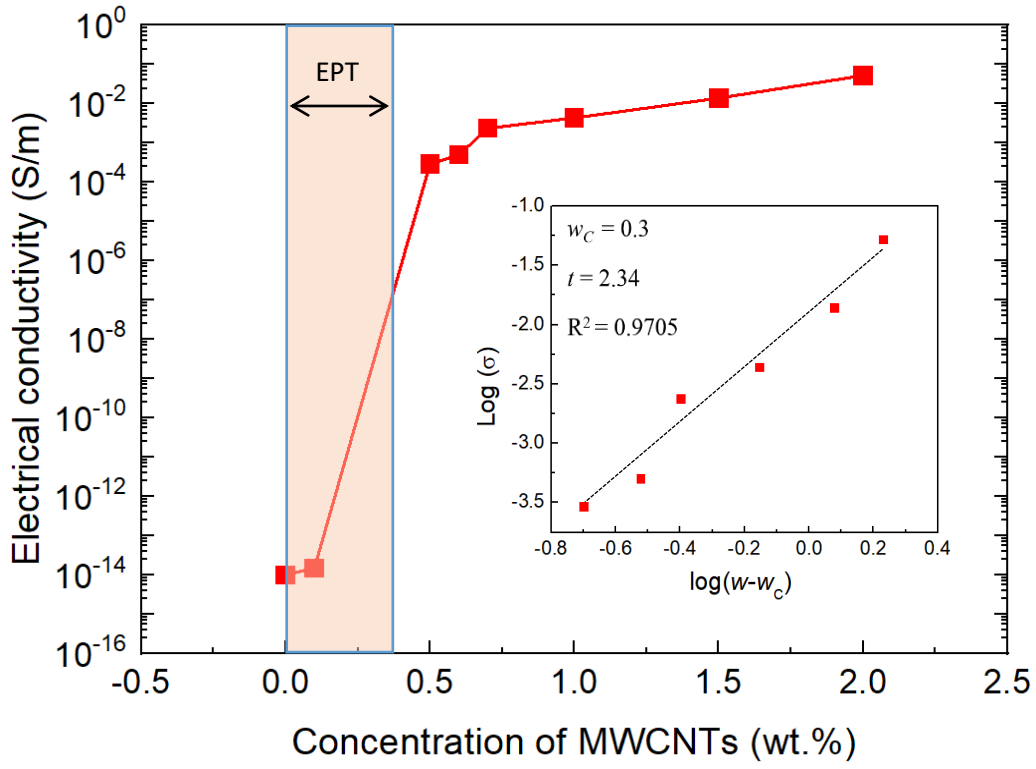

Figure 4.18: Electrical conductivity of MWCNTs/epoxy nanocomposites as a function of MWCNTs concentration. The inset shows the log-log plot of the nanocomposite electrical conductivity as a function of (w-w_c) with a linear fitting.

By altering the value of w_c, the best linear fit (using regression analysis) was obtained. The fitting results showed that t and w_c of MWCNTs had the values of ~2.34 and 0.3 wt. %, respectively.

Here, since to the obtained value of t being between 1.5-2.5, then this indicates that the MWCNTs conductive networks are deformed in a three-dimensional manner inside the nanocomposite matrix [54]. Moreover, the lower (EPT) value of MWCNTs nanocomposite is attributed to a good distribution of MWCNTs inside the matrix [152], as shown in Figure 4.17. In the present study, the maximum electrical conductivity of MWCNTs/epoxy composite reached was 5.25×10^{-2} S/m, and this occurred at 2.0 weight % MWCNTs. The observed increased in conductivity of the nanocomposite is most likely due to a well-developed MWCNTs network

structure (conducting pathways) created within the matrix material [80, 82, 89, 153]. At low concentrations of MWCNTs, the distance between adjacent MWCNT's is relatively large and this decreases as the concentration increases. As a consequence, the effectiveness of electron transfer (i.e. current flow) between the MWCNT's is very highly dependent on this MWCNTs spacing distance. With higher concentrations of MWCNTs the ease by which electron transfer occurs is considered [80] to be enhanced by way of a tunnelling mechanism.

4.2.3 Electromechanical Response

4.2.3.1 Under Monotonic Load

The piezo-resistive response of different samples, with different weight % content of MWCNTs, was tested in order to ascertain the sensitivity of the MWCNT/epoxy nanocomposite. Figure 4.19 shows the normalised change in resistance ($\Delta R/R_0$) which occurred when the nanocomposite was subjected to mechanical compression until it fractured. It can be seen that the piezo-resistive behaviour all samples was nonlinear. Regardless of the concentration of MWCNTs present, an increase in the resistance, with increasing compressive strain under the load, occurred. This piezo-resistive behaviour is similar to that observed by Yin *et al.* [144].

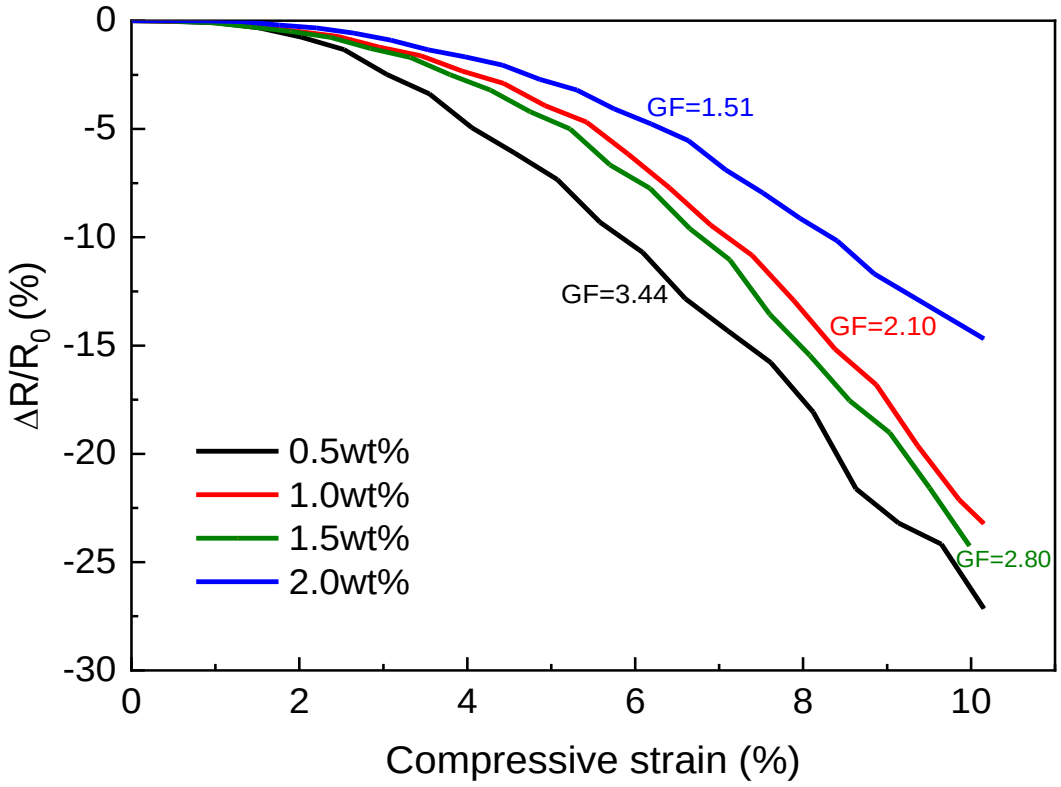

Figure 4.19: Normalised change in resistance as a function of applied compressive strain at 20 °C.

This behaviour is clearly dependent upon the MWCNT concentration, with the 0.5 weight % MWCNTs/epoxy nanocomposite showing the greatest change in the normalized change in resistance.

It has been suggested [80] that this type of response is due to the lower MWCNT concentration present. With lower concentration levels, the resistance to the charge tunnelling between the adjacent MWCNTs becomes more dominant, due to an increase in the inter-particle spacing. Similar results were observed by Shen *et al.* [82] and Yin *et al.* [144]. In addition, the strain sensitivity (GF), as defined by equation (3.4), is also dependent upon the MWCNT concentration. Using this equation to evaluate the strain sensitivity (GF) for all samples, it can be seen in the Figure 4.19, that the GF values increased when the concentration of the MWCNT is decreased, for

example it was 3.44 at 0.5 wt.% of MWCNTs, which is ≈ 128% greater than 2.0wt.% of MWCNTs content. Therefore, the magnitude of the strain sensitivity may depend on the concentration of MWCNTs present in the nanocomposite. Many nanocomposite based studies [59, 80, 81, 154, 155] making use of CNTs have reported similar findings. So here, it can be concluded that as the MWCNT content increases, so the resistance of the resulting nanocomposite is reduced, so decreasing the strain sensitivity, as shown in Figure 4.19. This could be due to the increasing CNTs, content decreasing the inter-particle distance between adjacent CNTs thus allowing the potential for greater possible contact between them. As a consequence of this, a reduction in the resistance will be seen. For this reason, at lower MWCNTs concentrations the electrical resistance of the nanocomposite material appears to be much more sensitive to strain [81].

4.2.3.2 Under cyclic load

With regards to the electromechanical response under cyclic loading conditions, Figure 4.20 a, b shows the absolute values of the measured changes in the normalised change in resistance ($\Delta R/R_0$) for the MWCNT/epoxy nanocomposite specimens when they were subjected to cyclic compressive loading. It can be seen that the change for all the samples, although alternating between zero and a maximum value, was relatively linear and showed excellent correspondence with the changes in the applied compressive strain as shown in blue in Figure 4.20 a for 2.0 wt. % of MWCNTs sample, respectively. From this observation, it can be concluded that the changing normalised resistance is directly related to the changing strain. This decreasing and increasing in electrical resistance during the compressing and subsequent releasing of the load can be ascribed to the gaps between MWCNTs as represented in Figure 4.21. This lockstep behaviour has been explained by Cao *et al.* [86] as being due to the

destruction, followed by the reforming, of the required conductive pathways between MWCNTs during the compressive cyclic loading. Additionally, the maximum values for MWCNTs/epoxy nanocomposite normalised change in resistance (%) were respectively 1.4%, 1.1%, 1.05% and 0.95% at 0.5 weight %, 1.0 weight %, 1.5 weight % and 2.0 weight % MWCNTs concentrations as seen in Figure 4.20b.

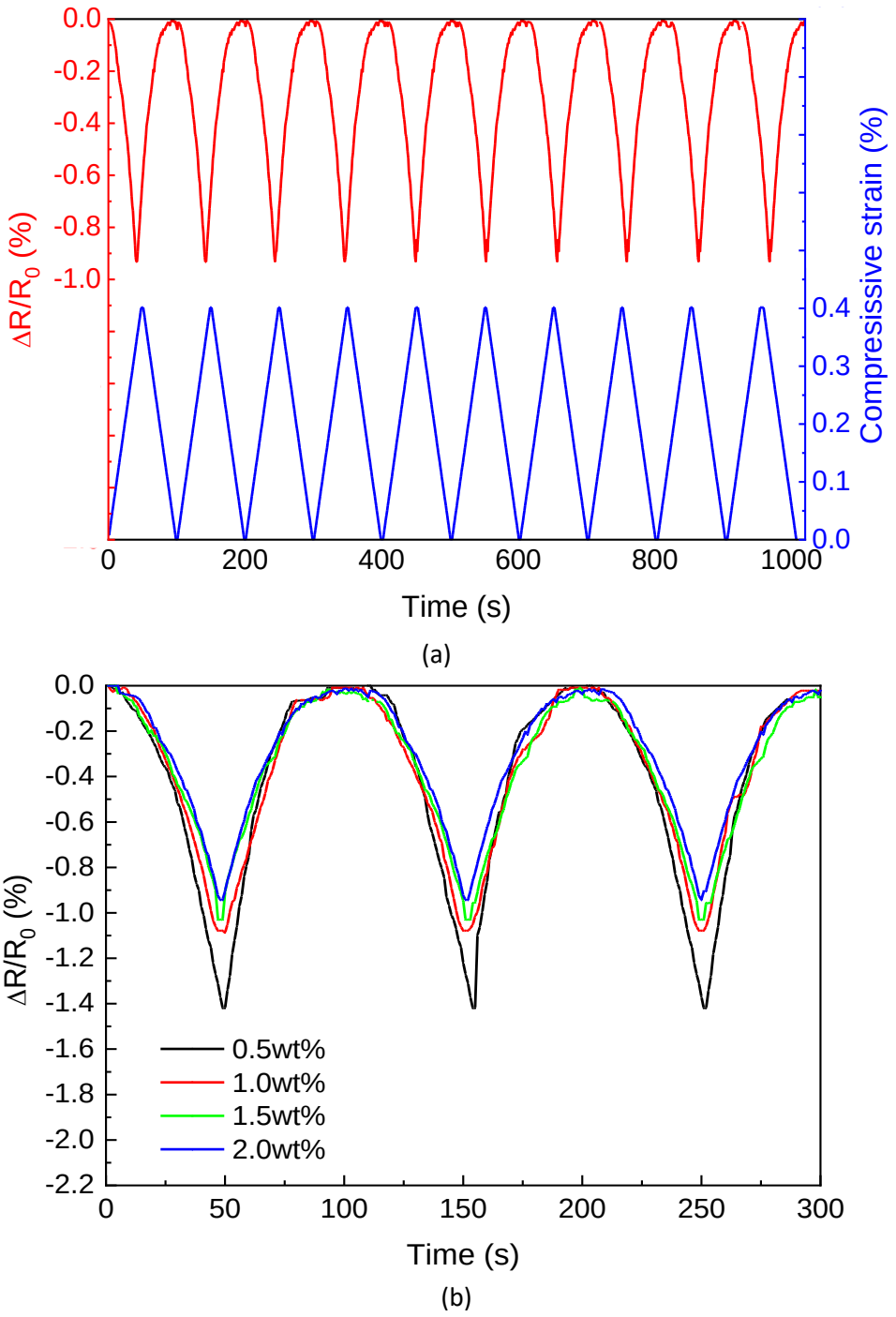

Figure 4.20: The piezo-resistive versus time response (a) ten loading cycles of 2.0 wt. % of MWCNTs, (b) maximum peak at three cycles for all samples.

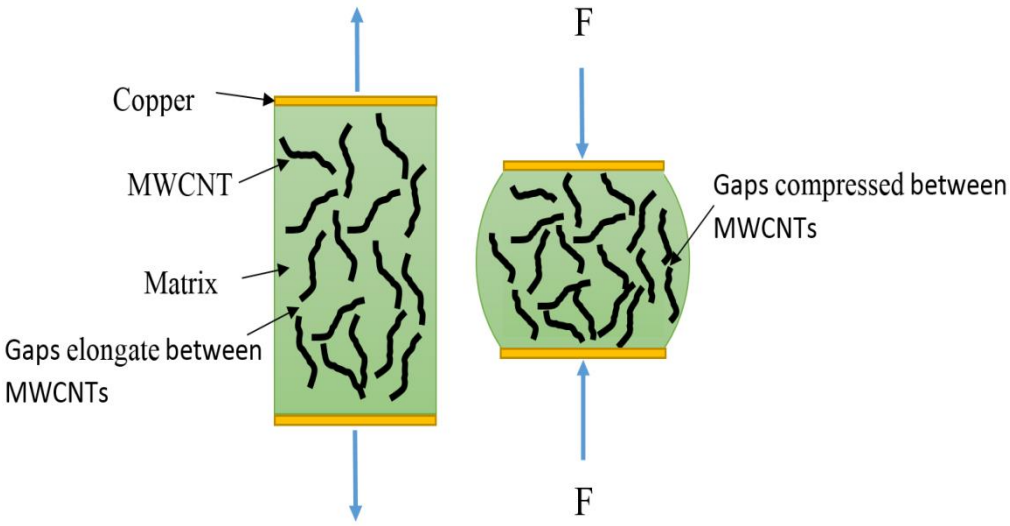

Figure 4.21: Schematic representation of nanocomposite sample under releasing and compressing load.

These results indicate that the maximum value of the normalised resistance ($\Delta R/R_0$) occurred at the lowest MWCNTs concentration. Thus, as the concentration decreases so the change in the resistance will increase. This is possibly due to the disruption caused to the potential tunnelling channels. In summary, during this type of cyclic loading, the resistance of the MWCNTs/epoxy nanocomposite shows a high degree of stability in terms of the observed piezo-resistive effect discussed. These results are comparable, and more accurate, than those obtained by [89, 144] during their study of the sensing behaviour of epoxy based CNTs subjected to compression cyclic load.

In their study Dinh *et al.* [89] observed a drift in normalised resistance during the first two cycles of five cycles when the samples were tested under cyclic compression. In addition, Yin *et al* [144], observed that the amplitude of the normalised resistance ($\Delta R/R_0$) decreased and did not return to its original level after each cycle. This was claimed to be due to hysteresis effects experienced by the nanocomposite during the compression loading.

4.2.4 Temperature Dependent Behaviour under Zero Load

It has been shown [87, 156] that temperature can affect the stability of the electrical resistance of CNTs/polymer nanocomposite materials. Consequently, this response can generate significant structural integrity issues for oil and gas pipeline structures when they are exposed to high, and varying, temperatures. Figure 4.22 shows the temperature versus normalised resistance profile in the range 20–80°C for MWCNTs/epoxy nanocomposite containing different MWCNTs concentrations but with no applied load.

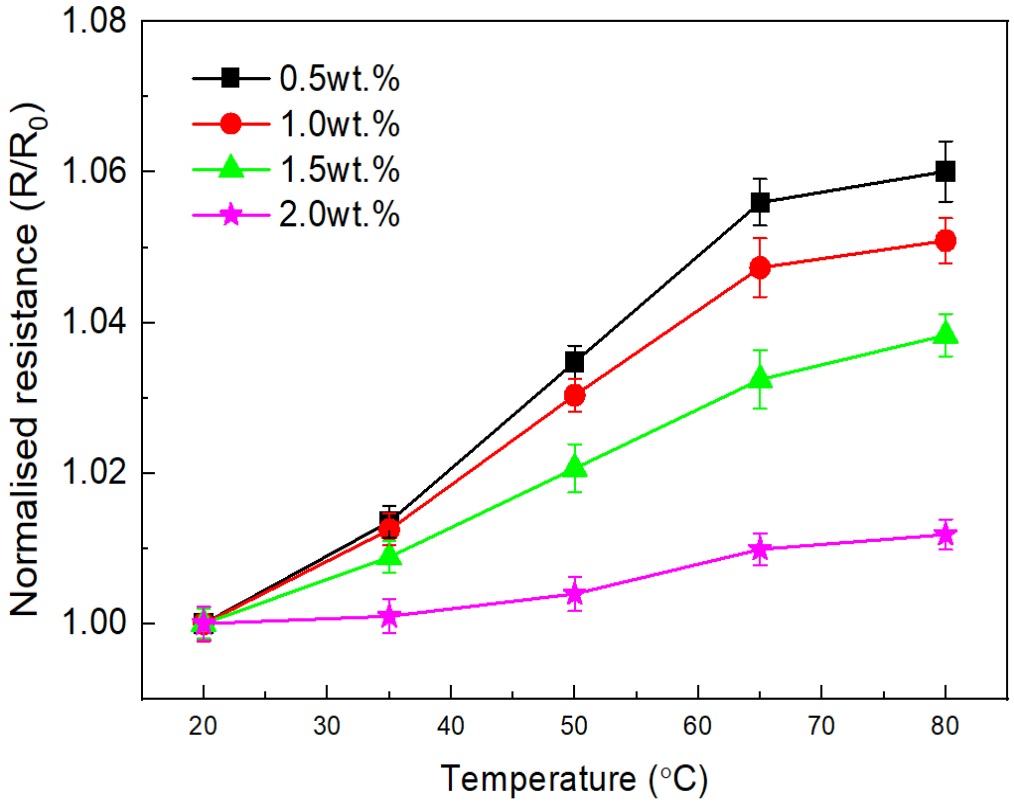

Figure 4.22: The influence of temperature on the normalised resistance of nanocomposite without load.

For each of the concentrations tested the normalised resistance was seen, as expected, to increase with increasing temperature. This increase in normalised nanocomposite resistance is due to the breakdown of MWCNTs network brought about by the

volumetric expansion of epoxy matrix as the temperature rises. These results are also observed previously by Njuguna *et al.* [157]. Further, it can be noted that the change, with temperature, in the normalised resistance for the sample with the highest MWCNTs concentration is smaller than for the lower concentration of MWCNTs. This behaviour can be associated with the better stability of the MWCNTs network structure, associated with the higher CNTs concentrations, facilitating better electron transfer through the inter-particle channels [158].

4.2.5 Temperature Dependent Behaviour during Cyclic Loading

Figure 4.23 shows the strain sensitivity (GF) for a 1.0 wt. % MWCNTs/epoxy nanocomposite obtained during cyclic compressive loading tests performed at a range of different temperatures. The values were obtained only during the first cycle of the test and are presented here for convenience against percentage strain. It can be seen that as the temperature increases from 20°C to 70°C, the strain sensitivity (GF) of the composite decreased significantly from a value of 4.33 to 1.18. This change in the strain sensitivity (GF) can be attributed to the observed behaviour of the matrix material when the tests were conducted above and below the glass transition temperature (Tg). The glass transition threshold temperature (Tg) is an important polymer property since it defines the temperature at which the polymer changes from a hard, glassy state to a more rubbery condition. Below Tg, i.e. between 20-70 °C, the strain sensitivity (GF) of the nanocomposite was reduced. However, above Tg the strain sensitivity of the nanocomposite increased sharply, reaching a value of 5.29 at 80 °C. At this temperature, above the threshold temperature (Tg), the effect on mobility of the internal structure of the nanocomposite is markedly enhanced as the material enters the rubbery stage.

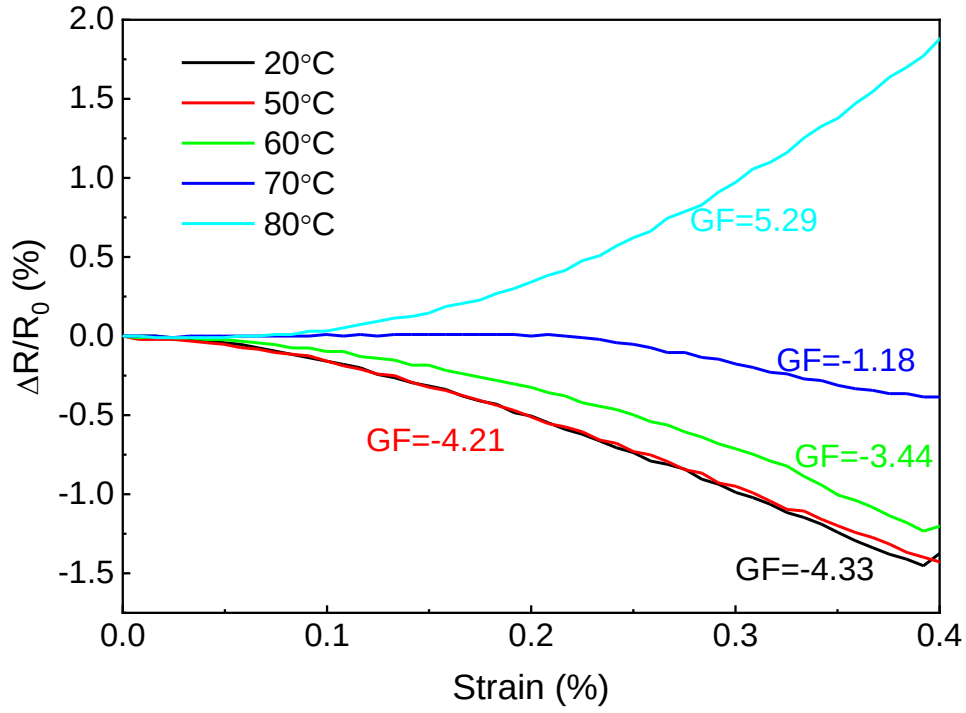

Figure 4.23: Strain sensitivity (GF) for one cycle for 1.0 wt.% MWCNTs at different temperatures.

To study the changes, which occurred in the resistance during cyclic loading of the CNT/epoxy nanocomposite, specimens were initially strained to 0.4% and then unloaded back down to zero. The resistance (R) which was calculated during the test, is presented in the Figure 4.24 as a function of time. It should be noted that when the test achieved at temperature below 70°C the value of (R) initially reduces steadily, with increasing the cyclic compressive loading, but then increases again as the load is released. Similar behaviour occurs for all five cycles. During testing the observed peaks and troughs, representing the maximum and minimum values reached, increased slightly with increasing temperature during each strain reversal. For those specimens tested between 20°C and 60°C the changes observed remained remarkably consistent in nature. However, above this temperature range those tested at 70°C and 80°C exhibited a different type of response, particularly that tested at 80°C, where the test temperature was above threshold temperature (Tg) for the nanocomposite. The

response of the material tested at 70°C appears to be in transition as the Tg threshold is crossed. This change in response above Tg can be attributed to the breakdown of the established conductive network structure present in the nanocomposite. Above the threshold temperature (Tg) for the nanocomposite, the structural changes which occur are considered to be irreversible [86, 159] due to hysteresis effects in the viscoelastic matrix material. Thus, the results obtained indicate that there are two possible modes of behaviour, with one occurring above the glass transition temperature (Tg) and the other below this temperature.

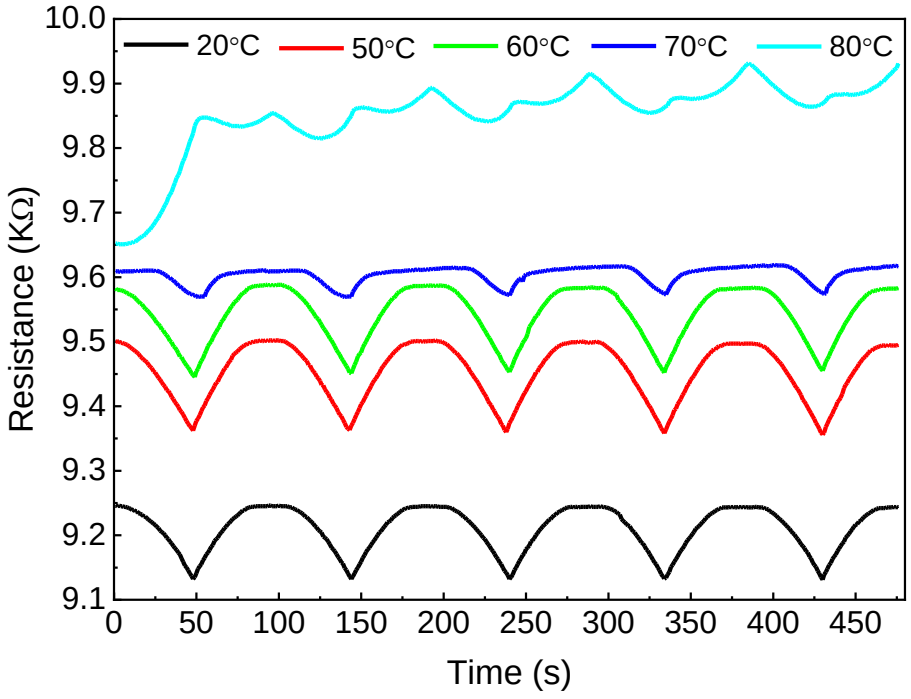

Figure 4.24: Temperature influence on the electrical resistance under cyclic load (1.0 wt. %).

For temperatures below the threshold (Tg) the response of electrical resistance (R) is seen be relatively stable and in step with the applied cyclic strain. However, above threshold (Tg) temperature the behaviour of CNT/epoxy nanocomposite changes as the observed electrical resistance steadily increases under compressive loading conditions. To understand why this happens two separate mechanisms need to be considered. Firstly, when the specimens are exposed to a higher test temperature, then

the resistance of MWCNTs/epoxy nanocomposite will naturally increase as the volume of the matrix material expands. Mohiuddin *et al.* [87] suggested that this volumetric change would increase in the spacing distance between the MWCNTs. Secondly, above the threshold (Tg) this change is further assisted by the partial breakdown of the MWCNTs network conducting pathways [89]. Taken together these two mechanisms make electron transfer within the structure more difficult, thus causing the resistance of the nanocomposite to increase.

4.2.6 Temperature Effect on the Mechanical Properties

Further evidence to support the above statement regarding the observed behaviour before and after the (Tg) threshold can be attributed to the observed visco-plastic behaviour of the material. Figure 4.25 shows the normalised behaviour of the elastic modulus of the nanocomposite over five applied strain cycles (0-0.4mm/mm) conducted at different temperatures. As expected, the normalised elastic modulus reduced as the temperature increased. For example, the normalised elastic modulus slightly reduces by ≈ 2% and ≈ 15% at temperature 50°C and 60°C respectively, when compared to the normalised elastic modulus at 20°C (as a reference). This is due to the visco-elastic behaviour of a material which is dependent on the magnitude of the applied temperature and loading time. In addition, if a constant strain is applied to this type of material, its elastic modulus will decrease gradually over a period of time. This is due to the matrix of the nanocomposite undergoing molecular reconfiguration in order to minimise the effect of localised stress [160]. However, a sharp reduction in the normalised elastic modulus was observed at 70°C (≈ 67%) and 80°C (≈ 87%) respectively. This reduction in elastic modulus of the nanocomposite may be due to the effect of broken of cross-linkings bonds between the matrix (epoxy) molecular

chains at the higher temperature, with a greater degree of damage seen when the temperature increases [186].

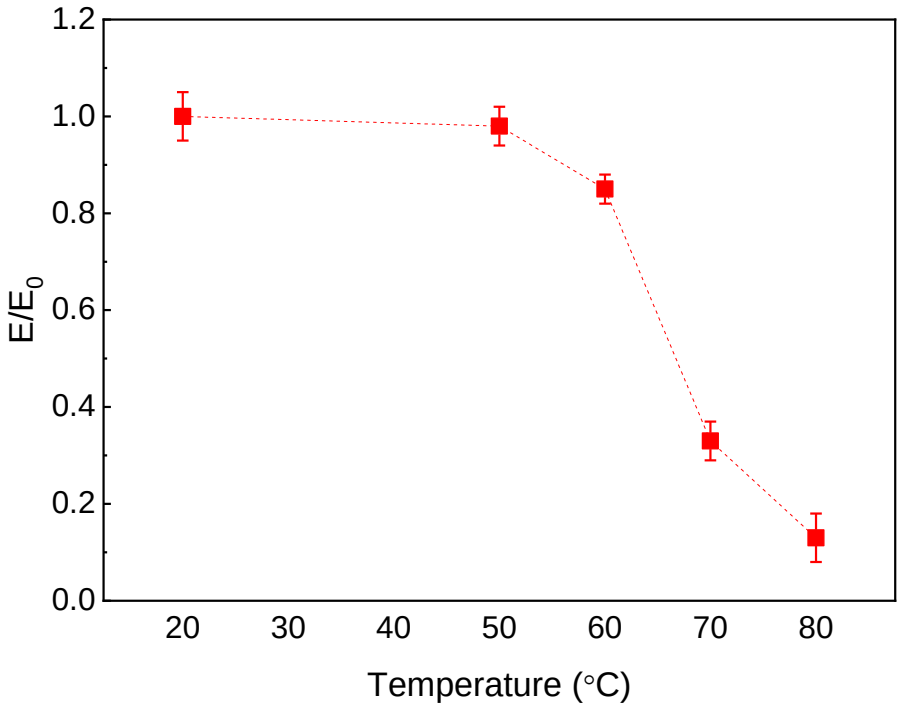

Figure 4.25: Temperature influence on normalised elastic modulus of 1.0 wt. % of MWCNTs nanocomposites under cyclic load.

4.3 Damage Sensing in Composites containing MWCNTs during Anticlastic Bending

4.3.1 Electrical Conductivity Test Results

The DC electrical conductivity of the composites laminate was measured as a function of MWCNTs concentration (wt.%), this was described previously in (section 3.2.2.1).

4.3.2 The Effect on Composite Properties of MWCNT Additions

4.3.2.1 Flexural Test Results

The flexural properties of composites, with and without MWCNTs obtained during testing are shown in Figure 4.26. These results indicates that embedding MWCNTs in the composites improves both the flexural strength and the flexural modulus of the composite. The flexural strength increased from 421.5 MPa (for the unmodified composite) to a maximum value of 473.4 MPa (nearly 12.3%) with the addition of 1.5% of MWCNTs. In addition, the flexural modulus was also improved and increased from 21.5 GPa to 31.1 GPa at 2.0 wt. % of MWCNTs. Yip *et al.* [161] studied the flexural behaviour of glass fibre reinforced polymer with MWCNT and obtained similar results in terms of flexural strength. Their observed increment was ≈ 9.2% for a 0.75 wt.% concentration of MWCNTs as compared to the unmodified composite. Similarly, Rathore *et al.* [95] added different concentrations of MWCNTs to composites (GFRP) and then conducted flexural tests. Their results indicated that the samples at 0.1 wt.% concentration of MWCNT had both a higher flexural strength and modulus, ≈ 32.8% and ≈ 11.5% respectively compared with the control samples.

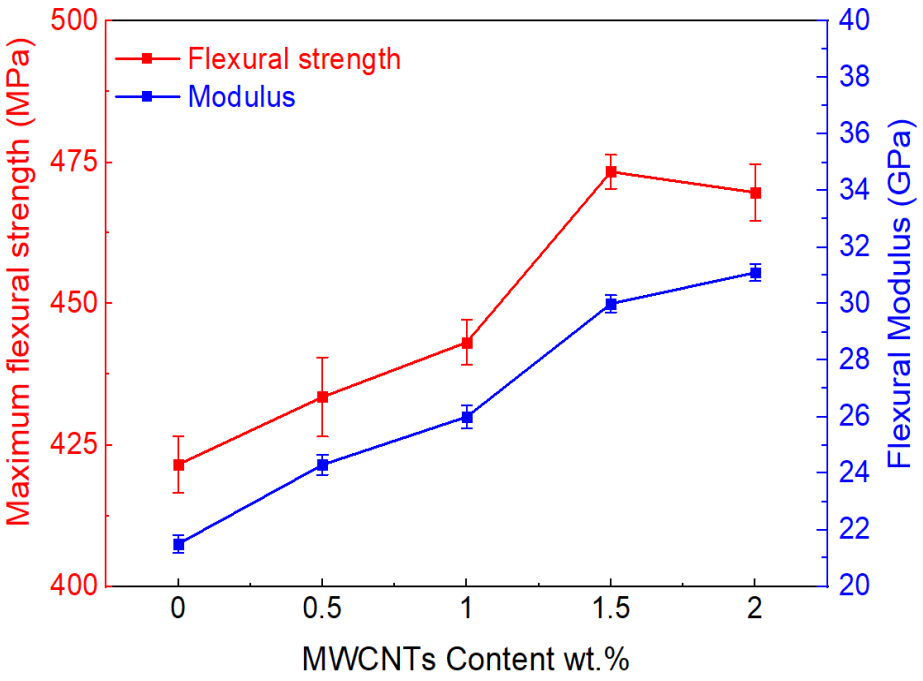

Figure 4.26: Effect of MWCNTs concentrations on flexural properties of GFRP composites.

This improvement in the strength and stiffness characteristics of the composites embedded with CNTs occurs due to good interfacial bonding between the CNTs, and the epoxy, with the fibre surface and the necessary effective distribution of the nanocomposite particles between the fibre tows as shown in Figure 4.27a. Therefore, these conditions ensure that the loads can be transferred efficiently throughout the composite structure. The good dispersion of CNTs inside the matrix increased the mechanical properties of composites. This enhancement can be explained as a strong synergetic effect between the polymer matrix and the MWCNTs, which benefits from the high stiffness property of MWCNTs [24, 116]. However, the flexural strength of composites decreased slightly, to 469.7 MPa, when the MWCNTs concentration reached 2.0%. This could be due to the poor interfacial bonds between the fibre and the matrix caused by MWCNTs agglomeration. At high concentration, MWCNTs tend to agglomerate due to relatively strong van der Waals force between them [9]. The agglomeration of CNTs, as shown in Figure 4.27b reduces the activity of CNTs surface

area characteristics (to be able to interact with the matrix) which in turn reduce the composite properties. However, in this study, the flexural strength continued to increase with wt.% additions related to the unmodified composite laminates (GRP) condition. Based on the results obtained, the composite showed the best improvement in mechanical properties for a 1.5 wt. % concentration of MWCNTs. Therefore, this wt.% was selected for subsequent experimental testing.

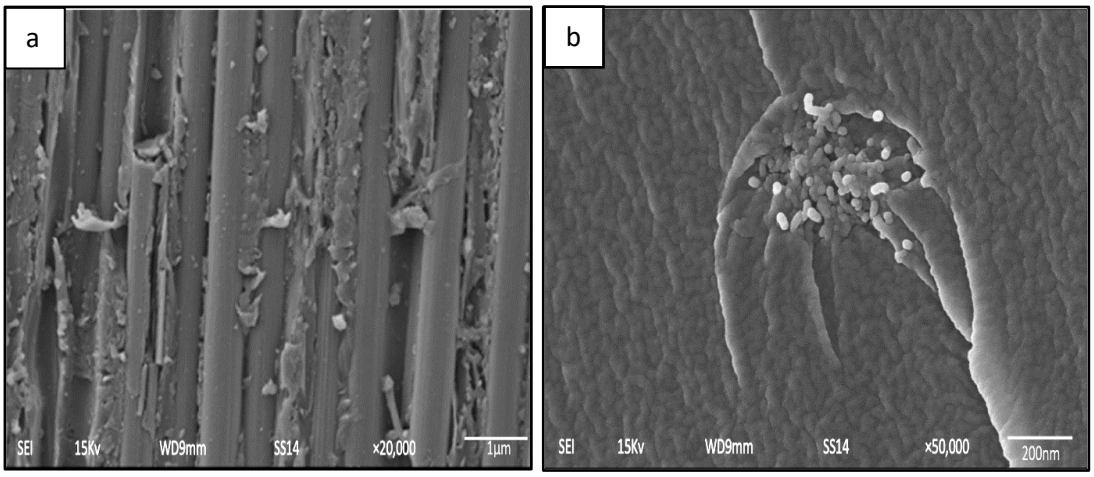

Figure 4.27: SEM images of (a) epoxy based MWCNTs nanocomposite between the fibre tows, (b) some MWCNTs agglomeration.

4.3.2.2 The Anticlastic tests

The anticlastic bend test considers a mode of plate deformation in which the plate is subjected to a twisting type of deformation and is characterised by two opposite plate curvatures into a so-called `saddle` shape (see Figure 4.33 later). The mechanical properties including the maximum stresses and elastic modulus values which were obtained, during anticlastic testing, for different concentrations of MWCNTs are shown in Figure 4.28. It can be seen that the addition of MWCNTs enhanced both the stress and the elastic modulus of the glass fibre/MWCNTs/epoxy composite. The stress increased to maximum value of 447.2 MPa at 1.5 wt. % MWCNTs concentration

and then decreased slightly to 431.5 MPa for 2.0 wt. % MWCNTs, due to MWCNTs agglomeration effects as shown in Figure 4.27b. However, the stress at 2.0 wt. % of MWCNTs still represents an increase relative to the control samples. Moreover, with respect to the modulus, it can be noted that there are two representative values, which are obtained from this test in the x-direction (E_x) and in the y-direction (E_y). As shown in Figure 4.28, both E_x, E_y increase significantly with increasing the MWCNTs concentration (note that the negative values are due to the negative strain ε_y). For example, the maximum modulus values were 39.1 GPa in x-direction and 35.1 GPa in the y-direction for 2.0 wt.% MWCNTs. Ideally, the Young's modulus should be identical in both directions since the composite is considered to be an isotropic in the in-plane direction. This small difference is likely due to slight asymmetry in the plates due to their hand lay-up manufacture.

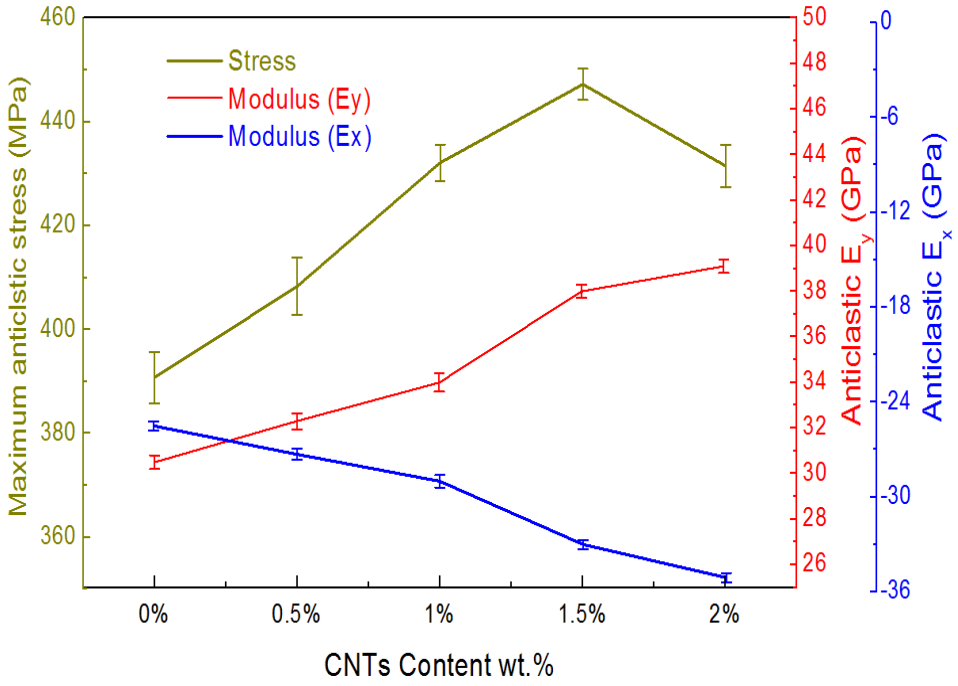

Figure 4.28: The effect of MWCNTs content on properties of (GFRP) during anticlastic testing anticlastic test.

For comparison with the flexural test results, the load deflection against MWCNTs concentration, obtained for both the flexural and anticlastic testing are shown in Figure 4.29. It can be seen that the glass fibre/MWCNTs the maximum sustained load, for a deflection of 6mm, for both tests increased with increasing MWCNTs concentration. The control composite demonstrated a bearing load of 647.7 N and 641.2 N at 6mm deflection. This increased to a maximum value of 776.9 N and 733.9 N for the flexural and anticlastic tests respectively. This observed increase is due to the incorporation of a secondary reinforcement effect at the nano-scale level where the MWCNTs in the composites increase the interfacial bonding between the matrix and fibre. However, the decrease of these loads with high MWCNTs content i.e. at 2.0% can be attributed to the inhomogeneous dispersion (agglomeration) of MWCNTs at higher concentration levels [22]. The results from the anticlastic test showed lower values relative to the flexural test in term of stress, whereas the values of Young's modulus (stiffness) were higher than those observed during flexural testing. This occurs in the anticlastic test, due to the geomentric behaviour of the test panel durin bending, which has a thickness t, and is subjected to external loads at the opposite corners. In this situation, there are two equal but opposite, bending moments in operation, i.e. $M_x = -M_y$, along the two pairs of edges as shown in Figure 3.7a. These two moments are can be calculated as indicated in equation (4.11);

$$M_x = \int_{-t/2}^{t/2} \sigma_x \times z \times dz\,,\ M_y = \int_{-t/2}^{t/2} \sigma_y \times z \times dz \qquad (4.11)$$

In the flexural test, only one bending moment is applied to the sample and for the other $M_x = 0$. Therefore, the loading in the flexural test is statically equal to two forces at

the corners of the composite plate that are applied exactly along the diagonal between the plate corners. In this case, the shear deformation is twice that experienced during the flexural test and, as a result, a lower bearing load is observed under this test. Moreover, in terms of actual displacement, the values of the strains experienced are shown in Figure 4.30. These were obtained from the anticlastic test within the elastic limit of the sample, and are lower than the values obtained from the flexural test. For this reason, and according to Hooke's law, the observed values of modulus from anticlastic tests appear higher.

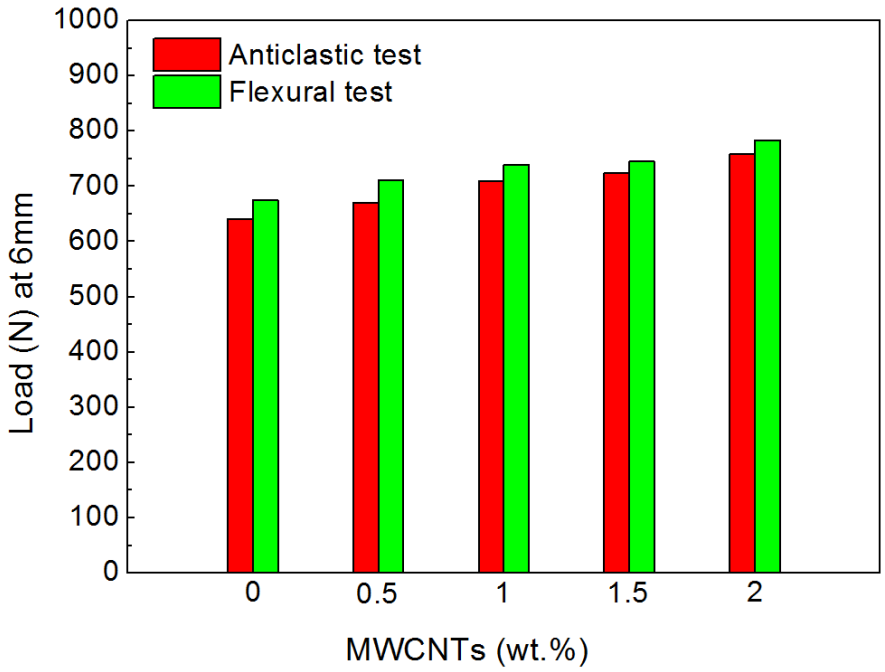

Figure 4.29: Maximum load for composite with different MWCNTs content.

4.3.3 Strain Deformation Under Flexural and Anticlastic Tests

Any stress applied to the glass fibre/MWCNTs/epoxy composite will lead to the development of strain. Therefore, to study the difference between these two tests i.e. flexural and anticlastic tests, strain measurements were carried out. To do this is, A

'T' type strain gauge rosette was bonded onto the (bottom) surface of glass fibre/MWCNTs/epoxy composite plates (i.e on the diagonal line of the specimen). This type of `T` strain gauge rosette can give two readings at the same time i.e. one in the x-direction and the other in the y-direction. The strain history readings from this gauge versus displacement are indicated in Figure 4.30. Because of a condition of uniaxial bending, it is observed that there is one set of strain readings for the flexural test (i.e. ε_y), whereas there are two obtained for the anticlastic test i.e. ε_x and ε_y. In general, the strains for both types of tests increased linearly as the displacement increased. At, 18 mm displacement, it can be seen that the strain from flexural test showed a larger magnitude ($\approx \times 4$) than for both anticlastic test strains. This is because when the load is applied to the composite plate four corners during the anticlastic test this causes four tension stresses and four compressions stresses to occur simultaneously in the plate as shown in Figure 4.33. During anticlastic testing, these stresses are distributed equally over the glass fibre/MWCNTs/epoxy composite plate so minimising the load concentration at a restricted position, as occurs in a flexural test. Moreover, although the strains for the anticlastic test are opposite in sign, they are very close in magnitude. The negative sign for the ε_x within the anticlastic test was ascribed to the surface compression that take places during the applied load on the composite plate corners, so creating the saddle shape (see Figure 4.33).

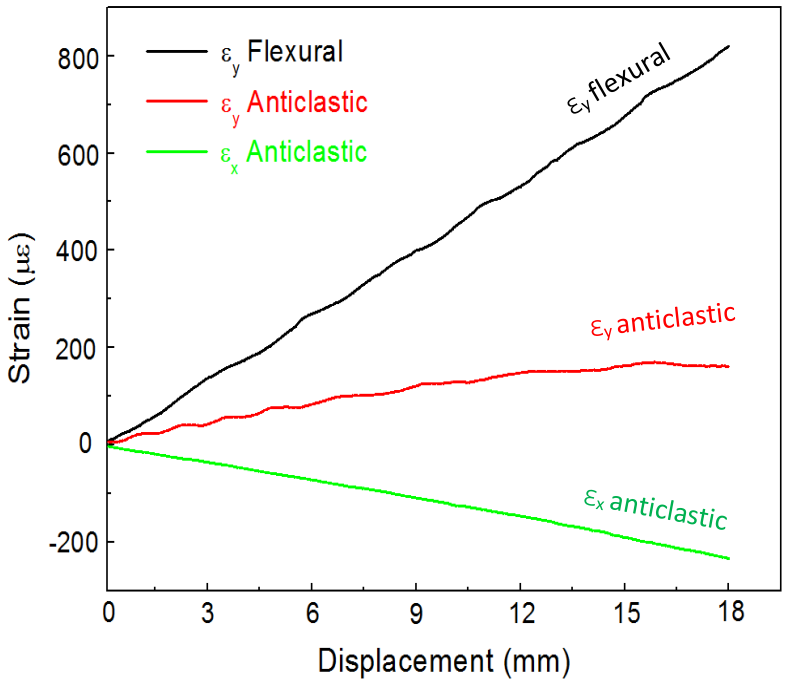

Figure 4.30: Strain versus displacement experimental readings for flexural and anticlastic tests.

4.3.4 Electromechanical Response

The major objective of this study was to investigate the electromechanical properties of the glass fibre/MWCNTs reinforced polymer when subjected to two different types of mechanical tests, (i.e. under flexural and anticlastic loading). Identical samples based on 1.5 wt. % MWCNTs were tested under both flexural and anticlastic test conditions using static loading. Figure 4.31 shows the change in the electric resistance, and the load, as a function of displacement for both types of tests. Clearly, from both tests, the change in the resistance with increasing the load follows a similar trend.

For the three-point flexural testing Figure 4.31a, it is clear that when the load increases then the normalised change in resistance ($\Delta R/R_0$) readings reduced slightly, and show negative values. This reduction in the readings continue up to a centre displacement of 8 mm for the composite plate. At this point, a sudden sharp increase was observed as the specimen fractured and broke. To explain this, note that the upper surface of the

sample, during flexural loading is compressed. Consequently and the lower surface is in tension see Figure 4.32a. Final failure occurred in the compression surface at the loading position.

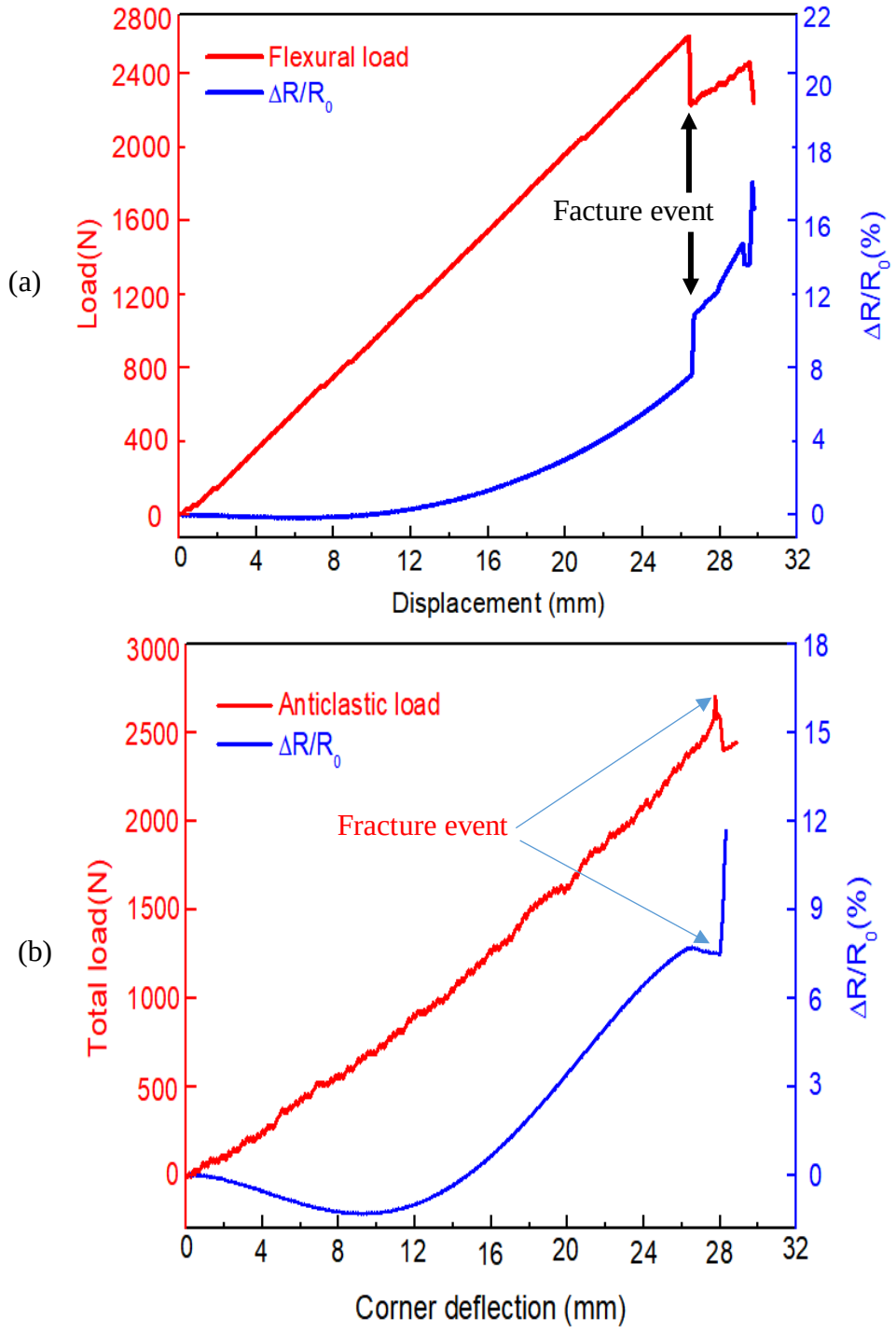

Figure 4.31: Load and resistance changes during (a) flexural test (b) anticlastic test.

To understand the relationship between the applied load and the changing resistance then the following needs to be considered. When the load starts to increase, there is a slight reduction in the spacing gap between MWCNTs within the network structure above its neutral axis and this reduces the resistance. Above 8 mm deflection, due to an increase in the applied load, the layers close to the bottom surface are exposed to a large tensile force. Consequently, the observed increasing resistance is due to the changing internal distances between the MWCNTs as shown in Figure 4.32b. The combination of these tensile and compression effects leads to the observed non-linear changes in $\Delta R/R_0$. These findings are consistent with other studies [25, 162, 163].

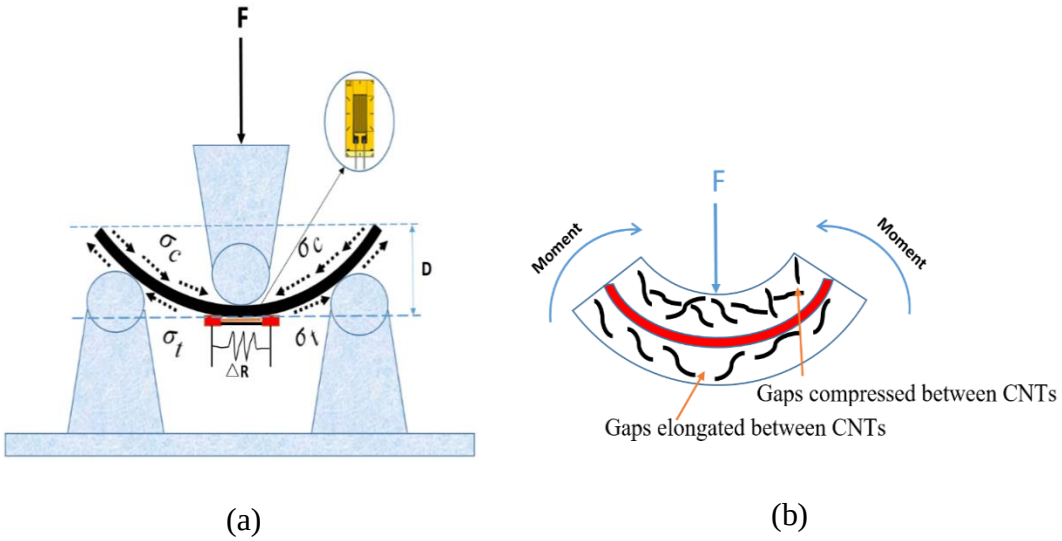

(a) (b)

Figure 4.32: Schematic of the 3-point flexural test showing the stress on the surfaces (a) and the tension/compression effect from force on the MWCNTs network (b).

For the anticlastic test (Figure 4.31b), the change in the resistance also shows non-linear behaviour with negative readings being possible, with a maximum value occurring at 9.3 mm corner deflection. This is ≈ 70% greater than for the flexural test. This is caused, in the anticlastic test, by the two combined moments which are imposed at the composite plate corners. These simultaneously create two compression and two

tension surfaces, as shown in Figure 4.33. Therefore, the spacing gaps between the MWCNTs in the out-plane region were reduced in the two compression surfaces and increased in the two tension surfaces. Consequently, this causes a larger, but still non-linear, variation in resistance when compared to the flexural test. Thus, this type of signal can be used to detect the damage at an early stage of crack initiation. In a previous study [164], using a carbon fibre composite, it was not possible to detect the crack at an early stage because there was no change in composite resistance during the applied load. Therefore, glass fibre based MWCNTs composite have the potential to detect early damage, by an observed change in the resistance, from the point at which any applied load will start to increase, as shown in Figure 4.31.

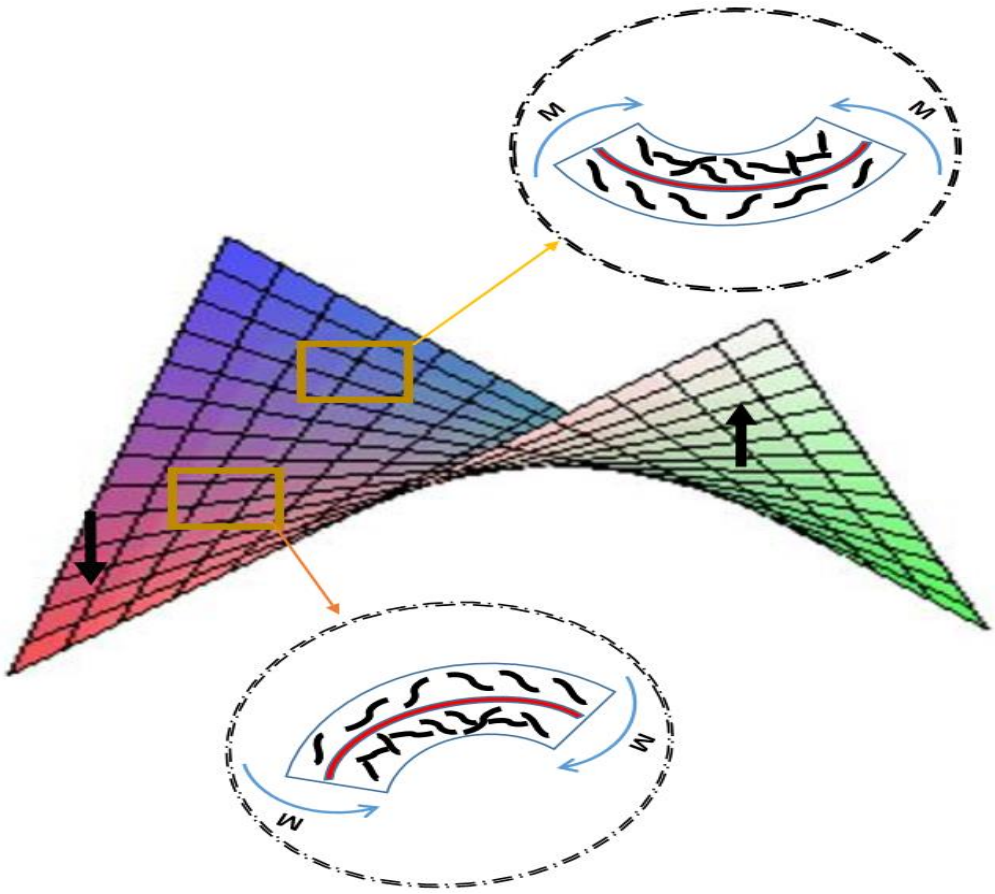

Figure 4.33: Anticlastic saddle shape during loading.

4.3.5 Strain Sensitivity

The local deformation in both flexural and anticlastic test specimens was detected using a conventional strain gauge fixed onto the surface of the composite plate. The history-recorded data were used in equation (3.6) to calculate the strain sensitivity or gauge factor (GF). Figure 4.34 and Figure 4.35 show the normalised change in resistance as a function of the strain for flexural and anticlastic test respectively. From these graphs it is clear that the correlation between the $\Delta R/R_0$ and the indicated strain in the flexural test shows almost linear behaviour, but to a greater degree than the anticlastic test. This might because there is only one moment in this test that can affect the curvature of the plate; while in the anticlastic test there were two moments available to cause the curvature as shown in Figure 4.33.

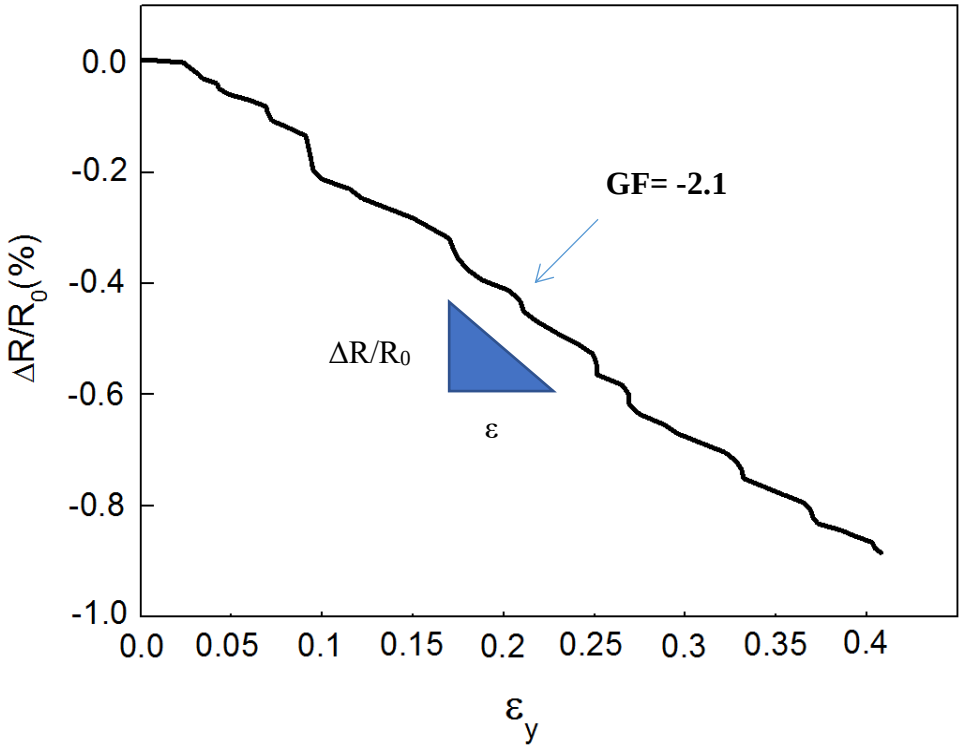

Figure 4.34: Normalised changes in resistance versus strain for flexural tests.

Moreover, it can also be observed that there are two measurable strain values i.e. ε_x, ε_y in the anticlastic test but only one i.e. ε_y in the flexural test. This means there are two GFs to consider in anticlastic test, and one only in the flexural test. In addition, the strain sensitivity in the flexural test is equal to -2.1 a lower value than those obtained from by the anticlastic test by about 47% as shown in Figure 4.35.

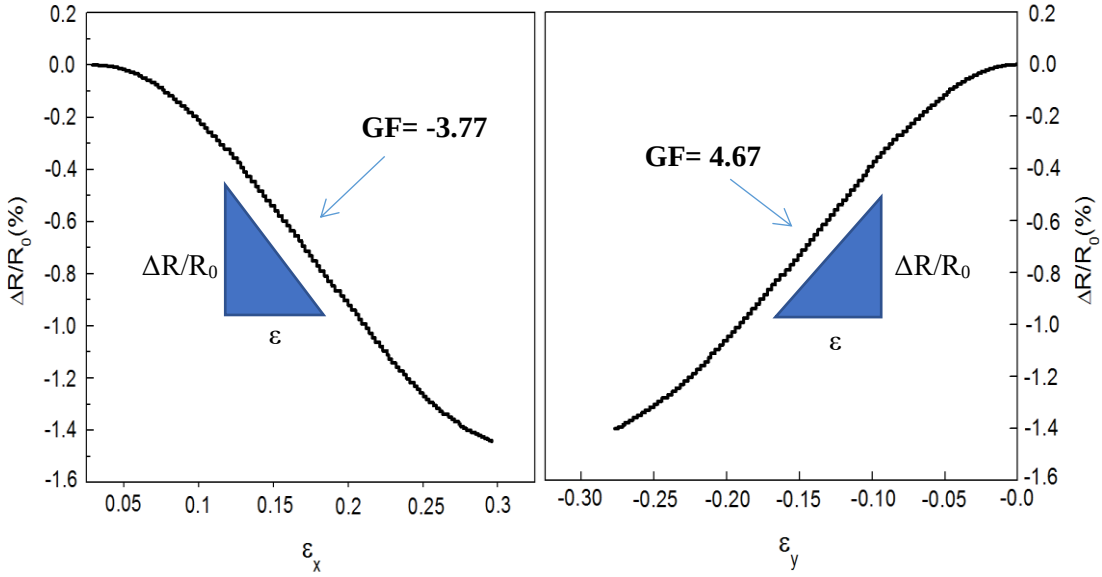

Figure 4.35: Normalised changes in resistance versus strain for anticlastic tests.

This is due to 3-dimensional natural of the curvatures developed in the surfaces during an anticlastic test. This leads to both tensile and compression surfaces being formed simultaneously during loading. As stated previously, the negative sign in the flexural test in x-direction in an anticlastic test comes from the compressive deformation on that curvature surface. Here, because the internal distance between MWCNTs decreases so the resistance also decreases, as shown in Figure 4.33. Ideally, the magnitude of the sensitivity strain in the anticlastic mode should be the same in both directions but in this study there is a slight difference possibly due to the strain gauge position being not exactly at the centre of the diagonal line of the composite plate.

4.4 The Drift Properties of MWCNTs in Composites during Manufacture

4.4.1 Mechanical Properties

For the MWCNTs shown in Figure 4.36, it was speculated that they could possibly drift during the infusion process. To investigate this possibility, test specimens were taken from different positions along the length of a test panel and then subjected to flexural tests. The test samples were chosen from three different zones (70 mm, 140 mm and 210 mm) along the panel length from the infusion point respectively as shown in Figure 4.36.

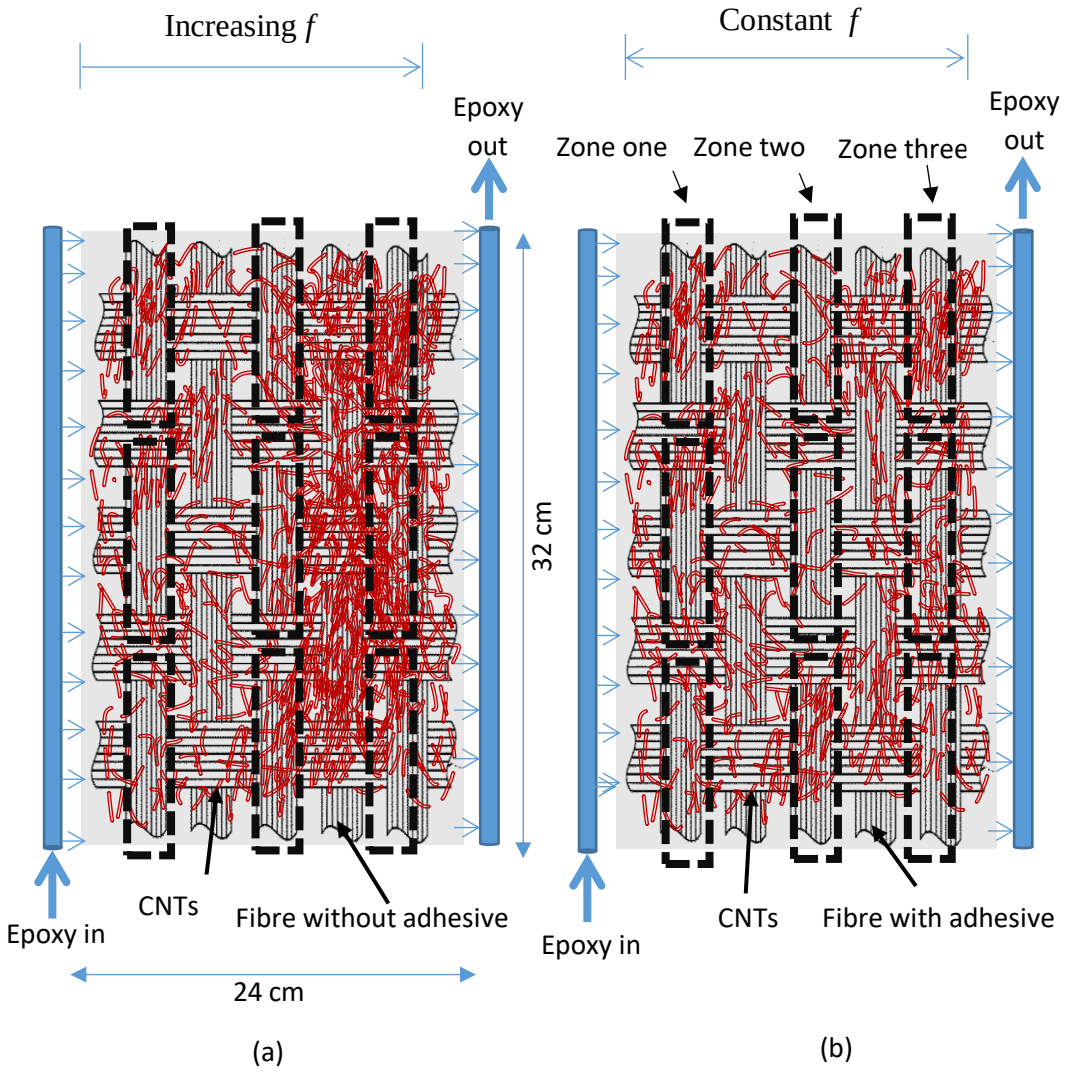

Figure 4.36: Schematic diagram used to explain the mobility the MWCNTs, with respect to time. (a) Without adhesive, (b) With adhesive.

Mechanical properties including flexural strength and elastic modulus were determined for both types of fabricated MWCNTs- GE composite using the standard flexural test.

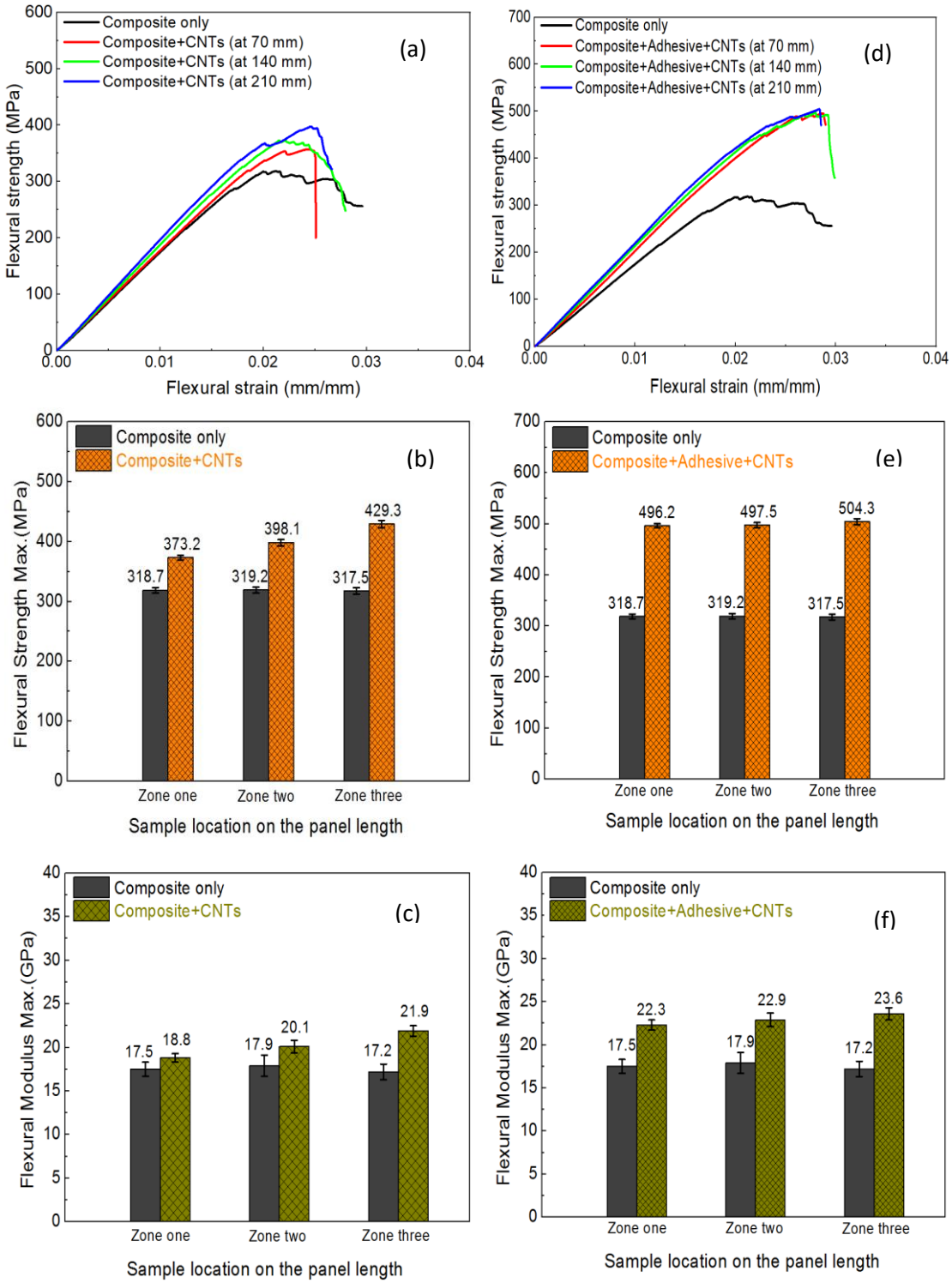

Figure 4.37: Representative individual flexural stress-strain curves, and collected results, for maximum flexural strength and modulus properties of MWCNT-GE composites without adhesive

Figure 4.37a, d shows the static flexural stress-strain curves obtained for both types of composites (with and without adhesive) at the different zones along the length of the composite panel. The changes in flexural strength, elastic modulus versus the collection locations for samples are shown in Figure 4.37b, c, e and f, respectively.

As shown in Figure 4.37a, d, both composite samples exhibited approximately similar stress-strain relationship for each zone tested. The flexural stress-strain curves initially present an almost linear response for the flexural stress up to ≈ 200-250 MPa for MWCNTs-GE composite (without adhesive) and ≈ 350-400 MPa for MWCNTs-GE composite (with adhesive). In Figure 4.37b, e, it can be seen, regardless of whether adhesive bonding was used or not, that the deposition of the MWCNTs on the fibre surface develops a significant increase in the flexural strength of the resultant MWCNTs-GE composite when compared to the unmodified (virgin) condition. These tests indicated that for the case of MWCNTs-GE composite, where no adhesive bonding was used, a gradual, and linear, increase in the flexural strength occurred along the length of the test panel. At the start position zone one (i.e. at 70 mm), the flexural strength was 373.2 MPa and at zone three (i.e. at 210 mm) the flexural strength was 429.3 MPa, so indicating a ≈ 13% and ≈ 26% increase for zone one and zone three, compared to control samples respectively.

This increase is due to the drift of the MWCNTs caused by the infusion process which creates an increase in the areal density of MWCNTs along the panel length. Figure 4.38 shows evidence for this effect using scanning electron microscopy (SEM) and optical microscopy. The advancing MWCNT front is clearly observed. For the case of MWCNTs-GE composite where adhesive bonding was used to fix the MWCNTs in place, the flexural strength was higher and remained reasonably constant at 504.3 MPa, with less than 1.6% change. Clearly, the use of bonding adhesive improves the

interfacial matrix/fibre properties, so keeping the MWCNTs in place. The improvement of the interfacial zone between the nanocomposite components is important since it helps the load to be transferred easily between them [165, 166]. This maintains a constant areal density along the panel length. Currently, no studies in the literature have considered the influence of MWCNTs drift during processing on the mechanical properties of MWCNTs-GE composites. In addition, the flexural modulus of MWCNTs- GE composite also increased following the addition of the MWCNTs as shown in Figure 4.37c, f. The flexural elastic modulus of both MWCNTs-GE composites varied in accordance with the specimen's location zone. These changes were highest where no adhesive was used. The elastic modulus steadily increased when the location of the specimen changed from zone one to zone three. The significant increase in the observed mechanical properties for both MWCNTs-GE composites is due to the greatly improved interfacial bonding that exists between the reinforcement material and the surrounding matrix [167]. This improvement was greatest for the adhesive assisted MWCNTs-GE composite, due to the inclusion of the adhesively bonded MWCNTs in this region. The adhesive facilitates better load transfer from the matrix to the fibre reinforcement.

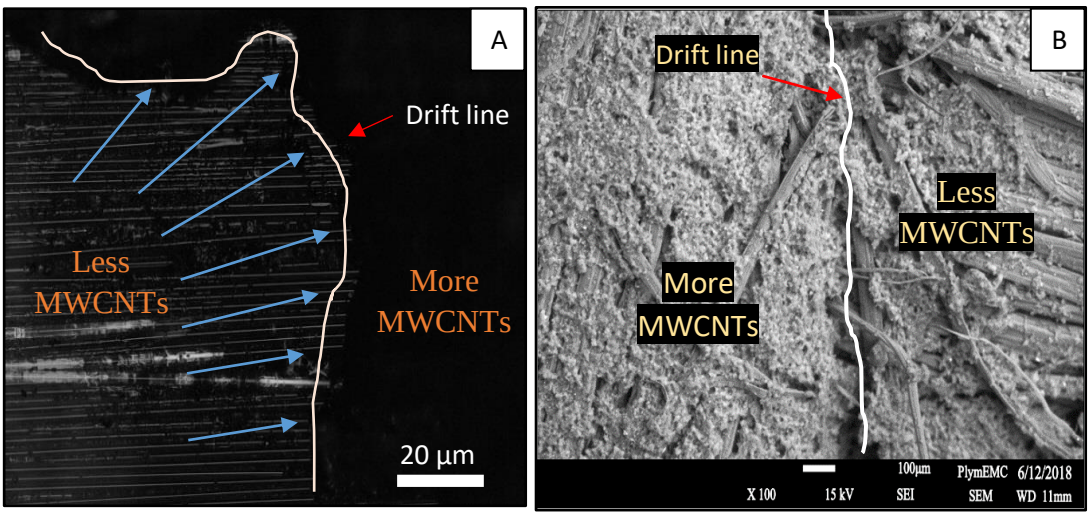

Figure 4.38: Illustration of the mobilisation of MWCNTs due to the epoxy flow rate (a) optical micrograph (b) SEM micrograph, both showing the drift line (white line), which separated the two phases.

The observed variation in the mechanical properties along the panel length can be attributed to the drift of MWCNTs from zone one to zone three, caused by the epoxy infusion flow pressure as shown in Figure 4.38. In this study, the boundary between the two phases is called drift line and highlighted with a white line.

Other studies have also investigated the improvement of composite properties through the addition of MWCNTs. Chang [114] studied the addition of MWCNTs on the mechanical properties of composite laminate/epoxy materials. The results obtained indicated an increase in the flexural strength properties of the resulting composite laminates. The observed increase was ≈ 22.1% as compared to the unmodified condition, a lower value when compared to the resent study. In addition, Zhang *et al.* [168] investigated the possible addition of different weight percentages of MWCNTs to the matrix material of glass/fibre composites to improve the mechanical properties. They observed that after adding only 0.4 wt.% of MWCNTs to the matrix improved flexural strength resulted. Neither of these studies considered the use of bonding adhesive, as was used here. Therefore, the results of the present study indicated that greater improvements to the mechanical properties of the resultant composite are possible when a simple bonding adhesive is used to lock the MWCNTs into place. However, the results obtained in this study showed lower values compared to those obtained by other researchers. For instance, Rahmanian *et al.* [169] used a CVD technique to deposit MWCNTs directly onto the fibre surfaces. Their results showed flexural strength and flexural modulus increases by 35% and 51% respectively. However, they did not study the variations in mechanical properties at various positions along the composite panel's length. They stated only average value.

4.4.2 In-situ Resistance Monitoring Test

Incorporating MWCNTs into glass fibre reinforced composite material will make the surface of glass fibre electrically conductive [27]. This is due to the formation of continuous conductive pathways between the MWCNTs on the surface of glass fibre. Consequently, the composite structure becomes very sensitive to external influences, particularly in terms of its internal electrical resistance. This provides the opportunity to create a sensor material, where changes in resistance can be monitored and related to any environmental or loading changes taking place. Here this change in the resistance behaviour also provides the opportunity to study, indirectly, the immovability of the MWCNTs in the interfacial region between matrix and reinforcement.

As described in section 3.4.1.2.2 the electrical tests were conducted on test panels to measure the changes in their resistance during the epoxy infusion process. Figure 4.39 shows the measured change in the electrical resistance, with time, for both types of treated (with and without bonding adhesive) MWCNTs-GE composites. Here it can be seen that a big difference for both types of composite test panels, in term of changing in resistance, occurred during the resin infusion. Where no bonding adhesive was used to fix the MWCNTs in place, the resistance of the panel increased steadily in an almost linear manner from the start of the epoxy infusion process. The increase observed here is due to two possible phenomena; firstly the MWCNTs have been moved during the resin infusion so increasing the tunnelling distance between adjacent MWCNTs. This distance has a direct effect on the total composite resistance [80]. Secondly, due also to the increase in temperature that occurs during the infusion process as the resin begins to chemically react with the coated composite layers [157, 170]. In addition, where the bonding adhesive was used, a good stability and no

obvious changes in resistance with time are observed up to 500 seconds. This stability is attributed to the adhesive material which holds the MWCNTs in place during the resin infusion process (see Figure 4.39b inset).

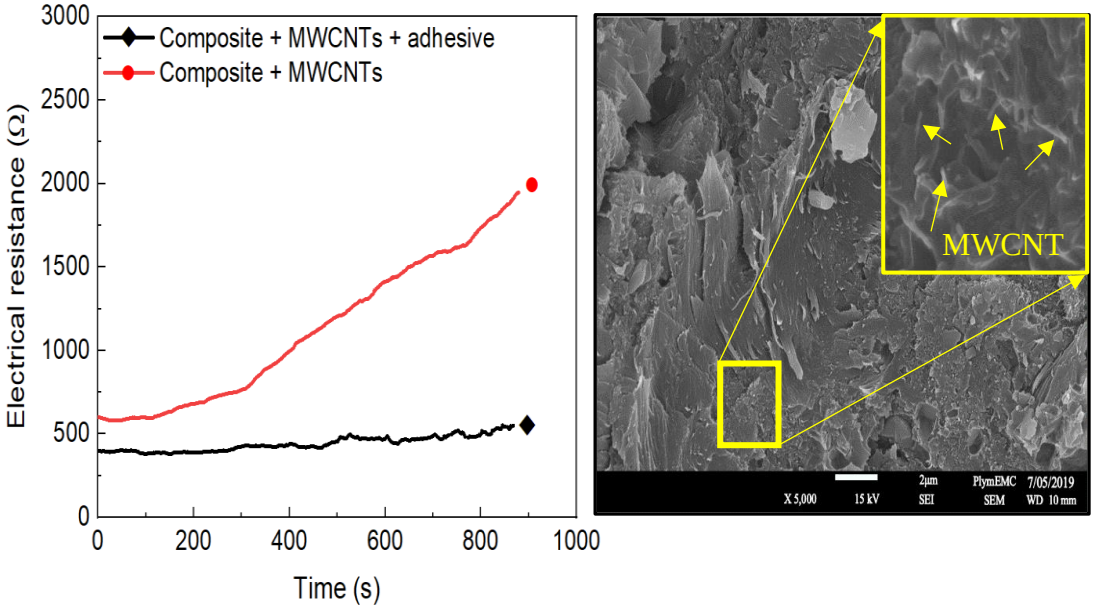

Figure 4.39: (a) Variation of electrical resistance with time during epoxy infusion for both type of fabricated self-sensing MWCNTs-GE nanocomposite and (b) SEM images for (adhesive) MWCNTs-GE composite.

It should be noted that, even with the use of adhesive, a small increase in the resistance was observed. This slight increment in resistance is probably not related to MWCNTs networks distortion, but is more likely due to the normal temperature increase in the matrix during hardening, which dominates at this stage [171]. In summary, without using bonding adhesive to fix the MWCNTs to the fabric surfaces, the conducting MWCNT network structure can become distorted, so altering the conduction pathway between MWCNTs particles. In addition, the change in the MWCNTs areal density, brought about by the infusion process, may also have an influence on the electrical conductivity. Therefore, the influence of MWCNTs mobility and the potential sweep of the MWCNTs by the advancing infusion front must not be disregarded.

4.4.3 Electrical Conductivity Measurement

The electrical conductivity of MWCNTs-GE composite is an important property. By monitoring the changing electrical conductivity, the fracture and strain can be predicted or sensed for structure health monitoring purposes. Figure 4.40 shows the variation in electrical conductivity for adhesive and non-adhesive composite as measured at the different zone locations, as previously shown in Figure 3.10.

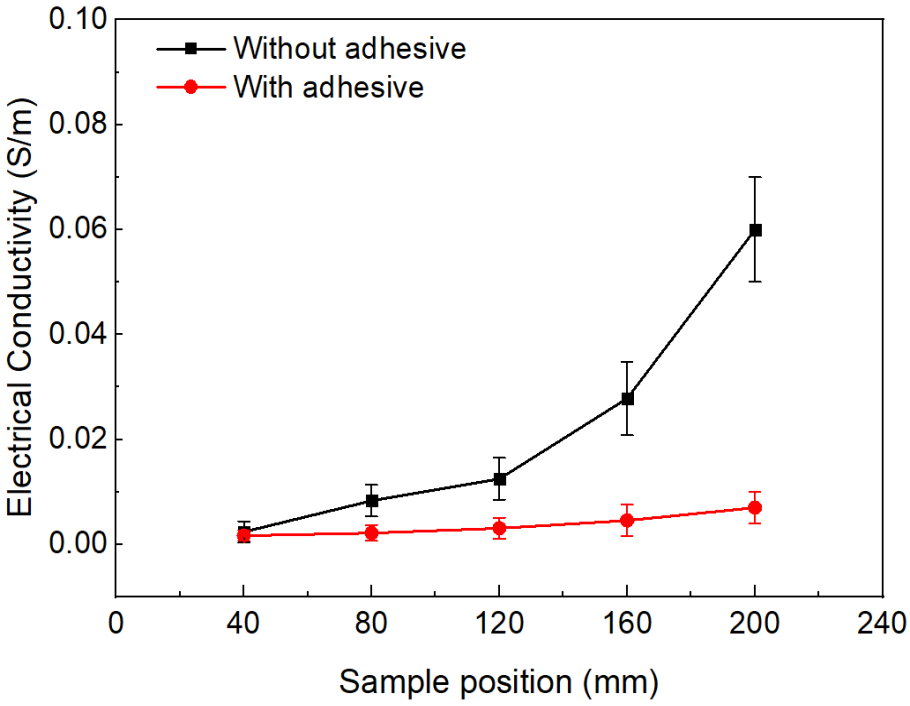

Figure 4.40: Variation in electrical conductivity against sample position.

It can be noted that the electrical conductivity of both types of specimens (with and without the use of bonding adhesive) increased in accordance with the sampling position i.e. the measured normalised conductivity values were highest at the end of the test panels and lowest at the beginning. This change was markedly higher where the bonding adhesive was not used due to the sweep of the MWCNTs, caused by the advancing epoxy infusion front, increasing the areal density of MWCNTs along the panel length. Thus, it is confirmed that any change in the MWCNT areal density,

brought about by the infusion process, will affect the electrical conductivity of the composite. It should also be noted that a greater areal density of MWCNTs can also cause a reduction in the overall magnitude of the composite resistance [80-82]. This is considered [172-174] to be due to the reduced distance between MWCNTs improving the efficiency of the conduction pathway. Since MWCNTs are randomly distributed above the fabric laminate surface and then covered by the epoxy resin, it is not realistic to estimate the exact distance between every two adjacent MWCNTs. This distance along the panel's zones especially for (non-adhesive composite), can be calculated using Simon's theoretical model [146]. This is stated as;

$$\sigma_m = \left(\frac{e^2 \sqrt{2m\beta}}{h^2} \right) \exp\left(\frac{4\pi d \sqrt{2m\beta}}{h}\right) \tag{4.12}$$

Where σ_m is the electrical conductivity polymer matrix, *e* the electron electric charge density ($1.60217662\times 10^{-19}$ coulombs), *m* is the electron mass (9.10938356×10^{-31} kg), *h* is Planck's constant (6.62607004×10^{-34} m^2 kg/s), and β is the energy barrier (0.5~5 eV) for most of polymers (in this study, β was 2.5 eV [59]). It should be noted that the tunnelling distance (*d*) is extremely dependent on both the matrix electrical conductivity and the energy barrier of the matrix (e). The electrical conductivity of most polymers is between 10^{-16} and 10^{-12} Sm^{-1}. Therefore, polymers (e.g. epoxy) have usually been considered as insulating materials. Nevertheless, when the epoxy contains MWCNTs, the electrons are than able to transfer between adjacent MWCNTs. This transfer could be defined, in a physical sense, as a quantum mechanical penetration of electrons through a potential barrier [175]. By considering the MWCNTs conductivity as isotropic and randomly oriented, the electrical conductivity of MWCNTs-GE composite material can be given as follows [176];

$$\sigma_e = \sigma_m + \frac{\chi f \sigma_m \sigma_c}{3 + (\sigma_m + H(\chi\alpha)} \tag{4.13}$$

Where σ_e is the electrical conductivity of the CNTs nanocomposite (in this study experimentally calculated and represented in Figure 4.40, σ_c and f indicate the electrical conductivity and the volume fraction of MWCNTs). It is well known that the electrical conductivity of MWCNTs is high and ranges from 10^3 S/m to 10^5 S/m [177]. Therefore, in our simulations, we use 10^4 S.m^{-1} in accordance with published data. The parameter χ in equation (4.13) represents the non-straightness of the CNTs, which can only apply when the aspect ratio of the CNTs is high. According to the current properties of the MWCNTs in this study, the aspect ratio (α) is approximately 400 and this is considered to be low, based on the recent studies [178]. These studies have demonstrated that as the aspect ratio of CNTs increases, then the fibre rigidity will also increase. Therefore, the non-straightness is taken as unity in this study. Moreover, H is the depolarisation factor which reflects the influence of the CNTs aspect ratio (α) to conductivity and is expressed as [179]:

$$H(\alpha) = [(\alpha / \sqrt{(\alpha^2 - 1)}) \times \ln[\alpha + \sqrt{(\alpha^2 - 1)}] - 1] / (\alpha^2 - 1) \tag{4.14}$$

Since the volume fraction (f) of the MWCNTs in this study is significantly altered due to their drift along the panel length then it can be considered as being high at the end of the panel (i.e. $0 < f < 0.155$), therefore, it was computed separately for each sample using Eq. (4.13). By substituting Eq. (4.13) and Eq. (4.14) in Eq. (4.12) then after separating the variables, the relation between the tunnelling distance (d) of CNT-CNT and their volume fraction can be stated as;

$$d = \frac{(-2\ln(-\sigma_c f - H + A + \sigma_e - 3) - 4(\ln eh) + \ln(8\lambda m))h\sqrt{2}}{16\pi\sqrt{\lambda m}} \tag{4.15}$$

$$A = \sqrt{\sigma_c^{\,2} f^{\,2} + 2f(H + \sigma_e + 3)\sigma_c + (H + \sigma_e + 3)^2} \tag{4.16}$$

The numerical results obtained using the above relationship, Eq. (4.15) and (4.16), are shown in Figure 4.41. It can be noted that the tunnelling distance (d) significantly decreases as the volume fraction (*f*) of the MWCNTs samples increases. This change in volume fraction is due to the drift of the MWCNTs. This can be clearly seen in Figure 4.42. The SEM micrographs, Figure 4.42 shows the difference in volume fraction of the MWCNTs after resin infusion at the inlet and outlet positions of the composite panel.

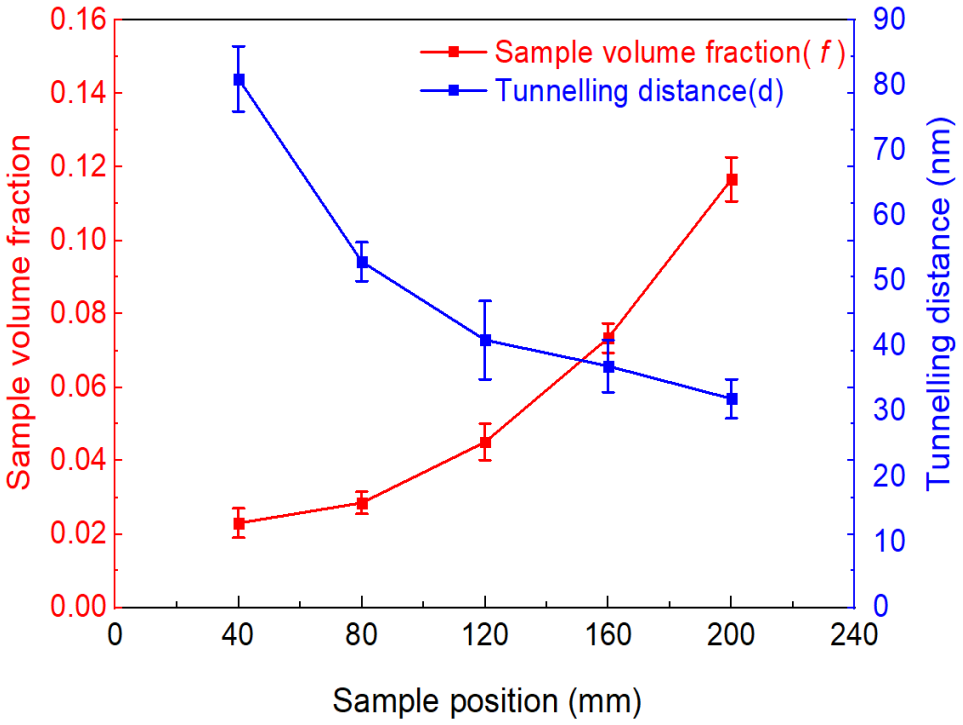

Figure 4.41: Tunnelling distance (d) of MWCNTs-GE composite samples as a function of the volume fraction (*f*) for each sample.

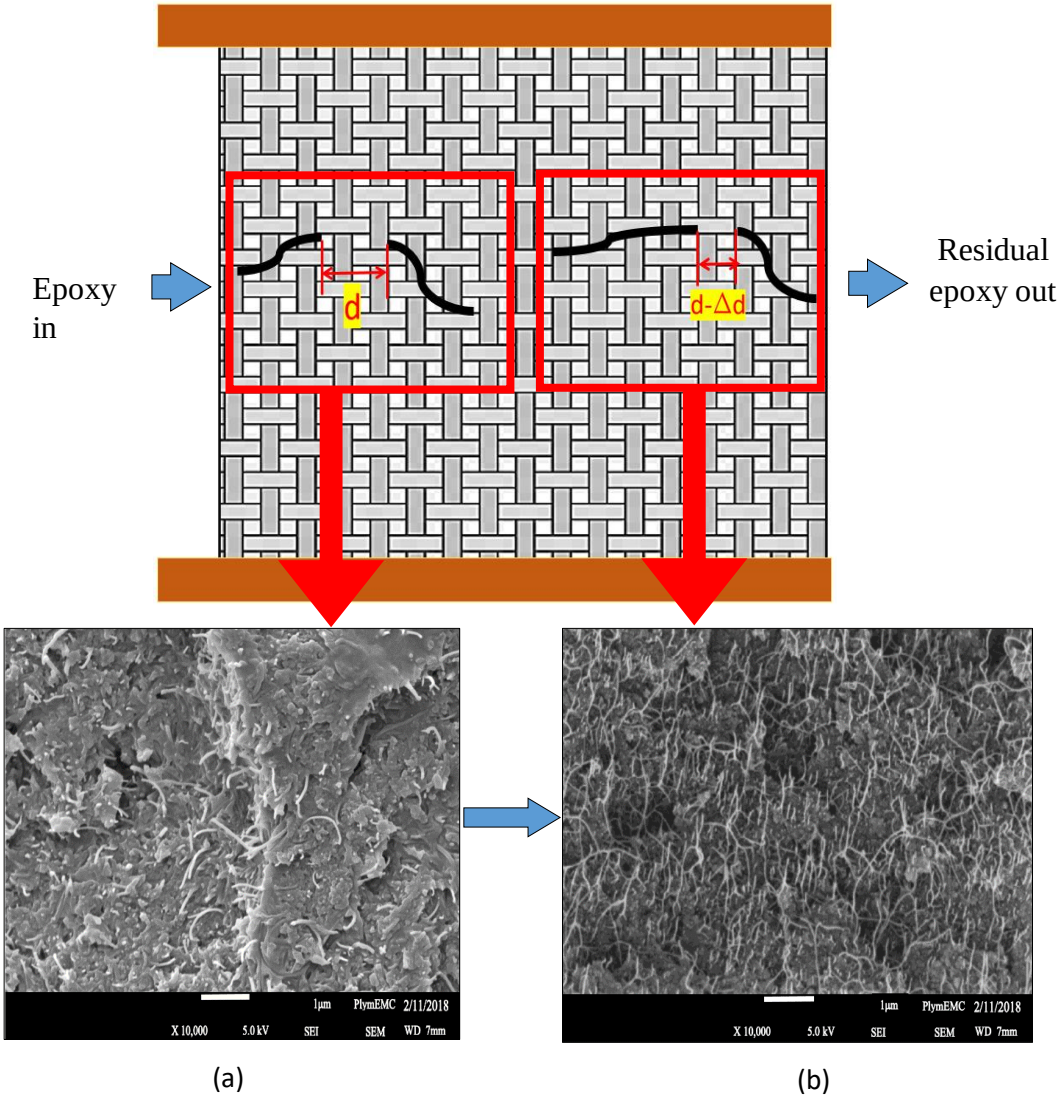

Figure 4.42: SEM micrographs of non-adhesive samples show MWCNTs volume fraction at (a) Panel inlet position, (b) End of panel (following infusion).

4.4.4 Piezoresistivity and Strain Sensitivity Properties

The major purpose of this study was to investigate the stability of MWCNTs coated fabric during epoxy infusion processing. Figure 4.43 shows the normalised electrical resistance change ($\Delta R/R_0$) versus strain curves obtained from experimental results for both types of fabricated composites (with and without adhesive). Both types of fabricated composites show a strong piezoresistive response when subjected to flexural loading. Regardless of the fixing method of the MWCNTs (fixed with adhesive or not), the behaviour of the normalised electric resistance changed linearly

and in negative piezoresistive manner, i.e. the resistance change ($\Delta R/R_0$) decreases linearly with the increase of applied strain for both types of fabricated composite as clearly shown in Figure 4.43a, c. This change in $\Delta R/R_0$ with applied flexural strain can be interpreted as the breakdown and disruption of the conductive network paths between adjacent MWCNTs, which increases the inter-CNTs distance during applied strain. Moreover, the slope of the graphs shows the strain sensitivity i.e. gauge factor (GF) of the composite specimens at different zone locations along the composite panel length.

The gauge factor is significantly dependent on the volume fraction (*f*) of the CNTs present [180]. Therefore, the change in volume fraction of MWCNTs along the panel length, as expected and demonstrated in Figure 4.36, can also be inferred from the gauge factor calculations. Therefore, Figure 4.43b, d shows that the gauge factor for the samples in the zone one is higher than that for the samples located at the end of the composite panel i.e. (zone three) for both type of composites. For example, the gauge factor at zone one (for non-adhesive composite) is 3.67 which is higher by 31.6 % and by 52.04 % than zone two and zone three, respectively. This is due to the drift of MWCNTs causing the areal density to gradually increase along the composite panel, becoming highest in zone three. This is shown clearly in SEM images in Figure 4.42. It was proved that the samples with CNTs concentrations closer to the percolation threshold, are more sensitive and behave in a highly linear way [181, 182]. This could be a reason for the higher gauge factor values in zone one, which has a lower MWCNTs concentration after resin infusion and, therefore, is closer to the percolation threshold.

Other studies [80, 144, 183-185] have also observed that when the volume fraction of MWCNTs increases, then the distance between neighbouring MWCNTs decreases and results in a reduction of both the electrical resistance and the strain sensitivity (GF) of the nanocomposite. However, for a composite coated with adhesively bonded MWCNTs, there is no significantly large change in the zone`s gauge factors (2.38 ± 0.13). This is due to the restricted movement of MWCNTs caused by the adhesive bonds between the MWCNTs and the fibres. This enables the MWCNTs to resist the sweeping pressure, which comes from the epoxy resin infusion.

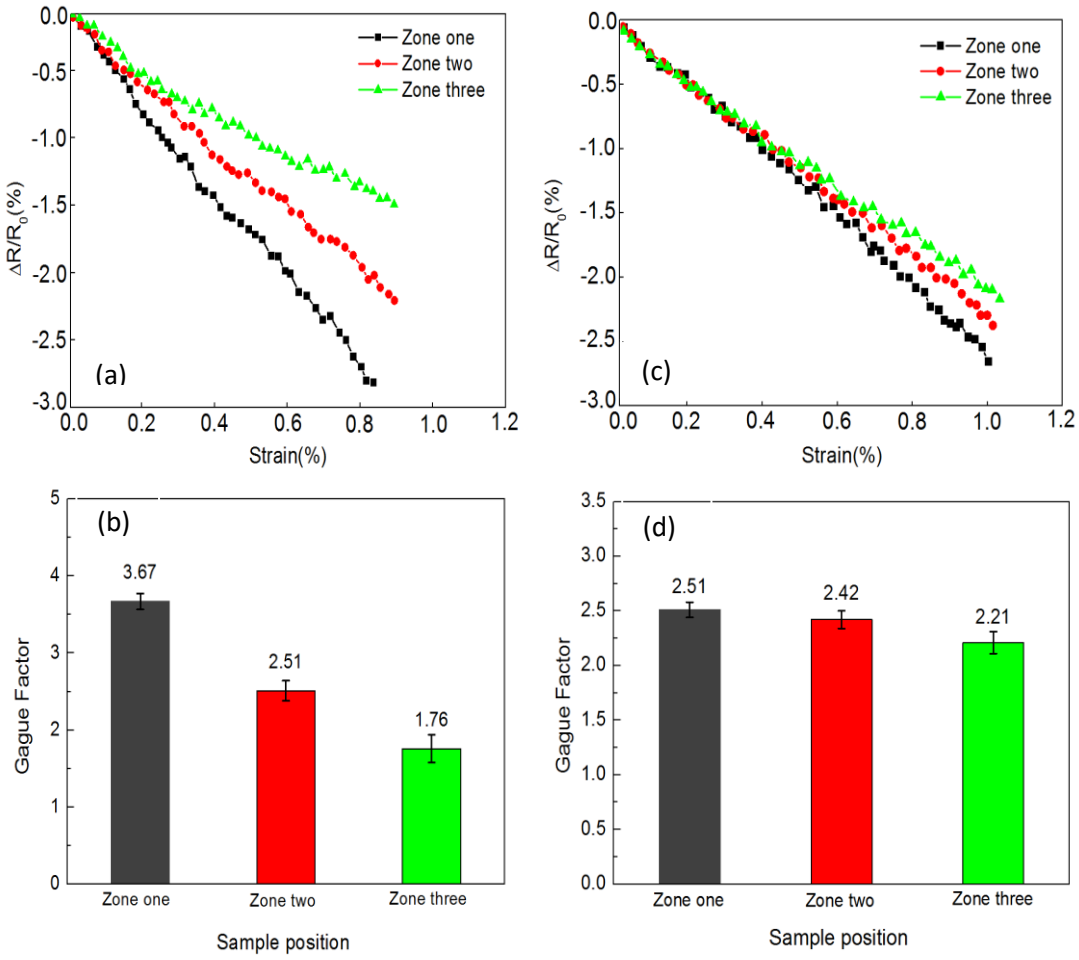

Figure 4.43: Normalised resistance change with strain and the gauge factors for different zones location. (a, b) without adhesive, (c, d) with adhesive.

The conclusions drawn from this chapter will be summarised in chapter 5.

Chapter 5
Conclusions

During the course of this study, the following major conclusions were reached for each of the areas of investigation concerned.

5.1 Impact Damage Assessment in Composites containing MWCNTs

In summary, a new criterion has been developed that enables assessment, detection and quantification of damage in real-time. This method is based on monitoring of how the electrical resistance of the permanent structure changes after an impact load. Self-sensing composites containing a quantity of MWCNTs were successfully prepared. The success of this method strongly depends on the employment of an optimal concentration of MWCNTs, with a good distribution, to detect the damage at any region in the composite structure when it is subjected to sudden impact. The results confirmed that;

1. The electrical conductivity of the self-sensing composite increased when the MWCNTs concentration increased.
2. SEM images revealed a good dispersion of 1.5% MWCNTs in the matrix of self-sensing composites and this was confirmed by Raman spectroscopy. In contrast, some agglomeration appeared when the MWCNTs concentration increased to 2.0 wt.%.

3. The maximum absorbed energy with the lowest damage factor occurred at 1.5 wt.% of MWCNTs concentration. However, the damage sensitivity decreases with increasing the MWCNTs content and a 0.5 wt.% of MWCNTs offered good damage sensitivity to impact.
4. The normalised changes in resistance, or the permanent damage parameter in the electrical resistance of the self-sensing composite, increased with increases in the impact energy and decreased when the MWCNTs content increased.
5. The statistical results showed that there were a significant difference between the properties of the nanocomposite samples containing different MWCNTs concentrations when these were impacted at different impact energies.

Therefore, it is believed that the *in-situ*, real-time, measurement of electrical resistance in self-sensing composite materials, and their stability during repeated impacts, offers the potential for an on-line method of sensing and evaluating sudden impact damage events in a structure, so minimising the possibility of catastrophic failure occurring.

5.2 The Electromechanical and Temperature Dependent Behaviour of Composites contaning MWCNTs

During these investigations the following major conclusions were reached.

1. The compressive strength and Young's modulus of the MWCNTs/epoxy nanocomposites were considerably enhanced by the addition of MWCNTs to the matrix material. These enhanced properties can be ascribed to the good interfacial bond between the MWCNTs and the matrix, so improving load transfer through the structure.

2. MWCNTs were added to epoxy resin, a conductive nanocomposite material was created. When the concentration (by weight %) of the MWCNTs was increased, a significant increase in the electrical conductivity of the nanocomposite was observed, reaching a maximum value of 0.01 $S.m^{-1}$ at 2.0 weight %.
3. The strain sensitivity, as measured in terms of the nanocomposite gauge factor, was dependent upon the MWCNTs concentration, with this being highest at the lowest concentration of MWCNTs. The strain sensitivity of the MWCNTs/epoxy nanocomposite decreased as the temperature increased up to 70°C. Thereafter, it increased sharply and reached a maximum value of 5.29 at 80 °C.
4. Under constant amplitude cyclic loadings the MWCNTs/epoxy nanocomposite exhibited a stable, and reproducible, piezo-resistive response up to a temperature of 60°C. Up to this temperature, the resistance decreased in step with the applied cyclic loading. As the glass transition temperature of the nanocomposite was approached, the response of the material was seen to change, being no longer directly in step with the applied cyclic loading. At 80°C, the observed behaviour was quite different, and now indicated by a steadily increasing (R) resistance.
5. As a self-sensing smart material, this type of nanocomposite shows considerable potential for structural health monitoring purposes, albeit within a limited working temperature range.

5.3 Damage Sensing in Composites containing MWCNTs during Anticlastic Bending

The damage sustained in composite materials is still a critical issue. Here, a self-sensing composite was manufactured by adding controlled concentrations of MWCNTs to the mixture (i.e. epoxy) of glass/fibre composite. Two different tests, viz. flexural and anticlastic, were conducted on this novel type of smart composites and the main finding obtained were:-

1. The mechanical properties of the smart composite were considerably enhanced by adding the MWCNTs as a second filler.

2. It is observed that at 1.5 wt.% of MWCNTs, the strength of the composite reached a maximum. Above this value (at 2.0 wt.%) of MWCNTs agglomeration reduce the mechanical performance in terms of strength but not stiffness (E).
3. The normalised change in resistance ($\Delta R/R_0$) reduced in the flexural and give a minimun value at 8 mm of displacement. Therefore, it increased sharply. During anticlastic testing the normalised resistance reduced by ≈ 70% more than that observed for the flexural for a 9.3 mm of displacement, after which, it increased and becomes positive. This was due to the formation of tensile/compressive saddle shape surfaces under loading.
4. The strain sensitivity was constant for the flexural test and had a value of - 2.1. This value was less than the value those obtained from the strain gauges used during anticlastic testing. The values decreased by about 47%. Therefore, the results obtained here provide a good understanding of the behaviour of the

composites based MWCNTs in terms of loads and strain sensitivity for complex loading conditions.

5.4 The Drift Properties of MWCNTs in Composites during Manufacture

In summary, MWCNTs-GE composite panels were fabricated using vacuum infusion techniques. These panels were additionally reinforced using MWCNTs, with these being incorporated into the composite structure with, and without, the use of a bonding adhesive. These panels were investigated, both experimentally and theoretically, and from this work; the following major conclusions can be drawn;

1. In general, both mechanical and electrical properties of the fabricated composites were greatly enhanced by the addition of MWCNTs to their structure, particularly where these were fixed in place using a simple bonding adhesive.
2. The flexural strength of the MWCNTs-GE composites, where bonding adhesive was used, was improved compared to the reference by ≈ 37 % for the samples located at the end of the panel, with changes of less than ≈ 1.6 % from this for the other zones. Where no bonding adhesive was used only a 26% increase occurred, this was maximum at the panel end with equally large values being observed at the first and second zones.
3. The flexural modulus increased by ≈ 27 % and ≈ 21.4 % for the composite with, and without, the use of bonding adhesive respectively.

4. The electrical conductivity measurements were also found to be high at the end of the MWCNTs-GE composite tests panels especially where no adhesive was used, with a maximum value of ≈ 0.06 S/m.
5. The epoxy infusion process also affected the electrical resistance and the gauge factors of the MWCNT-GE composites. Infusion brought about a change in the volume fraction of MWCNTs along the length of the composite. The electrical resistance was high, and the gauge factor was low, where no bonding adhesive was used at zone three.
6. Due to the drift of the MWCNTs to the end of the non-adhesive panel, the interparticle tunnelling distances between the MWCNTs had to be determined by theoretical analysis. The obtained results showed that there is an inverse relationship between the tunnelling distance and volume fraction of the MWCNTs. The samples having a high MWCNTs volume fraction at the end of panels exhibited a substantial reduction in the MWCNTs tunnelling distance.
7. From the results obtained, a variation in MWCNTs-GE composite properties of the test panels (with and without adhesive) were observed. The extent of the change depended upon where the test specimens were taken from in the fabricated panels. Test specimens taken from the zone three position exhibited higher mechanical, electrical properties, and lower strain sensitivity, than those taken from zone one. These properties are fully dependent on the areal density of the MWCNTs in each location.

Chapter 6

Overall Summary and Recommendations for Future Work

6.1 Thesis Summary

Multi-walled carbon nanotubes (MWCNTs) are currently considered to be very effective engineering materials due to their superior mechanical, electrical and thermal properties. They can also be used to reinforce epoxy resin as a means of preparing self-sensing nanocomposites. Embedding MWCNTs in the matrix of the glass/fibre composite (i.e. epoxy resin) or depositing them on the glass fibre surface to serve as strain and damage sensors was introduced in this thesis. The effects of adding different concentrations of multi-wall carbon nanotubes on the mechanical, electrical, strain sensitivity properties were studied in detail. Standard mixing techniques using an ultrasonic probe were also used and studied during the manufacture of appropriate specimens for testing.

A variety of mechanical tests such as flexural, compression, anticlastic bending, impact, and flexural testing after impact tests, were studied under both static and dynamic (cyclic) conditions. The results of these tests were then evaluated in detail. In addition to the microstructure, was also studied using Scanning Electronics Microscope (SEM), with Raman spectroscopy and optical microscopy being used to visualise the degree and state of dispersion of the MWCNTs within the matrix of the self-sensing nanocomposite. The main aim of this study was to make the composite into a self-sensing structure which could monitor any change in response to different types of mechanical loading during service.

To a large degree this was accomplished through establishing an electromechnical coupling between the effect of the structure geometry and the developed strain in the structure as indicated by the electrical resistance change under different experimental conditions. From this experimental and theoretical work the following overarching conclusions can be drawn;

1. The addition of MWCNTs into polymer matrix composites and onto fibres surface, which were studied in this work, can be exploited as self-sensing elements in composites for *in-situ* structural health monitoring (SHM) purposes.
2. The electrical conductivity measurements for the MWCNTs nanocomposites indicated a steadily increasing directly proportional relationship with increasing MWCNTs concentration. This was due to the formation of MWCNTs conductive networks.
3. The resistance change of the self-sensing nanocomposite, when subjected to mechanical loading, is ascribed to the contribution of several effects. These are; the orientation of MWCNTs, an increase in the tunnelling resistance, and the change in contact area between neighbouring MWCNT and the inherent piezoresistive influence.
4. Damage sensitivity and damage factor properties were studied experimentally and statistically as the specimens were subjected to different levels of impact energies. The results showed that the changes in electrical resistance of specimens increased with an increasing impact energy. Moreover, the specimens containing a high MWCNTs concentration showed a lower damage sensitivity and a lower damage factor under all impact energy levels.

5. The piezo-resistive properties of MWCNTs/epoxy nanocomposites were also investigated at different temperatures, under both static and cyclic compressive loading conditions. For zero loading, the results obtained indicated that the normalised resistance of the nanocomposite increased with increasing temperature and decreased with increases in the MWCNTs concentration. However, under cyclic loading conditions, the normalised resistance showed different types of behaviour since it decreased with increasing the compressive load up to 65°C. Thereafter, it started to increase, and only increased more slowly when 70°C was reached. It then sharply increased when the temperature reached 80°C. The strain sensitivity measurements for static loads indicated that it increased as the MWCNTs concentration decreased. Nevertheless, for cyclic loading, it showed a different type of behaviour, especially when the temperature increased above 65°C.
6. The strain deformation due to the flexural test was only in one direction (i.e. in y-direction) and indicated higher value compared to both strain values (in the x and y directions) obtained from the anticlastic test. In addition, two strain sensitivities, but with opposite signs, where obtained from anticlastic tests while only one was obtained from the flexural test and had a magnitude equal to approximately half the value when compared to those obtained from the anticlastic test.
7. The self-sensing composites with adhesively bonded MWCNTs exhibited a more consistent response in their properties than the composites where no adhesive was used. In addition, the electrical resistance of both types of self-sensing composites was monitored during the epoxy infusion process. The results showed that the electrical resistance was not obviously affected for the

composite with non-adhesive bonded MWCNTs but was high for the specimens where the MWCNTs were not adhesively bonded. Moreover, the numerical study indicated that the relationship between the tunnelling distance between the MWCNTs filler and their volume fraction was inverse in nature.

6.2 Recommendations for Future Work

In order to make the initial finding of this thesis more general or comprehensive to the readers, additional experimental work and further studies are required. These could include the following;

1. Numerous numbers of studies have tried to embed different types and concentrations of CNTs to fabricate strain sensors for damage detecting. However, the electromechanical behaviour of these types of self-sensing nanocomposites is still unclear, complicated and not fully understood. Therefore, carrying more experiments need to be carried out to understand the sensing mechanism and to elucidate details of their piezoresistive response. This is important in order to utilise this type of self-sensing material for strain and damage sensing.
2. Based on the results obtaind in this thesis regarding the behaviour of the composite matrix exposed to heat. It is important to evaluate the properties of the composite when subjected to high velocity impact of nanocomposites under different temperature conditions. This needs to be better understood, particularly at different conditions of temperature and impact loading conditions, including strain rate at impact.
3. Comparison of the current results with self-sensing nanocomposite made from different types of polymer resins, either thermosetting or thermoplastic, is

needed to find the relationship between the results obtained and the matrix type (i.e. polymers).

4. Additional fatigue tests must be carried out on the nanocomposite based CNTs to study the behaviour of the changing electric resistance of the specimens as a function of possible fatigue test parameters, viz. random loading conditions, static over load effects and the influence of temperature.
5. Glass and carbon fibre reinforced composites are widely used in the many practical engineering of applications. Therefore, it is also necessary to develop new and easier techniques to deposit the CNTs into fibre surfaces of composite structures in order to monitor any changes when they are subjected to mechanical loading during service. Here 'real-time' variations must be investigated.
6. Due to self-sensing nanocomposites having the ability to monitor the propagation of the cracks that occurred inside the structure, it is also important to exploit the superior properties of the CNTs for self-healing purposes. To date very little research has been done in this important area.

References

1. Barbero, E. J. (2017) *Introduction to composite materials design*. CRC press.
2. Agarwal, B. D., Broutman, L. J. & Chandrashekhara, K. (2017) *Analysis and performance of fiber composites*. John Wiley & Sons.
3. Abot, J. L., Song, Y., Vatsavaya, M. S., Medikonda, S., Kier, Z., Jayasinghe, C., Rooy, N., Shanov, V. N. & Schulz, M. J. (2010) '*Delamination detection with carbon nanotube thread in self-sensing composite materials*'. Composites Science and Technology, 70 (7), pp. 1113-1119.
4. Ramakrishnan, M., Rajan, G., Semenova, Y. & Farrell, G. (2016) '*Overview of fiber optic sensor technologies for strain/temperature sensing applications in composite materials*'. Sensors, 16 (1), pp. 99.
5. Wen, J., Xia, Z. & Choy, F. (2011) '*Damage detection of carbon fiber reinforced polymer composites via electrical resistance measurement*'. Composites Part B: Engineering, 42 (1), pp. 77-86.
6. Chung, D. (2012) '*Carbon materials for structural self-sensing, electromagnetic shielding and thermal interfacing*'. Carbon, 50 (9), pp. 3342-3353.
7. Spitalsky, Z., Tasis, D., Papagelis, K. & Galiotis, C. (2010) '*Carbon nanotube–polymer composites: chemistry, processing, mechanical and electrical properties*'. Progress in polymer science, 35 (3), pp. 357-401.
8. Varshney, K. (2014) '*Carbon nanotubes: a review on synthesis, properties and applications*'. International Journal of Engineering Research, 2 (4), pp. 660-677.
9. Cha, J., Jun, G. H., Park, J. K., Kim, J. C., Ryu, H. J. & Hong, S. H. (2017) '*Improvement of modulus, strength and fracture toughness of CNT/Epoxy nanocomposites through the functionalization of carbon nanotubes*'. Composites Part B: Engineering, 129 pp. 169-179.
10. Chu, K., Lee, S.-C., Lee, S., Kim, D., Moon, C. & Park, S.-H. (2015) '*Smart conducting polymer composites having zero temperature coefficient of resistance*'. Nanoscale, 7 (2), pp. 471-478.
11. Ku-Herrera, J., Avilés, F. & Seidel, G. (2013) '*Self-sensing of elastic strain, matrix yielding and plasticity in multiwall carbon nanotube/vinyl ester composites*'. Smart Materials and Structures, 22 (8), pp. 085003.
12. Bhushan, B. (2017) *Springer handbook of nanotechnology*. Springer.
13. Yadav, T. P., Yadav, R. M. & Singh, D. P. (2012) '*Mechanical milling: a top down approach for the synthesis of nanomaterials and nanocomposites*'. Nanoscience and Nanotechnology, 2 (3), pp. 22-48.
14. Iijima, S. & Ichihashi, T. (1993) '*Single-shell carbon nanotubes of 1-nm diameter*'. nature, 363 (6430), pp. 603.
15. Ansari, S. (2017) '*Combination of molecularly imprinted polymers and carbon nanomaterials as a versatile biosensing tool in sample analysis: Recent applications and challenges*'. TrAC Trends in Analytical Chemistry, 93 pp. 134-151.

16. Roch, A., Stepien, L., Roch, T., Dani, I., Leyens, C., Jost, O. & Leson, A. (2014) '*Optical absorption spectroscopy and properties of single walled carbon nanotubes at high temperature*'. Synthetic Metals, 197 pp. 182-187.

17. Kumar, M. & Ando, Y. (2010) '*Chemical vapor deposition of carbon nanotubes: a review on growth mechanism and mass production*'. Journal of nanoscience and nanotechnology, 10 (6), pp. 3739-3758.

18. Kulkarni, M., Carnahan, D., Kulkarni, K., Qian, D. & Abot, J. L. (2010) '*Elastic response of a carbon nanotube fiber reinforced polymeric composite: a numerical and experimental study*'. Composites Part B: Engineering, 41 (5), pp. 414-421.

19. Eftekhari, M., S. Mohammadi, and A.R. Khoei, *Effect of defects on the local shell buckling and post-buckling behavior of single and multi-walled carbon nanotubes.* Computational Materials Science, 2013. **79**: p. 736-744.

20. Esawi, A. M. K. & Farag, M. M. (2007) '*Carbon nanotube reinforced composites: Potential and current challenges*'. Materials & Design, 28 (9), pp. 2394-2401.

21. Wang, P.-N., Hsieh, T.-H., Chiang, C.-L. & Shen, M.-Y. (2015) '*Synergetic effects of mechanical properties on graphene nanoplatelet and multiwalled carbon nanotube hybrids reinforced epoxy/carbon fiber composites*'. Journal of Nanomaterials, 2015 pp. 7.

22. Bal, S. (2007) '*Influence of dispersion states of carbon nanotubes on mechanical and electrical properties of epoxy nanocomposites*'. Journal of scientific and industrial reasearch, 66 (9).

23. Kim, B. C. & Park, S. W. (2008) '*Fracture toughness of the nano-particle reinforced epoxy composite*'. Composite Structures, 86 (1), pp. 69-77.

24. Gkikas, G., Barkoula, N.-M. & Paipetis, A. (2012) '*Effect of dispersion conditions on the thermo-mechanical and toughness properties of multi walled carbon nanotubes-reinforced epoxy*'. Composites Part B: Engineering, 43 (6), pp. 2697-2705.

25. Alexopoulos, N., Bartholome, C., Poulin, P. & Marioli-Riga, Z. (2010) '*Structural health monitoring of glass fiber reinforced composites using embedded carbon nanotube (CNT) fibers*'. Composites Science and Technology, 70 (2), pp. 260-271.

26. Bhattacharya, M. (2016) '*Polymer nanocomposites—a comparison between carbon nanotubes, graphene, and clay as nanofillers*'. Materials, 9 (4), pp. 262.

27. Mittal, G., Dhand, V., Rhee, K. Y., Park, S.-J. & Lee, W. R. (2015) '*A review on carbon nanotubes and graphene as fillers in reinforced polymer nanocomposites*'. Journal of industrial and engineering chemistry, 21 pp. 11-25.

28. Qiu, J., Zhang, C., Wang, B. & Liang, R. (2007) '*Carbon nanotube integrated multifunctional multiscale composites*'. Nanotechnology, 18 (27), pp. 275708.

29. Gao, L., Chou, T.-W., Thostenson, E. T., Godara, A., Zhang, Z. & Mezzo, L. (2010a) '*Highly conductive polymer composites based on controlled agglomeration of carbon nanotubes*'. Carbon, 48 (9), pp. 2649-2651.

30. An, F., Lu, C., Guo, J., He, S., Lu, H. & Yang, Y. (2011) '*Preparation of vertically aligned carbon nanotube arrays grown onto carbon fiber fabric and evaluating its wettability on effect of composite*'. Applied Surface Science, 258 (3), pp. 1069-1076.

31. Bekyarova, E., Thostenson, E., Yu, A., Kim, H., Gao, J., Tang, J., Hahn, H., Chou, T.-W., Itkis, M. & Haddon, R. (2007) '*Multiscale carbon nanotube− carbon fiber reinforcement for advanced epoxy composites*'. Langmuir, 23 (7), pp. 3970-3974.

32. Zhang, H., Liu, Y., Kuwata, M., Bilotti, E. & Peijs, T. (2015b) '*Improved fracture toughness and integrated damage sensing capability by spray coated CNTs on carbon fibre prepreg*'. Composites Part A: Applied Science and Manufacturing, 70 pp. 102-110.

33. Roh, S. C., Choi, E. Y., Choi, Y. S. & Kim, C. (2014) '*Characterization of the surface energies of functionalized multi-walled carbon nanotubes and their interfacial adhesion energies with various polymers*'. Polymer, 55 (6), pp. 1527-1536.

34. Fejes, D. & Hernádi, K. (2010) 'A review of the properties and CVD synthesis of coiled carbon nanotubes'. Materials, 3 (4), pp. 2618-2642.

35. Ayatollahi, M. R., Shadlou, S., Shokrieh, M. M. & Chitsazzadeh, M. (2011) '*Effect of multi-walled carbon nanotube aspect ratio on mechanical and electrical properties of epoxy-based nanocomposites*'. Polymer Testing, 30 (5), pp. 548-556.

36. Wu, D., Wu, L., Zhou, W., Sun, Y. & Zhang, M. (2010) '*Relations between the aspect ratio of carbon nanotubes and the formation of percolation networks in biodegradable polylactide/carbon nanotube composites'*. Journal of Polymer Science Part B: Polymer Physics, 48 (4), pp. 479-489.

37. Li, J., Ma, P. C., Chow, W. S., To, C. K., Tang, B. Z. & Kim, J. K. (2007) '*Correlations between percolation threshold, dispersion state, and aspect ratio of carbon nanotubes*'. Advanced Functional Materials, 17 (16), pp. 3207-3215.

38. Huang, Y., Ahir, S. & Terentjev, E. (2006) '*Dispersion rheology of carbon nanotubes in a polymer matrix*'. Physical Review B, 73 (12), pp. 125422.

39. Wang, W., Ciselli, P., Kuznetsov, E., Peijs, T. & Barber, A. H. (2008) '*Effective reinforcement in carbon nanotube-polymer composites'*. Philos Trans A Math Phys Eng Sci, 366 (1870), pp. 1613-1626.

40. Ma, P.-C., Siddiqui, N. A., Marom, G. & Kim, J.-K. (2010) '*Dispersion and functionalization of carbon nanotubes for polymer-based nanocomposites: a review*'. Composites Part A: Applied Science and Manufacturing, 41 (10), pp. 1345-1367.

41. Nanni, F., Mayoral, B. L., Madau, F., Montesperelli, G. & McNally, T. (2012) '*Effect of MWCNT alignment on mechanical and self-monitoring properties of extruded PET–MWCNT nanocomposites*'. Composites Science and Technology, 72 (10), pp. 1140-1146.

42. Kim, S. W., Kim, T., Kim, Y. S., Choi, H. S., Lim, H. J., Yang, S. J. & Park, C. R. (2012) '*Surface modifications for the effective dispersion of carbon nanotubes in solvents and polymers*'. Carbon, 50 (1), pp. 3-33.

43. Moreno Marcelino, J. E., Vigueras Santiago, E., Lopez-Tellez, G. & Hernández López, S. (2014) '*Chemical functionalization of carbon nanotubes and its effects on electrical conductivity*', Journal of Nano Research. Trans Tech Publ, pp. 51-61.

44. Khan, S. U., Pothnis, J. R. & Kim, J.-K. (2013) '*Effects of carbon nanotube alignment on electrical and mechanical properties of epoxy nanocomposites*'. Composites Part A: Applied Science and Manufacturing, 49 pp. 26-34.

45. Sulong, A. B. & Park, J. (2011) '*Alignment of multi-walled carbon nanotubes in a polyethylene matrix by extrusion shear flow: mechanical properties enhancement*'. Journal of composite materials, 45 (8), pp. 931-941.

46. Parmar, K., Mahmoodi, M., Park, C. & Park, S. S. (2013) '*Effect of CNT alignment on the strain sensing capability of carbon nanotube composites*'. Smart Materials and Structures, 22 (7), pp. 075006.

47. Oliva-Avilés, A., Avilés, F. & Sosa, V. (2011) *'Electrical and piezoresistive properties of multi-walled carbon nanotube/polymer composite films aligned by an electric field*'. Carbon, 49 (9), pp. 2989-2997.

48. Tijing, L. D., Park, C.-H., Choi, W. L., Ruelo, M. T. G., Amarjargal, A., Pant, H. R., Im, I.-T. & Kim, C. S. (2013) '*Characterization and mechanical performance comparison of multiwalled carbon nanotube/polyurethane composites fabricated by electrospinning and solution casting*'. Composites Part B: Engineering, 44 (1), pp. 613-619.

49. Dijkstra, D. J., Cirstea, M. & Nakamura, N. (2010) '*The orientational behavior of multiwall carbon nanotubes in polycarbonate in simple shear flow*'. Rheologica acta, 49 (7), pp. 769-780.

50. Mahmoodi, M., Arjmand, M., Sundararaj, U. & Park, S. (2012) '*The electrical conductivity and electromagnetic interference shielding of injection molded multi-walled carbon nanotube/polystyrene composites*'. Carbon, 50 (4), pp. 1455-1464.

51. Jogi, B. F., Sawant, M., Kulkarni, M. & Brahmankar, P. K. (2012) '*Dispersion and performance properties of carbon nanotubes (CNTs) based polymer composites: a review*'. Journal of Encapsulation and Adsorption Sciences, 2 (04), pp. 69.

52. Cui, L.-J., Wang, Y.-B., Xiu, W.-J., Wang, W.-Y., Xu, L.-H., Xu, X.-B., Meng, Y., Li, L.-Y., Gao, J. & Chen, L.-T. (2013) '*Effect of functionalization of multi-walled carbon nanotube on the curing behavior and mechanical property of multi-walled carbon nanotube/epoxy composites*'. Materials & Design, 49 pp. 279-284.

53. Zhang, Q., Huang, J.-Q., Zhao, M.-Q., Qian, W.-Z., Wang, Y. & Wei, F. (2008) '*Radial growth of vertically aligned carbon nanotube arrays from ethylene on ceramic spheres*'. Carbon, 46 (8), pp. 1152-1158ز

54. Bauhofer, W. & Kovacs, J. Z. (2009) '*A review and analysis of electrical percolation in carbon nanotube polymer composites*'. Composites Science and Technology, 69 (10), pp. 1486-1498.

55. Liu, H., Li, Q., Zhang, S., Yin, R., Liu, X., He, Y., Dai, K., Shan, C., Guo, J. & Liu, C. (2018) '*Electrically conductive polymer composites for smart flexible strain sensors: a critical review*'. Journal of Materials Chemistry C, 6 (45), pp. 12121-12141.

56. Pandey, G. & Thostenson, E. T. (2012) '*Carbon nanotube-based multifunctional polymer nanocomposites*'. Polymer Reviews, 52 (3), pp. 355-416.

57. Naebe, M., Abolhasani, M. M., Khayyam, H., Amini, A. & Fox, B. (2016) '*Crack damage in polymers and composites: A review*'. Polymer reviews, 56 (1), pp. 31-69.

58. Kim, K. J., Yu, W.-R., Lee, J. S., Gao, L., Thostenson, E. T., Chou, T.-W. & Byun, J.-H. (2010) '*Damage characterization of 3D braided composites using carbon nanotube-based in situ sensing*'. Composites Part A: Applied Science and Manufacturing, 41 (10), pp. 1531-1537.

59. Hu, N., Karube, Y., Arai, M., Watanabe, T., Yan, C., Li, Y., Liu, Y. & Fukunaga, H. (2010) '*Investigation on sensitivity of a polymer/carbon nanotube composite strain sensor*'. Carbon, 48 (3), pp. 680-687.

60. Güemes, A., Fernandez-Lopez, A. & Fernandez, P. (2014) '*Damage detection in composite structures from fibre optic distributed strain measurements*', EWSHM-7th European Workshop on Structural Health Monitoring.

61. Chung, D. D. (2010) Composite materials: *science and applications*. Springer Science & Business Media.

62. Shi, Y., Swait, T. & Soutis, C. (2012) '*Modelling damage evolution in composite laminates subjected to low velocity impact*'. Composite Structures, 94 (9), pp. 2902-2913.

63. Kostopoulos, V., Baltopoulos, A., Karapappas, P., Vavouliotis, A. & Paipetis, A. (2010) '*Impact and after-impact properties of carbon fibre reinforced composites enhanced with multi-wall carbon nanotubes*'. Composites Science and Technology, 70 (4), pp. 553-563.

64. Faggiani, A. & Falzon, B. (2010) *'Predicting low-velocity impact damage on a stiffened composite panel*'. Composites Part A: Applied Science and Manufacturing, 41 (6), pp. 737-749.

65. Siegfried, M., Tola, C., Claes, M., Lomov, S. V., Verpoest, I. & Gorbatikh, L. (2014) '*Impact and residual after impact properties of carbon fiber/epoxy composites modified with carbon nanotubes*'. Composite Structures, 111 pp. 488-496.

66. Bull, D. J., Helfen, L., Sinclair, I., Spearing, S. & Baumbach, T. (2013) '*A comparison of multi-scale 3D X-ray tomographic inspection techniques for assessing carbon fibre composite impact damage*'. Composites Science and Technology, 75 pp. 55-61.

67. García-Martín, J., Gómez-Gil, J. & Vázquez-Sánchez, E. (2011) '*Non-destructive techniques based on eddy current testing*'. Sensors, 11 (3), pp. 2525-2565.

68. Meola, C. & Carlomagno, G. M. (2010) '*Impact damage in GFRP: new insights with infrared thermography*'. Composites Part A: Applied Science and Manufacturing, 41 (12), pp. 1839-1847.

69. Katunin, A., Dragan, K. & Dziendzikowski, M. (2015) '*Damage identification in aircraft composite structures: A case study using various non-destructive testing techniques*'. Composite Structures, 127 pp. 1-9.

70. Di Sante, R. (2015) '*Fibre optic sensors for structural health monitoring of aircraft composite structures: Recent advances and applications*'. Sensors, 15 (8), pp. 18666-18713.

71. Rauf, A., Hand, R. & Hayes, S. (2012) '*Optical self-sensing of impact damage in composites using E-glass cloth*'. Smart Materials and Structures, 21 (4), pp. 045021.

72. Ikikardaslar, K. & Delale, F. (2018) '*Self-sensing damage in CNT infused epoxy panels with and without glass-fibre reinforcement*'. Strain, pp. e12268.

73. De Volder, M. F., Tawfick, S. H., Baughman, R. H. & Hart, A. J. (2013) '*Carbon nanotubes: present and future commercial applications*'. science, 339 (6119), pp. 535-539.

74. Bedsole, R. W., Park, C., Bogert, P. B. & Tippur, H. V. (2015) '*A critical evaluation of the enhancement of mechanical properties of epoxy modified using CNTs*'. Materials Research Express, 2 (9), pp. 095020.

75. Gao, L., Chou, T.-W., Thostenson, E. T., Zhang, Z. & Coulaud, M. (2011) *'In situ sensing of impact damage in epoxy/glass fiber composites using percolating carbon nanotube networks*'. Carbon, 49 (10), pp. 3382-3385.

76. Naghashpour, A. & Van Hoa, S. (2013a) '*In situ monitoring of through-thickness strain in glass fiber/epoxy composite laminates using carbon nanotube sensors*'. Composites Science and Technology, 78 pp. 41-47.

77. Monti, M., Natali, M., Petrucci, R., Kenny, J. M. & Torre, L. (2011) '*Impact damage sensing in glass fiber reinforced composites based on carbon nanotubes by electrical resistance measurements*'. Journal of Applied Polymer Science, 122 (4), pp. 2829-2836.

78. Arronche, L., La Saponara, V., Yesil, S. & Bayram, G. (2013) '*Impact damage sensing of multiscale composites through epoxy matrix containing carbon nanotubes*'. Journal of Applied Polymer Science, 128 (5), pp. 2797-2806.

79. Costa, P., Silva, J., Ansón-Casaos, A., Martinez, M., Abad, M., Viana, J. & Lanceros-Mendez, S. (2014) '*Effect of carbon nanotube type and functionalization on the electrical, thermal, mechanical and electromechanical properties of carbon nanotube/styrene–butadiene–styrene composites for large strain sensor applications*'. Composites Part B: Engineering, 61 pp. 136-146.

80. Hu, N., Fukunaga, H., Atobe, S., Liu, Y. & Li, J. (2011) '*Piezoresistive strain sensors made from carbon nanotubes based polymer nanocomposite*s'. Sensors, 11 (11), pp. 10691-10723.

81. Bouhamed, A., Al-Hamry, A., Müller, C., Choura, S. & Kanoun, O. (2017) '*Assessing the electrical behaviour of MWCNTs/epoxy nanocomposite for strain sensing*'. Composites Part B: Engineering, 128 pp. 91-99.

82. Shen, J., Buschhorn, S., De Hosson, J. T. M., Schulte, K. & Fiedler, B. (2015) '*Pressure and temperature induced electrical resistance change in nano-carbon/epoxy composites*'. Composites Science and Technology, 115 pp. 1-8.

83. Li, J., Lu, Y., Ye, Q., Cinke, M., Han, J. & Meyyappan, M. (2003) '*Carbon nanotube sensors for gas and organic vapor detection*'. Nano letters, 3 (7), pp. 929-933.

84. Li, C., Thostenson, E. T. & Chou, T.-W. (2008) '*Sensors and actuators based on carbon nanotubes and their composites: a review*'. Composites Science and Technology, 68 (6), pp. 1227-1249.

85. Park, J.-M., Jang, J.-H., Wang, Z.-J., Kwon, D.-J. & DeVries, K. L. (2010) '*Self-sensing of carbon fiber/carbon nanofiber–epoxy composites with two different nanofiber aspect ratios investigated by electrical resistance and wettability measurements*'. Composites Part A: Applied Science and Manufacturing, 41 (11), pp. 1702-1711.

86. Cao, X., Wei, X., Li, G., Hu, C., Dai, K., Guo, J., Zheng, G., Liu, C., Shen, C. & Guo, Z. (2017) '*Strain sensing behaviors of epoxy nanocomposites with carbon nanotubes under cyclic deformation*'. Polymer, 112 pp. 1-9.

87. Mohiuddin, M. & Hoa, S. (2011) '*Temperature dependent electrical conductivity of CNT–PEEK composites*'. Composites Science and Technology, 72 (1), pp. 21-27.

88. Ou, J. & Zhou, Z. (2008) '*Applications of optical fiber sensors of SHM in infrastructures*', Smart Sensor Phenomena, Technology, Networks, and Systems 2008. International Society for Optics and Photonics, pp. 693311.

89. Dinh, N. T. & Kanoun, O. (2015) '*Temperature-compensated force/pressure sensor based on multi-walled carbon nanotube epoxy composites*'. Sensors, 15 (5), pp. 11133-11150.

90. Vollebregt, S., Banerjee, S., Beenakker, K. & Ishihara, R. (2013) '*Size-dependent effects on the temperature coefficient of resistance of carbon nanotube vias*'. IEEE Transactions on Electron Devices, 60 (12), pp. 4085-4089.

91. Zhang, H., Kuwata, M., Bilotti, E. & Peijs, T. (2015a) *'Integrated damage sensing in fibre-reinforced composites with extremely low carbon nanotube loadings*'. Journal of Nanomaterials, 16 (1), pp. 243.

92. Zhang, H., Bilotti, E. & Peijs, T. (2015) '*The use of carbon nanotubes for damage sensing and structural health monitoring in laminated composites: a review*'. Nanocomposites, 1 (4), pp. 167-184.

93. Karapappas, P., Vavouliotis, A., Tsotra, P., Kostopoulos, V. & Paipetis, A. (2009) '*Enhanced fracture properties of carbon reinforced composites by the addition of multi-wall carbon nanotubes*'. Journal of composite materials, 43 (9), pp. 977-985.

94. Davis, D. C., Wilkerson, J. W., Zhu, J. & Ayewah, D. O. (2010) '*Improvements in mechanical properties of a carbon fiber epoxy composite using nanotube science and technology*'. Composite Structures, 92 (11), pp. 2653-2662.

95. Rathore, D. K., Prusty, R. K., Kumar, D. S. & Ray, B. C. (2016) '*Mechanical performance of CNT-filled glass fiber/epoxy composite in in-situ elevated temperature environments emphasizing the role of CNT content*'. Composites Part A: Applied Science and Manufacturing, 84 pp. 364-376.

96. Awan, F. S., Fakhar, M. A., Khan, L. A., Zaheer, U., Khan, A. F. & Subhani, T. (2018) '*Interfacial mechanical properties of carbon nanotube-deposited carbon fiber epoxy matrix hierarchical composites*'. Composite Interfaces, 25 (8), pp. 681-699.

97. Iijima, S. (1991) '*Helical microtubules of graphitic carbon*'. nature, 354 (6348), pp. 56.

98. Bautista-Quijano, J., Avilés, F., Aguilar, J. & Tapia, A. (2010) '*Strain sensing capabilities of a piezoresistive MWCNT-polysulfone film*'. Sensors and Actuators A: Physical, 159 (2), pp. 135-140.

99. Kathi, J., Rhee, K.-Y. & Lee, J. H. (2009) '*Effect of chemical functionalization of multi-walled carbon nanotubes with 3-aminopropyltriethoxysilane on mechanical and morphological properties of epoxy nanocomposites*'. Composites Part A: Applied Science and Manufacturing, 40 (6-7), pp. 800-809.

100. Kim, M., Rhee, K., Lee, J., Hui, D. & Lau, A. K. (2011) *'Property enhancement of a carbon fiber/epoxy composite by using carbon nanotubes'*. Composites Part B: Engineering, 42 (5), pp. 1257-1261.

101. Fan, Z., Santare, M. H. & Advani, S. G. (2008) '*Interlaminar shear strength of glass fiber reinforced epoxy composites enhanced with multi-walled carbon nanotubes*'. Composites Part A: Applied Science and Manufacturing, 39 (3), pp. 540-554.

102. Zhao, J., Dai, K., Liu, C., Zheng, G., Wang, B., Liu, C., Chen, J. & Shen, C. (2013) '*A comparison between strain sensing behaviors of carbon black/polypropylene and carbon nanotubes/polypropylene electrically conductive composites*'. Composites Part A: Applied Science and Manufacturing, 48 pp. 129-136.

103. Vertuccio, L., Guadagno, L., Spinelli, G., Lamberti, P., Tucci, V. & Russo, S. (2016) '*Piezoresistive properties of resin reinforced with carbon nanotubes for health-monitoring of aircraft primary structures*'. Composites Part B: Engineering, 107 pp. 192-202.

104. Park, J.-M., Kim, D.-S., Kim, S.-J., Kim, P.-G., Yoon, D.-J. & DeVries, K. L. (2007) '*Inherent sensing and interfacial evaluation of carbon nanofiber and nanotube/epoxy composites using electrical resistance measurement and micromechanical technique*'. Composites Part B: Engineering, 38 (7-8), pp. 847-861.

105. Thostenson, E. T. & Chou, T. W. (2006) '*Carbon nanotube networks: sensing of distributed strain and damage for life prediction and self healing*'. Advanced Materials, 18 (21), pp. 2837-2841.

106. Böger, L., Sumfleth, J., Hedemann, H. & Schulte, K. (2010) '*Improvement of fatigue life by incorporation of nanoparticles in glass fibre reinforced epoxy*'. Composites Part A: Applied Science and Manufacturing, 41 (10), pp. 1419-1424.

107. Azwa, Z., Yousif, B., Manalo, A. & Karunasena, W. (2013) '*A review on the degradability of polymeric composites based on natural fibres*'. Materials & Design, 47 pp. 424-442.

108. Gaztelumendi, I., Chapartegui, M., Seddon, R., Flórez, S., Pons, F. & Cinquin, J. (2017) '*Enhancement of electrical conductivity of composite structures by integration of carbon nanotubes via bulk resin and/or buckypaper films*'. Composites Part B: Engineering, 122 pp. 31-40.

109. Shi, S., Wang, L., Pan, Y., Liu, C., Liu, X., Li, Y., Zhang, J., Zheng, G. & Guo, Z. (2019) '*Remarkably Strengthened microinjection molded linear low-density polyethylene (LLDPE) via multi-walled carbon nanotubes derived nanohybrid shish-kebab structure*'. Composites Part B: Engineering.

110. Li, Z., Wang, B., Qin, X., Wang, Y., Liu, C., Shao, Q., Wang, N., Zhang, J., Wang, Z. & Shen, C. (2018b) '*Superhydrophobic/superoleophilic polycarbonate/carbon nanotubes porous monolith for selective oil adsorption from water*'. ACS Sustainable Chemistry & Engineering, 6 (11), pp. 13747-13755.

111. Lin, C., Hu, L., Cheng, C., Sun, K., Guo, X., Shao, Q., Li, J., Wang, N. & Guo, Z. (2018) '*Nano-TiNb2O7/carbon nanotubes composite anode for enhanced lithium-ion storage*'. Electrochimica Acta, 260 pp. 65-72.

112. Zhou, B., Li, Y., Zheng, G., Dai, K., Liu, C., Ma, Y., Zhang, J., Wang, N., Shen, C. & Guo, Z. (2018) '*Continuously fabricated transparent conductive polycarbonate/carbon nanotube nanocomposite films for switchable thermochromic applications*'. Journal of Materials Chemistry C, 6 (31), pp. 8360-8371.

113. Cheng, C., Fan, R., Ren, Y., Ding, T., Qian, L., Guo, J., Li, X., An, L., Lei, Y. & Yin, Y. (2017) '*Radio frequency negative permittivity in random carbon nanotubes/alumina nanocomposites*'. Nanoscale, 9 (18), pp. 5779-5787.

114. Chang, M. S. (2010) '*An investigation on the dynamic behavior and thermal properties of MWCNTs/FRP laminate composites*'. Journal of Reinforced Plastics and Composites, 29 (24), pp. 3593-3599.

115. Liu, W., Wei, B. & Xu, F. (2017) '*Investigation on the mechanical and electrical properties of carbon nanotube/epoxy composites produced by resin transfer molding*'. Journal of composite materials, 51 (14), pp. 2035-2043.

116. Frømyr, T. R., Hansen, F. K. & Olsen, T. (2012) '*The optimum dispersion of carbon nanotubes for epoxy nanocomposites: evolution of the particle size distribution by ultrasonic treatment*'. Journal of Nanotechnology, 2012.

117. De Greef, N., Zhang, L., Magrez, A., Forró, L., Locquet, J.-P., Verpoest, I. & Seo, J. W. (2015) '*Direct growth of carbon nanotubes on carbon fibers: Effect of the CVD parameters on the degradation of mechanical properties of carbon fibers*'. Diamond and Related Materials, 51 pp. 39-48.

118. Deng, C., Jiang, J., Liu, F., Fang, L., Wang, J., Li, D. & Wu, J. (2015) '*Influence of carbon nanotubes coatings onto carbon fiber by oxidative treatments combined with electrophoretic deposition on interfacial properties of carbon fiber composite*'. Applied Surface Science, 357 pp. 1274-1280.

119. Jamnani, B. D., Hosseini, S., Rahmanian, S., Rashid, S. A. & Balavandy, S. K. (2015) '*Grafting carbon nanotubes on glass fiber by dip coating technique to enhance tensile and interfacial shear strength*'. Journal of Nanomaterials, 16 (1), pp. 306.

120. Xu, Z., Huang, Y., Zhang, C., Liu, L., Zhang, Y. & Wang, L. (2007) '*Effect of γ-ray irradiation grafting on the carbon fibers and interfacial adhesion of epoxy composites*'. Composites Science and Technology, 67 (15-16), pp. 3261-3270.

121. Vavouliotis, A., Paipetis, A. & Kostopoulos, V. (2011) '*On the fatigue life prediction of CFRP laminates using the electrical resistance change method*'. Composites Science and Technology, 71 (5), pp. 630-642.

122. Nofar, M., Hoa, S. & Pugh, M. (2009) '*Failure detection and monitoring in polymer matrix composites subjected to static and dynamic loads using carbon nanotube networks*'. Composites Science and Technology, 69 (10), pp. 1599-1606.

123. Thostenson, E. T. & Chou, T.-W. (2008) '*Real-time in situ sensing of damage evolution in advanced fiber composites using carbon nanotube networks*'. Nanotechnology, 19 (21), pp. 215713.

124. Gao, S. l., Zhuang, R. C., Zhang, J., Liu, J. W. & Mäder, E. (2010c) '*Glass fibers with carbon nanotube networks as multifunctional sensors*'. Advanced Functional Materials, 20 (12), pp. 1885-1893.

125. Obitayo, W. & Liu, T. (2012) '*A review: Carbon nanotube-based piezoresistive strain sensors*'. Journal of Sensors, 2012.

126. Zhang, J., Liu, J., Zhuang, R., Mäder, E., Heinrich, G. & Gao, S. (2011) *'Single MWNT-glass fiber as strain sensor and switch*'. Advanced Materials, 23 (30), pp. 3392-3397.

127. Gao, L., Chou, T.-W., Thostenson, E. T. & Zhang, Z. (2010b) '*A comparative study of damage sensing in fiber composites using uniformly and non-uniformly dispersed carbon nanotubes*'. Carbon, 48 (13), pp. 3788-3794.

128. Grammatikos, S. & Paipetis, A. (2012) '*On the electrical properties of multi scale reinforced composites for damage accumulation monitoring*'. Composites Part B: Engineering, 43 (6), pp. 2687-2696.

129. Naghashpour, A. & Van Hoa, S. (2013b) '*A technique for real-time detection, location and quantification of damage in large polymer composite structures made of electrically non-conductive fibers and carbon nanotube networks*'. Nanotechnology, 24 (45), pp. 455502.

130. Yesil, S., Winkelmann, C., Bayram, G. & La Saponara, V. (2010) '*Surfactant-modified multiscale composites for improved tensile fatigue and impact damage sensing*'. Materials Science and Engineering: A, 527 (27-28), pp. 7340-7352.

131. Grammatikos, S., Kordatos, E., Matikas, T. & Paipetis, A. (2014) '*Real-time debonding monitoring of composite repaired materials via electrical, acoustic, and thermographic methods*'. Journal of materials engineering and performance, 23 (1), pp. 169-180.

132. Sebastian, J., Schehl, N., Bouchard, M., Boehle, M., Li, L., Lagounov, A. & Lafdi, K. (2014) '*Health monitoring of structural composites with embedded carbon nanotube coated glass fiber sensors*'. Carbon, 66 pp. 191-200.

133. Deng, N. & Korkolis, Y. P. (2018) '*Determination of the shear modulus of orthotropic thin sheets with the anticlastic-plate-bending experiment*'. Journal of Engineering Materials and Technology, 140 (4), pp. 041011.

134. Yamamoto, N., de Villoria, R. G. & Wardle, B. L. (2012) '*Electrical and thermal property enhancement of fiber-reinforced polymer laminate composites through controlled implementation of multi-walled carbon nanotubes*'. Composites Science and Technology, 72 (16), pp. 2009-2015.

135. Zhang, J., Zhang, X., Chen, S., Gong, T. & Zhu, Y. (2016a) '*Surface-enhanced Raman scattering properties of multi-walled carbon nanotubes arrays-Ag nanoparticles*'. Carbon, 100 pp. 395-407.

136. Hadjiev, V., Warren, G., Sun, L., Davis, D., Lagoudas, D. & Sue, H.-J. (2010) '*Raman microscopy of residual strains in carbon nanotube/epoxy composites*'. Carbon, 48 (6), pp. 1750-1756.

137. Tehrani, M., Boroujeni, A., Hartman, T., Haugh, T., Case, S. & Al-Haik, M. (2013) '*Mechanical characterization and impact damage assessment of a woven carbon*

fiber reinforced carbon nanotube–epoxy composite'. Composites Science and Technology, 75 pp. 42-48.

138. Quaresimin, M., Ricotta, M., Martello, L. & Mian, S. (2013) '*Energy absorption in composite laminates under impact loading'*. Composites Part B: Engineering, 44 (1), pp. 133-140.

139. Belingardi, G. & Vadori, R. (2002) '*Low velocity impact tests of laminate glass-fiber-epoxy matrix composite material plates*'. International Journal of Impact Engineering, 27 (2), pp. 213-229.

140. Sarasini, F., Tirillò, J., Ferrante, L., Valente, M., Valente, T., Lampani, L., Gaudenzi, P., Cioffi, S., Iannace, S. & Sorrentino, L. (2014) '*Drop-weight impact behaviour of woven hybrid basalt–carbon/epoxy composites*'. Composites Part B: Engineering, 59 pp. 204-220.

141. Liu, Q., Guo, O., Ju, Y., Lin, Y. & Li, Q. (2014) '*Impact responses and residual flexural properties of narrow CFRP laminates*'. Composite Structures, 111 pp. 332-339.

142. De Rosa, I., Marra, F., Pulci, G., Santulli, C., Sarasini, F., Tirillò, J. & Valente, M. (2011) '*Post-impact mechanical characterisation of E-glass/basalt woven fabric interply hybrid laminates*'. Express Polymer Letters, 5 (5).

143. Montgomery, D. C. (2013) '*Design and Analysis of Experiments, eight edition*'. Joh Wiley and Sons.

144. Yin, G., Hu, N., Karube, Y., Liu, Y., Li, Y. & Fukunaga, H. (2011) '*A carbon nanotube/polymer strain sensor with linear and anti-symmetric piezoresistivity*'. Journal of composite materials, 45 (12), pp. 1315-1323.

145. Mecklenburg, M., Mizushima, D., Ohtake, N., Bauhofer, W., Fiedler, B. & Schulte, K. (2015) '*On the manufacturing and electrical and mechanical properties of ultra-high wt.% fraction aligned MWCNT and randomly oriented CNT epoxy composites*'. Carbon, 91 pp. 275-290.

146. Perets, Y., Aleksandrovych, L., Melnychenko, M., Lazarenko, O., Vovchenko, L. & Matzui, L. (2017) '*The Electrical Properties of Hybrid Composites Based on Multiwall Carbon Nanotubes with Graphite Nanoplatelets*'. Nanoscale research letters, 12 (1), pp. 406.

147. Romanov, V. S., Lomov, S. V., Verpoest, I. & Gorbatikh, L. (2015) '*Modelling evidence of stress concentration mitigation at the micro-scale in polymer composites by the addition of carbon nanotubes*'. Carbon, 82 pp. 184-194.

148. De Villoria, R. G. & Miravete, A. (2007) '*Mechanical model to evaluate the effect of the dispersion in nanocomposites*'. Acta Materialia, 55 (9), pp. 3025-3031.

149. Coleman, J. N., Khan, U., Blau, W. J. & Gun'ko, Y. K. (2006) '*Small but strong: a review of the mechanical properties of carbon nanotube–polymer composites*'. Carbon, 44 (9), pp. 1624-1652.

150. Bokobza, L. (2017) '*Mechanical and electrical properties of elastomer nanocomposites based on different carbon nanomaterials*'. C, 3 (2), pp. 10.

151. Zhang, J. & Jiang, D. (2011) '*Interconnected multi-walled carbon nanotubes reinforced polymer-matrix composites*'. Composites Science and Technology, 71 (4), pp. 466-470.

152. Chen, J., Shi, Y.-y., Yang, J.-h., Zhang, N., Huang, T., Chen, C., Wang, Y. & Zhou, Z.-w. (2012) '*A simple strategy to achieve very low percolation threshold via the selective distribution of carbon nanotubes at the interface of polymer blends*'. Journal of Materials Chemistry, 22 (42), pp. 22398-22404.

153. Jang, S.-H., Kawashima, S. & Yin, H. (2016) '*Influence of carbon nanotube clustering on mechanical and electrical properties of cement pastes*'. Materials, 9 (4), pp. 220.

154. Pham, G. T., Park, Y.-B., Liang, Z., Zhang, C. & Wang, B. (2008) '*Processing and modeling of conductive thermoplastic/carbon nanotube films for strain sensing*'. Composites Part B: Engineering, 39 (1), pp. 209-216.

155. Hu, N., Karube, Y., Yan, C., Masuda, Z. & Fukunaga, H. (2008) '*Tunneling effect in a polymer/carbon nanotube nanocomposite strain sensor*'. Acta Materialia, 56 (13), pp. 2929-2936.

156. Njuguna, M. K., Yan, C., Bell, J. & Yarlagadda, P. (2012) '*Temperature Dependent Electrical Resistivity in Epoxy—Multiwall Carbon Nanotube Nanocomposites*', Engineering Asset Management and Infrastructure Sustainability. Springer, pp. 713-723.

157. Njuguna, M. K., Galpaya, D., Yan, C., Colwell, J. M., Will, G., Hu, N., Yarlagadda, P. & Bell, J. M. (2015) '*Investigation on Temperature-Dependent Electrical Conductivity of Carbon Nanotube/Epoxy Composites for Sustainable Energy Applications*'. Journal of nanoscience and nanotechnology, 15 (9), pp. 6957-6964.

158. Zeng, Y., Lu, G., Wang, H., Du, J., Ying, Z. & Liu, C. (2014) '*Positive temperature coefficient thermistors based on carbon nanotube/polymer composites*'. Scientific reports, 4 pp. 6684.

159. Mohiuddin, M. & Van Hoa, S. (2011) '*Electrical resistance of CNT-PEEK composites under compression at different temperatures*'. Nanoscale research letters, 6 (1), pp. 419.

160. Bandyopadhyay, A., Valavala, P. K., Clancy, T. C., Wise, K. E. & Odegard, G. M. (2011) '*Molecular modeling of crosslinked epoxy polymers: The effect of crosslink density on thermomechanical properties*'. Polymer, 52 (11), pp. 2445-2452.

161. Yip, M.-C., Lin, Y.-C. & Wu, C.-L. (2011) '*Effect of Multi-Walled Carbon Nanotubes Addition on Mechanical Properties of Polymer Composites Laminate'*. Polymers & Polymer Composites, 19 (2/3), pp. 131.

162. Takeda, T., Shindo, Y., Fukuzaki, T. & Narita, F. (2014) '*Short beam interlaminar shear behavior and electrical resistance-based damage self-sensing of woven carbon/epoxy composite laminates in a cryogenic environment*'. Journal of composite materials, 48 (1), pp. 119-128.

163. Böger, L., Wichmann, M. H., Meyer, L. O. & Schulte, K. (2008) '*Load and health monitoring in glass fibre reinforced composites with an electrically conductive*

nanocomposite epoxy matrix'. Composites Science and Technology, 68 (7-8), pp. 1886-1894.

164. Muto, N., Arai, Y., Shin, S., Matsubara, H., Yanagida, H., Sugita, M. & Nakatsuji, T. (2001) '*Hybrid composites with self-diagnosing function for preventing fatal fracture*'. Composites Science and Technology, 61 (6), pp. 875-883.

165. Wu, Z., Cui, H., Chen, L., Jiang, D., Weng, L., Ma, Y., Li, X., Zhang, X., Liu, H. & Wang, N. (2018) '*Interfacially reinforced unsaturated polyester carbon fiber composites with a vinyl ester-carbon nanotubes sizing agent*'. Composites Science and Technology, 164 pp. 195-203.

166. Gu, H., Zhang, H., Ma, C., Xu, X., Wang, Y., Wang, Z., Wei, R., Liu, H., Liu, C. & Shao, Q. (2019) '*Trace electrosprayed nanopolystyrene facilitated dispersion of multiwalled carbon nanotubes: simultaneously strengthening and toughening epoxy*'. Carbon, 142 pp. 131-140.

167. He, Y., Yang, S., Liu, H., Shao, Q., Chen, Q., Lu, C., Jiang, Y., Liu, C. & Guo, Z. (2018) '*Reinforced carbon fiber laminates with oriented carbon nanotube epoxy nanocomposites: magnetic field assisted alignment and cryogenic temperature mechanical properties*'. Journal of colloid and interface science, 517 pp. 40-51.

168. Zhang, X., Wang, P., Neo, H., Lim, G., Malcolm, A. A., Yang, E.-H. & Yang, J. (2016b) '*Design of glass fiber reinforced plastics modified with CNT and pre-stretching fabric for potential sports instruments*'. Materials & Design, 92 pp. 621-631.

169. Rahmanian, S., Thean, K., Suraya, A., Shazed, M., Salleh, M. M. & Yusoff, H. (2013) '*Carbon and glass hierarchical fibers: influence of carbon nanotubes on tensile, flexural and impact properties of short fiber reinforced composites*'. Materials & Design, 43 pp. 10-16.

170. Danisman, M., Tuncol, G., Kaynar, A. & Sozer, E. M. (2007) '*Monitoring of resin flow in the resin transfer molding (RTM) process using point-voltage sensors*'. Composites Science and Technology, 67 (3-4), pp. 367-379.

171. Sorrentino, L., Esposito, L. & Bellini, C. (2017) '*A new methodology to evaluate the influence of curing overheating on the mechanical properties of thick FRP laminates*'. Composites Part B: Engineering, 109 pp. 187-196.

172. Liu, H., Gao, J., Huang, W., Dai, K., Zheng, G., Liu, C., Shen, C., Yan, X., Guo, J. & Guo, Z. (2016) '*Electrically conductive strain sensing polyurethane nanocomposites with synergistic carbon nanotubes and graphene bifillers*'. Nanoscale, 8 (26), pp. 12977-12989.

173. Sun, K., Xie, P., Wang, Z., Su, T., Shao, Q., Ryu, J., Zhang, X., Guo, J., Shankar, A. & Li, J. (2017) '*Flexible polydimethylsiloxane/multi-walled carbon nanotubes membranous metacomposites with negative permittivity*'. Polymer, 125 pp. 50-57.

174. Zhang, S., Liu, H., Yang, S., Shi, X., Zhang, D., Shan, C., Mi, L., Liu, C., Shen, C. & Guo, Z. (2019) '*Ultrasensitive and Highly Compressible Piezoresistive Sensor Based on Polyurethane Sponge Coated with Cracked Cellulose Nanofibril/Silver Nanowire Layer*'. ACS applied materials & interfaces.

175. Nelin, E. A. (2007) '*Impedance model for quantum-mechanical barrier problems*'. Physics-Uspekhi, 50 (3), pp. 293.

176. Deng, F. & Zheng, Q. (2009) '*Interaction models for effective thermal and electric conductivities of carbon nanotube composites*'. Acta Mechanica Solida Sinica, 22 (1), pp. 1-17.

177. Lekawa-Raus, A., Patmore, J., Kurzepa, L., Bulmer, J. & Koziol, K. (2014) '*Electrical properties of carbon nanotube based fibers and their future use in electrical wiring*'. Advanced Functional Materials, 24 (24), pp. 3661-3682.

178. Kumar, R. M., Sharma, S. K., Kumar, B. M. & Lahiri, D. (2015) '*Effects of carbon nanotube aspect ratio on strengthening and tribological behavior of ultra high molecular weight polyethylene composite*'. Composites Part A: Applied Science and Manufacturing, 76 pp. 62-72.

179. Deng, F., Zheng, Q.-S., Wang, L.-F. & Nan, C.-W. (2007) '*Effects of anisotropy, aspect ratio, and nonstraightness of carbon nanotubes on thermal conductivity of carbon nanotube composites*'. Applied Physics Letters, 90 (2), pp. 021914.

180. Rahman, R. & Servati, P. (2012) *'Effects of inter-tube distance and alignment on tunnelling resistance and strain sensitivity of nanotube/polymer composite films*'. Nanotechnology, 23 (5), pp. 055703.

181. García-Macías, E., D'Alessandro, A., Castro-Triguero, R., Pérez-Mira, D. & Ubertini, F. (2017) '*Micromechanics modeling of the uniaxial strain-sensing property of carbon nanotube cement-matrix composites for SHM applications*'. Composite Structures, 163 pp. 195-215.

182. D'Alessandro, A., Rallini, M., Ubertini, F., Materazzi, A. L. & Kenny, J. M. (2016) '*Investigations on scalable fabrication procedures for self-sensing carbon nanotube cement-matrix composites for SHM applications*'. Cement and Concrete Composites, 65 pp. 200-213.

183. Al-Bahrani, M., Aljuboury, M. & Cree, A. (2018) '*Damage sensing and mechanical properties of laminate composite based MWCNTs under anticlastic test*'. Materials Research Express, 6 (3), pp. 035704.

184. Ferreira, A., Martínez, M., Ansón-Casaos, A., Gómez-Pineda, L., Vaz, F. & Lanceros-Mendez, S. (2013) '*Relationship between electromechanical response and percolation threshold in carbon nanotube/poly (vinylidene fluoride) composites*'. Carbon, 61 pp. 568-576.

185. Li, Y., Zhou, B., Zheng, G., Liu, X., Li, T., Yan, C., Cheng, C., Dai, K., Liu, C. & Shen, C. (2018a) '*Continuously prepared highly conductive and stretchable SWNT/MWNT synergistically composited electrospun thermoplastic polyurethane yarns for wearable sensing*'. Journal of Materials Chemistry C, 6 (9), pp. 2258-2269

186. Pearce, E., 2012. Flame-retardant polymeric materials. Springer Science & Business Media.